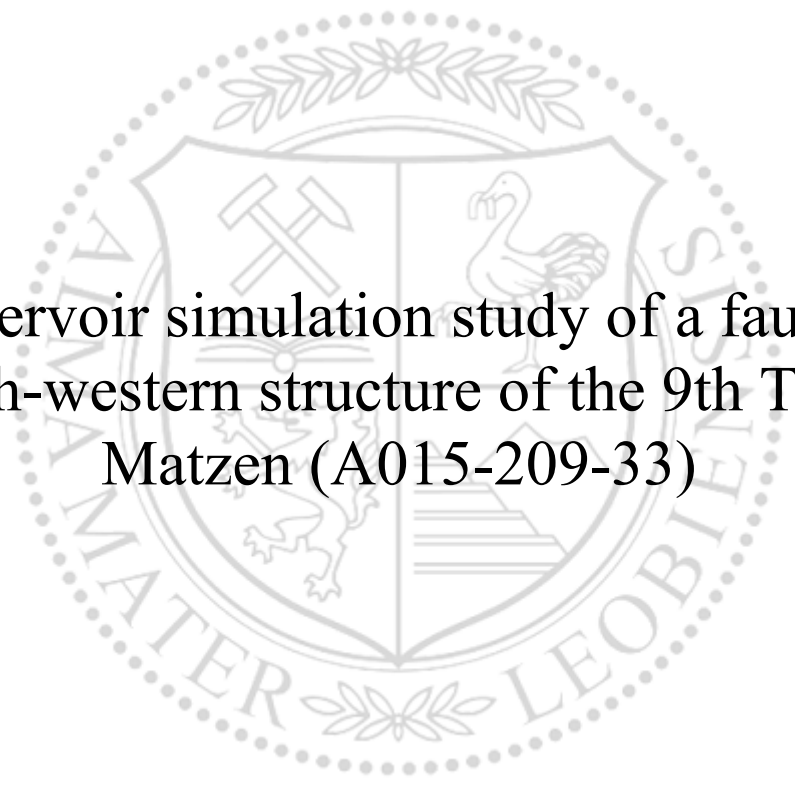




Chair of Reservoir Engineering

Master's Thesis



Reservoir simulation study of a faulted
north-western structure of the 9th TH in
Matzen (A015-209-33)

Bastian Kumhofer, BSc

September 2019

Bastian Kumhofer, BSc

Master Thesis 2019

Supervisor: Univ.-Prof. Dipl.-Phys. Dr.rer.nat. Holger Ott

Co-Supervisor: DI Matthias Maierhofer

Reservoir simulation study of a faulted north-western structure of the 9th TH in Matzen (A015-209-33)



EIDESSTÄTTLICHE ERKLÄRUNG

Ich erkläre an Eides statt, dass ich diese Arbeit selbständig verfasst, andere als die angegebenen Quellen und Hilfsmittel nicht benutzt, und mich auch sonst keiner unerlaubten Hilfsmittel bedient habe.

Ich erkläre, dass ich die Richtlinien des Senats der Montanuniversität Leoben zu "Gute wissenschaftliche Praxis" gelesen, verstanden und befolgt habe.

Weiters erkläre ich, dass die elektronische und gedruckte Version der eingereichten wissenschaftlichen Abschlussarbeit formal und inhaltlich identisch sind.

Datum 06.09.2019

Unterschrift Verfasser/in
Bastian, Kumhofer
Matrikelnummer: 01435281

Acknowledgements

First of all, I would like to thank Matthias Maierhofer and Manfred Leitner for selecting this topic. Without their proposal and their organizational work, writing this thesis would not have been possible.

Once more, I would like to extend my thanks to my supervisor Matthias Maierhofer for answering all my question, constantly reviewing my work, and especially for sharing his experience and knowledge with me. All our technical discussions enabled me do get a different view on specific problems, which in turn led to new conclusions.

Special thanks also go to Albert Gauer for his comprehensive expertise in the fields of geology and geo-modelling. Without him, the use of the integrated reservoir simulation approach would not have been possible.

Finally, I want to thank my parents, who made it possible for me to live a worry-free life and to fully concentrate on my studies. This master thesis marks the successful end of all my efforts.

Abstract

The efficient and effective recovery of hydrocarbons is one of the major challenges for any oil and gas company. This is especially true in countries in which the potential for significant new discoveries of these resources is limited. Optimizing and improving the recovery from brown fields can be achieved in various ways ranging from target-oriented infill drilling (based on new and more detailed information about the subsurface geology) to the implementation of enhanced recovery methods.

The main aim of this thesis was to develop an optimized production strategy for the production unit 209-33 in the Matzen oil field. Unit 209-33 is a part of the 9th Tortonian Horizon and located in the geologically complex Matzen fault system. It can be considered as a kind of satellite production unit to the main compartment of the 9th Tortonian layer.

Production in this reservoir started in the 1960s. By 2016 a primary recovery factor of approximately 60 % had been reached, which was also reflected by the very high water cut of 95 %. In the same year an already existing production well was relocated from a deeper oil-bearing rock formation to production unit 209-33. Since then the water cut of this new well has remained stable at around 13 %.

As this was quite unusual, it was decided to carry out a reassessment of the oil field to achieve a better understanding of the characteristic features. Special emphasis was put on the influence of geological faults. After all, the development of an economically viable production strategy is only possible, if the fundamental characteristics of an oil field are well known. To achieve this, a fully integrated reservoir simulation approach was used.

In this thesis a representative reservoir model for the production unit 209-33 has been developed. It is also shown that the production behaviour of the latest well cannot be deduced from the actual reservoir behaviour. Therefore, possible technical causes for water production have been proposed. Based on this model various future development scenarios have been investigated, with the result that a single new vertical infill well holds the greatest economic potential. Within the first 10 years an additional recovery of about 22,000 sm³ of crude oil can be expected, which corresponds to a recovery factor increase from 38.9 % to 41.5 %.

Zusammenfassung

Eine der größten Herausforderungen für Erdöl und Erdgas produzierende Unternehmen ist die effektive und effiziente Förderung dieser Rohstoffe. Das betrifft vor allem jene Länder, in denen das Potential für signifikante Neuentdeckungen limitiert ist. Die Produktionsoptimierung kann auf verschiedenste Arten erreicht werden und reicht von Neubohrungen (aufgrund detaillierterer Untergrundmodelle) bis hin zur Anwendung von technisch komplexeren Produktionsmethoden (EOR).

Das Ziel dieser Arbeit bestand darin, eine optimierte Produktionsstrategie für die Lagerstätte 209-33 im Matzen-Feld zu entwickeln. Diese Produktionseinheit ist Teil des 9. Tortonhorizontes und liegt im strukturell komplexen Matzen-Bruchsystem.

Die Erschließung der Lagerstätte datiert zurück ins Jahr 1960. Bis 2016 wurden in etwa 60 % der damals errechneten Erdölmenge gefördert. Das spiegelt sich auch in dem sehr hohen Wasseranteil (ca. 95 %) der produzierten Flüssigkeit wider. Im selben Jahr wurde eine vorhandene Fördersonde von einem tieferen Gesteinshorizont in die Produktionseinheit 209-33 verlegt. Der Wasseranteil in dieser Sonde liegt seither kontinuierlich bei 13 %.

Aufgrund dieses untypischen Verhaltens wurden eine neue Untersuchung und Analyse der Lagerstätte beschlossen. Die Entwicklung einer optimierten Produktionsstrategie ist nur dann möglich, wenn die grundlegenden Charakteristiken der Lagerstätte bekannt sind. Besonderes Augenmerk wurde dabei auf den Einfluss von geologischen Störungen gelegt.

Im Zuge dieser Arbeit wurde ein Lagerstättenmodell, das eine genaue Reproduktion der historischen Produktionsdaten ermöglicht, entwickelt. Darüber hinaus wurde gezeigt, dass das Produktionsverhalten der neuesten Bohrung nicht aus dem Lagerstättenverhalten abgeleitet werden kann und mögliche technische Ursachen für die Wasserproduktion wurden vorgeschlagen. Im Anschluss wurden, auf diesem Modell basierend, verschiedene Produktionsstrategien untersucht. Dabei zeigte sich, dass eine einzelne vertikale Neubohrung den größten wirtschaftlichen Erfolg bringt. Innerhalb der ersten 10 Jahre wird eine zusätzliche Rohölproduktion von zirka 22,000 sm³ erwartet. Das entspricht einer Steigerung der prozentuellen Ausbeute von 38.9 % auf 41.5 %.

Table of Contents

Chapter 1	Introduction.....	1
1.1	Background and Context.....	1
1.2	Scope and Objectives.....	3
1.3	Technical Issues.....	4
Chapter 2	Literature Review.....	5
2.1	Matzen Field.....	5
2.2	9 th Tortonian Horizon.....	9
2.3	Analogous Fields.....	13
Chapter 3	Methodology.....	17
3.1	Analytic Description of 209-33.....	17
3.2	Analogous Investigation.....	23
3.3	Resource & Reserve Estimation.....	27
3.4	Model Setup and Initialization.....	32
3.5	History Matching.....	34
3.6	Development Scenarios & Production Forecasting.....	48
3.7	Economic Assessment.....	51
Chapter 4	Results & Discussion.....	55
Chapter 5	Conclusion.....	59
5.1	Summary.....	59
5.2	Evaluation.....	59
5.3	Future Work.....	60
Chapter 6	References.....	61

Chapter 1

Introduction

1.1 Background and Context

One of the major challenges for every oil and gas company is the successful maintenance of a sustainable level of proven reserves. A company's ability to replace the produced volumes by new reserves is measured by the so-called reserve replacement ratio. This ratio simply compares the amount of annually added reserves to the amount of annually produced hydrocarbon volumes. Having a reserve replacement ratio of less than one means that the production is higher than the newly discovered hydrocarbon volumes and the company's reserve basis will gradually decrease over time. Long-term, a reserve replacement ratio of 100 % or more is required in order to stay competitive.

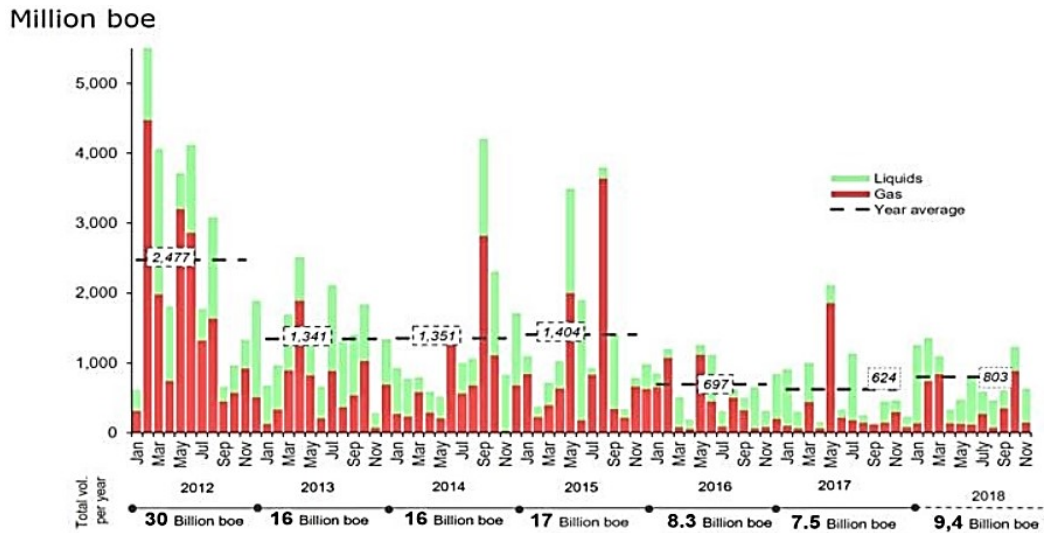
Additions to proven reserves basically come from (Eia.gov, 2019):

- discoveries of entirely new fields
- discoveries of new reservoirs in old fields
- extension of the proven area of a reservoir
- revision of the proven reserves of a reservoir due to new information
- improved recovery methods (beyond primary recovery)
- purchase of reserves.

Several factors, from the current economic conditions (including the oil price, CAPEX, OPEX, etc.) to technical challenges, innovations and limitations influence the reserve basis. The two actions that actively increase or reduce the total amount of proven reserves are production and successful reserve addition.

In the past oil and gas companies were often able to achieve sufficient reserve replacement by their own exploration activities. Changes date back to the 1990s when exploration expenditures

were reduced. Not only that, but also several other reasons like e.g. fewer discoveries of major fields caused this transformation (Bjørndal et al., 2013). With a globally discovered volume of about 9.4 billion boe, according to Palzor Shenga, 2018 was the most successful year in terms of exploration of conventional hydrocarbons since 2015 (Palzor Shenga, 2018). Nevertheless, discovered volumes had decreased by more than two-thirds since 2012 (shown in Figure 1).



Source: Rystad Energy ECube December 2018

Figure 1: Development of global conventional oil & gas discoveries (Palzor Shenga, 2018)

Due to previously mentioned facts, other methods and possibilities to ensure reserve replacement have become more important. Having a look at the global net proven reserve changes from 2016 to 2017 (shown in Figure 2), it can be seen that improved recovery (improved & enhanced recovery methods), extensions of existing fields (infill drilling in undrained areas) and discoveries of both entirely new fields as well as new reservoirs in existing fields accounted for approximately 50 % of the changes in proven reserves. The remaining additions were due to revisions and purchase. Generally, the regions and continents displayed in this analysis can be split into three groups (Barron, 2018):

- the United States, the Middle East and Latin America where exploration, extensions and improved recovery contributed the most to reserve additions.
- Russia, Central Asia, the Asia-Pacific region, where revisions as well as exploration, extensions and improved recovery methods added nearly the same amount of proven reserves.
- Europe and Canada, where revisions of existing fields made the largest contribution to the addition of proven reserves.

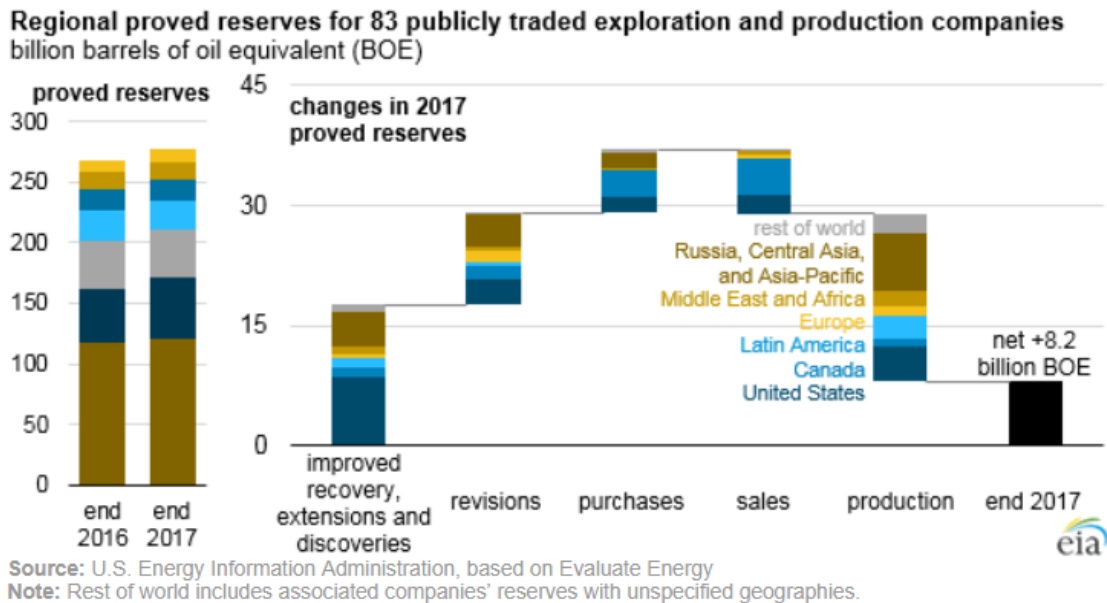


Figure 2: Changes in proved reserves 2016 to 2017
(Barron, 2018)

As a result, it can be seen that countries with a limited potential to discover new major fields, like Austria, can increase their proven reserves by applying improved and enhanced recovery methods, clearly evaluating the extent of the existing fields and revising the initial reserve estimates based on new information and more detailed field characterization. Beside several other influencing factors, the development and implementation of the optimum production strategy for each individual production unit are other important aspects to stay competitive on a long-term basis.

1.2 Scope and Objectives

The main objective of this thesis is to identify such an optimum technical and economic development scenario for the production unit A015-209-33 and consequently to increase the achievable URF. This can include:

- potential infill drilling location(s)
- workover (e.g. re-perforation) potentials of existing wells.

In order to do that, a clear understanding of the geological extent of the reservoir has to be developed and a reasonable number of the expected OIIP has to be estimated. In order to get a first estimate of achievable URF and the respective OIIP, different calculation methods, starting with the investigation of several neighbouring analogous fields, were applied. After that, material balance calculations and reservoir simulations of the reservoir were used to verify and refine this initial estimate.

1.3 Technical Issues

The production unit A015-209-33 is located in the 9th Tortonian horizon in the Matzen field. The main challenges in this rock layer are related to the complex internal layering scheme created during the time of deposition. Another issue is that the horizon consists of a number of independent production units and only the largest one represents an appropriate target for the economic application of enhanced oil recovery. Details regarding the structural and stratigraphic settings of both, the entire Matzen field and the 9th Tortonian horizon are given in Chapter 2.

In order to increase sweep and displacement efficiency, different enhanced oil recovery techniques were tested back in the 1980s. As none of them showed the expected success, water injection was the only implemented enhanced recovery method until 2018. Since then, a pilot project for polymer injection has gone on stream in the main compartment. Hydrolyzed polyacrylamide has been injected through the central well of a horizontal three-well linear pattern, whereas the two external wells have been used as producers.

For all the other units an optimum exploitation scenario using primary recovery methods and possibly water injection via existing infrastructure (conversion of already existing wells) has to be developed.

Chapter 2

Literature Review

2.1 Matzen Field

2.1.1 Historical Overview

The Vienna Basin in Austria covers an area from the Austrian-Czech border in the north-east and stretching down to the regions south-west of Eisenstadt. Along its main direction the Vienna Basin stretches over approximately 200 km (Kröll., 1984).

According to Fuchs the actual formation of the basin is best described by a sequence of three geological events, starting with a phase of subsidence, which was subsequently followed by an extension and another subsidence (Fuchs et al., 2006). As seen in Figure 3, the Matzen field is located in the north-east of Vienna and therefore belongs to the central part of the Vienna Basin.

The first indications for possible hydrocarbon accumulations in the Vienna Basin date back to the year 1913. Raggendorf 1, the very first exploration well in this area was spudded in 1915 and stopped two years later in a depth of 1070 m. It took another 32 years of geological mapping, structural drilling and basic 2D-seismic surveys until the first successful well

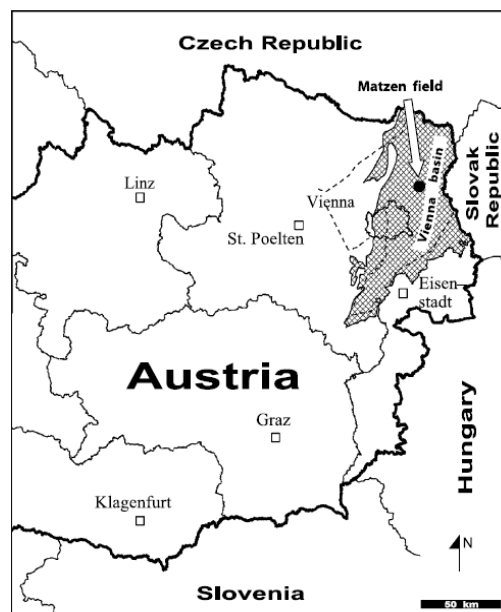


Figure 3: Location of the Matzen field (Fuchs et al., 2006)

was drilled in the Matzen field in 1949 (Kröll, 1984).

Important historical events described by Kröll (1984) and Fuchs (2006) as well as the latest developments are summarized below:

- 1948**
 - 62 shallow wells were drilled to investigate the structural and stratigraphic setting.
 - Natural gas eruption from the well Matzen K3, which was drilled to a depth of 554 m, was the first evidence for hydrocarbons in this region.
- 1949**
 - Exploration well Matzen 3 penetrated an oil bearing sand layer at a depth of 1644 m. This layer was the 16th Tortonian horizon, also called “Matzen Sand”, which is the largest oil reservoir in Austria.
- 1949-1955**
 - Drilling of more than 420 additional wells (exploration, appraisal and production).
 - Start of production in 1950.
 - Peak production level was reached in 1955.
- 1956-1992**
 - Drilling of about 1000 additional wells. Besides the conventional appraisal and production wells, reservoir management also required the drilling of water- and gas injection wells. During that period natural gas storage operations were initiated and enforced the drilling of related storage wells.
 - Drilling of the gas production well Schönkirchen Tief 32 into the Main Dolomite, which is the largest gas reservoir in Austria. With a total depth of about 6009 m, it was not only the deepest well so far, but also the first well that reached a depth of more than 6000 m in the Vienna Basin.
 - First 3D-seismic surveys were conducted.
- 1994-1996**
 - Successful re-development project of the Matzen field was proven by the first incremental oil in 1996.
- 2001**
 - Recovered volumes reached 90 % of the initially expected recoverable hydrocarbon volumes in place.
- 2011**
 - Start of a polymer injection pilot project in the 8th Tortonian horizon (Gumpenberger et al., 2011).
- 2018-2019**
 - New 3D-seismic surveys with the focus on the Main Dolomite in the Schönkirchen area and the Tortonian horizons in the Matzen area have been conducted.

2.1.2 Structural and Stratigraphic Conditions

Nowadays Matzen is known as a so-called multi-pool field. This term is used to describe that the entire field is not only made up of one single, continuous reservoir. It actually consists of about 70 productive horizons that contain more than 400 individual production units. Overall, these units initially contained producible hydrocarbon volumes of about 550 million barrels of oil and 1,500 billion cubic feet of gas (Fuchs et al., 2006). Based on the most recent definition given by Carmalt and Moscariello (2017):

“A giant oil or gas field is an accumulation of oil, natural gas, or a combination of these that has an estimated final recovery of 500 million barrels of oil and/or natural gas hydrocarbons of no less than 10° API gravity and that are trapped in the subsurface in a single or similar geological manner and that are a contiguous (or nearly contiguous) feature in map view, with gas being converted to oil equivalent at a ratio of 1 barrel 5 6000 cubic feet.”

the Matzen field can be considered to be a giant oil and gas field. At the same time, it is also the largest one in Central Europe (Fouad et al., 2001).

As mentioned previously, the structural setting of the Matzen field is the result of a sequence of geological events. Figure 4 indicates the main characteristics created by these tectonic movements. Basically the field consists of one central anticline surrounded by three fault zones. The axis of this anticline (indicated by the black arrow) is oriented in a north-east to south-west

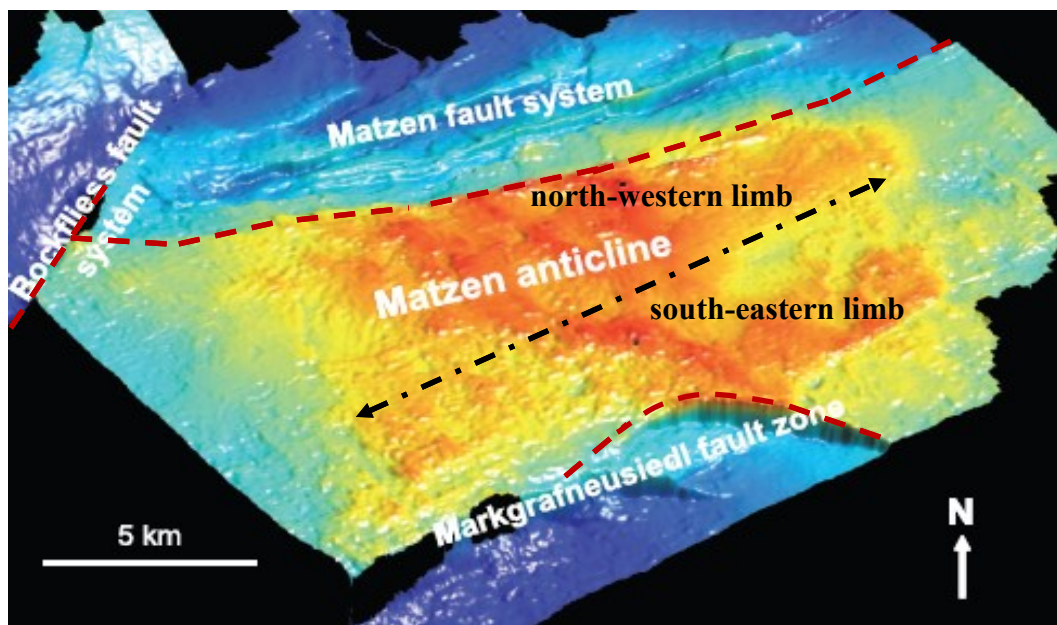


Figure 4: Structure of the Matzen field
(adapted from Fuchs et al. 2006)

direction and is dipping towards deeper layers in the north-east. In the direction of the axis the anticline extends over a length of about 10 km, whereas the width is only about 5 km. Both limbs of this anticlinal structure are bounded by adjacent fault zones (indicated by the red lines). The north-western limb is limited by the two intersecting faults that separate the anticline from the Matzen fault system and the Bockfliess fault system. On the other side of the anticline there is the Markgrafneusiedl fault zone that represents the bound for the south-eastern limb (Fouad et al., 2001 and Fuchs et al., 2006).

Fouad described the depositional history of the Matzen Field by three main sedimentary cycles (2nd order cycles) (Fouad et al. 2001). These cycles are further classified into several subsequences which are finally used to define the individual stratigraphic horizons.

The deposition took place during the middle and late Miocene ages and is characterized by the shallow marine, deltaic and fluvial facies. The horizons of the Badenian age are referred to as Tortonian and the ones of the Sarmatian age are called Sarmatian. The first of these three main Matzen cycles ends with the completed deposition of the 16th Tortonian horizon. After that the second cycle, also called the Matzen main cycle, during which most of the important oil and gas bearing layers were deposited, took place. As can be seen in Figure 5, all the major oil bearing horizons are part of the Tortonian sequence. Furthermore, it shows that all the Sarmatian horizons mainly contain gas. Only the 8th and the 10th Sarmatian horizons also produce minor amounts of oil. The final cycle started simultaneously with the beginning of the Pannonian age. Similar to the underlying Sarmatian horizons only natural gas is trapped here (Fouad et al., 2001 and Fuchs et al., 2006). Some of these depleted gas production units located in the 3rd and 4th Pannonian horizons, in the 5th Sarmatian horizon and in the 5th and 6th Tortonian horizons are currently still used as underground gas storage reservoirs in the Matzen field (Poldlehner, 2009).

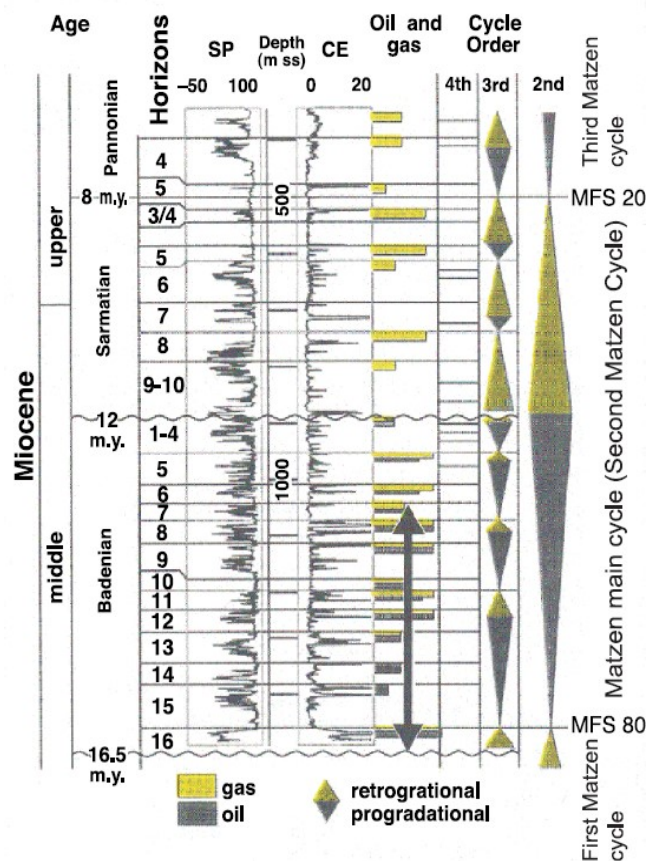


Figure 5: Type log of the Matzen field
(Fuchs et al., 2006 modified after Fouad et al., 2001)

2.2 9th Tortonian Horizon

2.2.1 Historical Overview

Similar to the entire Matzen field, the 9th Tortonian horizon itself is made up of a number of independent production units. The 9th Tortonian extends up to the Matzen and Bockfliess fault systems and these two features are also the main reason for the creation of the multi-pool setting (Gronister, 2004). Altogether, these production units cover an area of about 57 km². Since its discovery, more than 330 wells drilled in the Matzen field have been completed in this horizon. Approximately 90 production wells and 11 injection wells are still active (Finsterwalder et al., 2013). Some important historical events described by Finsterwalder (2013) and Gronister, (2004) as well as the latest developments are summarized below:

- 1950-1951** ➤ A gas blowout, which started on November 1, 1950 and stopped at the end of August 1951, marked the start of the production history.
 - The first oil was produced in March 1951 – production started although the blowout was still not under control.

- 1953-1957** ➤ Initial and largest drilling campaign took place.
 - Peak production rate of more than 600 tonnes per day was reached in July 1956 and May 1957.

- 1968** ➤ Start of water injection in the central PU via a peripheral flood pattern. The main injectors were located down the dip of the structure and in the vicinity of the Matzen fault system (northern part of the main PU).

- 1980-1985** ➤ Implementation and field-testing of various EOR methods with poor success. Tested techniques included caustic flooding using a 0.5 % sodium hydroxide solution as well as a polymer injection. The first one only showed marginal results due to the bad sweep efficiency, whereas the second method failed mainly due to bacterial degradation and related viscosity losses of the polymer slug.

- 2003** ➤ Streamline simulation of the flooding pattern for future optimization of the water injection efficiency.

- 2017** ➤ Drilling of three horizontal wells (one central injector and two producers) in the main compartment in a linear pattern and start of water injection.

- 2018-2019** ➤ Switch from water to polymer injection.
 - Drilling of a second horizontal injector-producer pattern.

2.2.2 Structural and Stratigraphic Conditions

As mentioned in chapter 2.1, the deposition of the Matzen field sediments took place in shallow marine, deltaic and fluvial environments. This is clearly reflected in the stratigraphic sequence of the 9th Tortonian horizon as well. The deposition took place during a period of a regressing sea level and caused a progression of the shelf line towards the south (Knox et al., 2000).

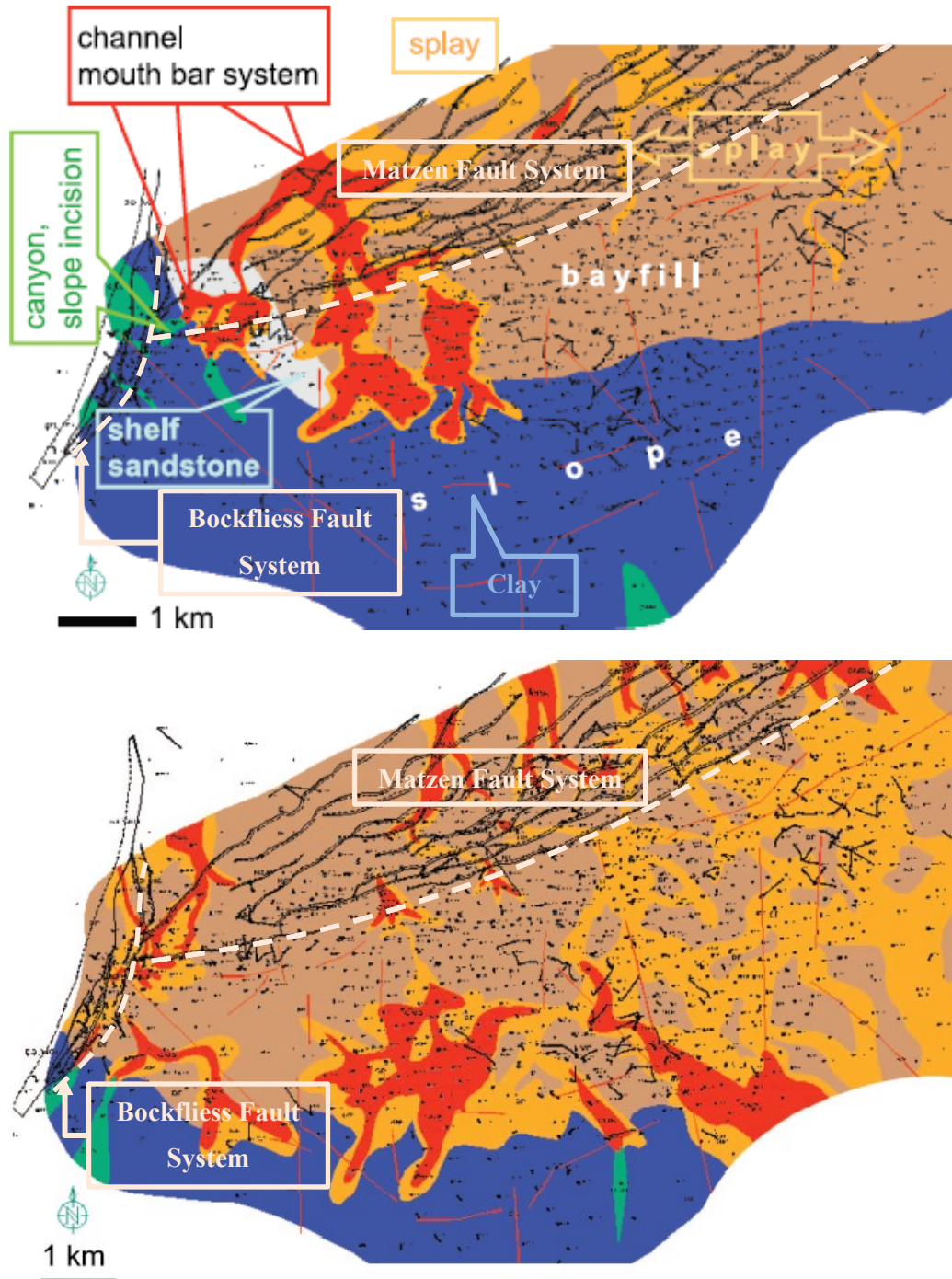


Figure 6: Paleographic setting of the 6th layer (top) and 1st layer (bottom)
(adapted from Fuchs et al. 2006)

Detailed investigations by Knox (2000) show that the horizon can be divided into six sub-layers. This classification is based on marine flooding surfaces that separate the individual layers. The numbering of the layers is done from top to bottom and consequently layer 6 was deposited first and layer 1 last. Details regarding these six sub-layers are given below according to the interpretations of Knox (2000), Fuchs (2001) and Fuchs (2006).

A schematic visualization of the initial and final stage of this sequence of sedimentation processes is shown in Figure 6. In layer 6 mainly proximal deposition took place in the northern part of the system. According to these interpretations, its thickness varies from 3 to 20 m and there is a distinct change in sediments from east to west. A channel mouth bar system essentially determines the character of the western areas, whereas the east side is mainly composed of splay and bayfill sediments.

The minimum thickness of layer 5 is the same as of layer 6, but the maximum extends up to 40 m. Interestingly, mainly vertical deposition took place. Layer 5 stacked on top of layer 6, and simultaneously the shelf line remained nearly unchanged. With respect to the type of sediments, layer 5 exhibits an inverse composition of layer 6. Bayfill and splay sediments are predominately present in the west, whereas channel mouth bar features are predominate in the east.

Layer 4 is the most complex sublayer present in the 9th Tortonian horizon. With a minimum thickness of 2 m and a maximum of 100 m, it shows the strongest variations of all layers. Additionally, it can be further classified into three zones of changing depositional processes. The thinnest zone (~2 m) is composed of extremely eroded and reworked sandstones that are located in the northeast of layer 4. This zone is interpreted as a delta plain. Channels along the Matzen fault system transported sediments coming from the north and enhanced the growth of the shelf line in the southern direction, consequently creating an area of very thick sediments (up to 100 m). The third zone, located in the very west, is a zone of low transportation-energy in which the very fine particles were deposited.

Compared to layer 4, layer 3 has just a small thickness variation of 4 to 40 m. The channel mouth bars are rather continuously distributed over the whole area. In case of a direct contact between layer 3 and layer 4 sandstones, fluid and pressure communication between these layers can be established.

The channel system of layer 2 (thickness of 4 to 35 m) and the Matzen fault system are perpendicular to each other. Pressure communication to the subjacent layers is possible in the case that layer 2 channels penetrate layer 3.

Layer 1, the uppermost layer, represents the final stage of deposition in the 9th Tortonian horizon. Compared to layer 6, the shelf line progressed approximately two kilometres to the south. As there was a very limited supply of clastic sediments from the north, this layer is

primarily composed of algal limestone. A rather uniform sedimentation is reflected in the small variation (8 to 25 m) in thickness as well. The schematic representation of the layering scheme in the 9th Tortonian horizon is shown in Figure 7.

The 9th Tortonian horizon clearly reflects the overall structural setting of the entire Matzen field. In Figure 8 it can be seen that the main structure is developed in a peripheral pattern. The majority of the wells was drilled along the limbs, away from the crest of the anticline in order to delay the breakthrough of the gas-cap gas as long as possible.

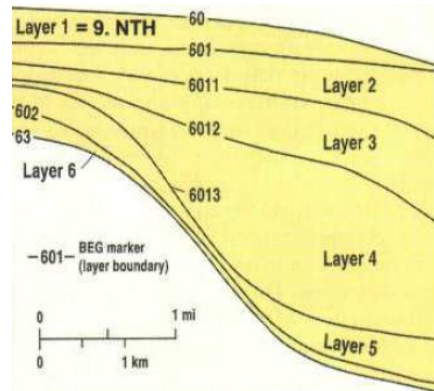


Figure 7: Schematic layering of the 9th TH (North-South cross section)
(Fuchs et al., 2001)

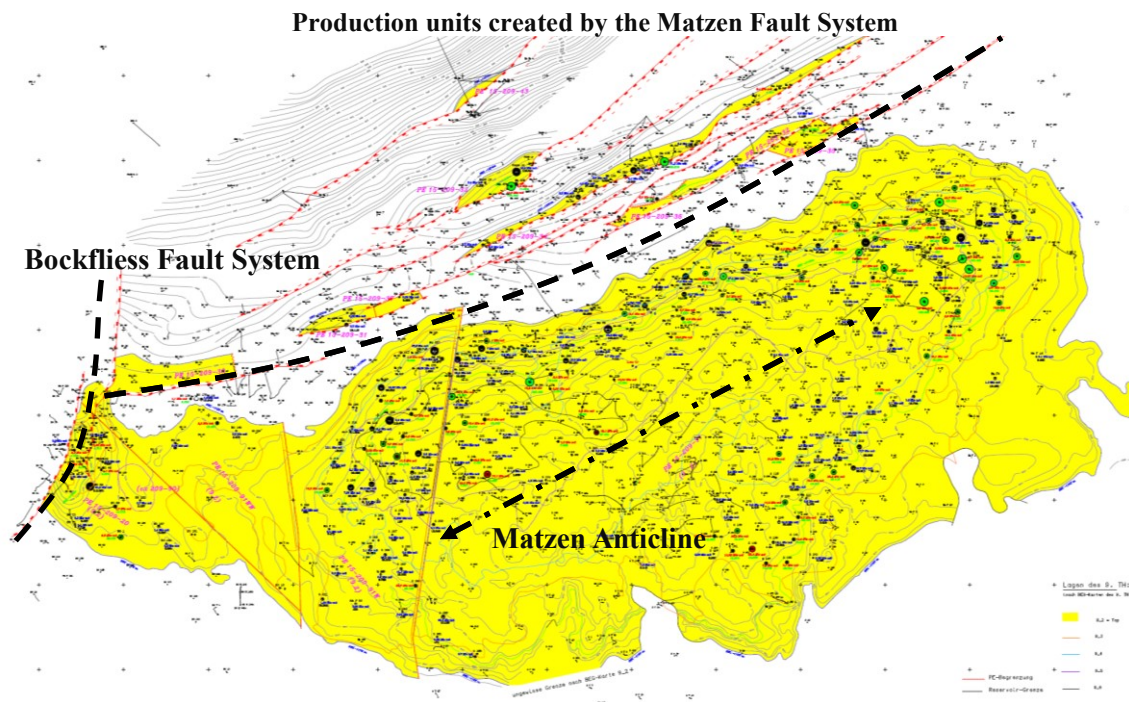


Figure 8: Current iso-map of the 9th TH

Beside the 16th Tortonian horizon, which is the most important oil bearing horizon in the Matzen field, the 9th Tortonian horizon is also among the top oil producing layers (Fuchs et al., 2006). After more than 65 years of production from the main compartment, a total of 5.3 mio tonnes of oil has been recovered. This is equivalent to a recovery factor of approximately 28 %. As seen in Figure 9, peak production of 600 tonnes of oil per day was first achieved in July 1956 and in May 1957. These rates were reached with a production WC of about 30 %. In 1984, the WC approached 90 % and has remained nearly constant since then – only a slight increase

of approximately 5 % has been observed over the last 35 years. In 1998, the oil production rate dropped below one third of the peak production rate. The historically lowest production of 100 tonnes of oil per day occurred in November 2017, since then it has increased again and current oil production is back to about 140 tonnes per day.

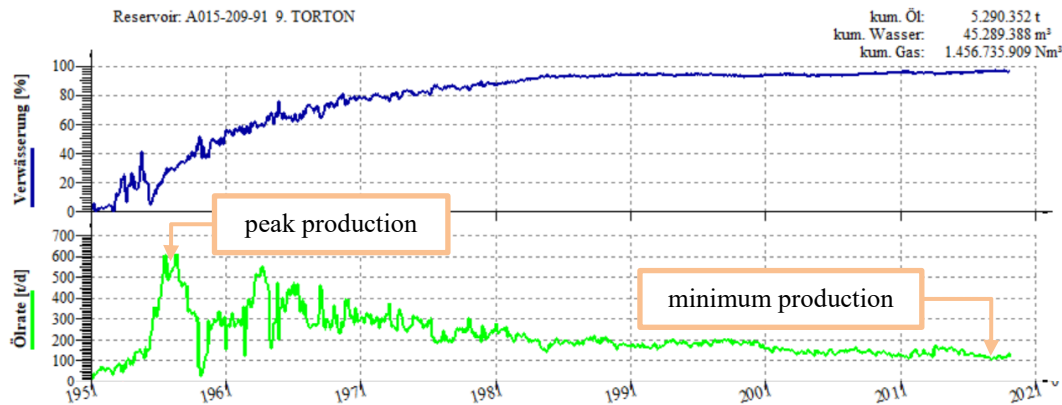


Figure 9: Oil production history and WC of the main compartment in the 9th TH

Generally, Fuchs (2006) suggested

- re-completion (especially re-perforation and the implementation of water shut off techniques) and
- infill drilling

as methods to cope with the re-development challenges that are related to the complex layering structure of the 9th Tortonian horizon.

2.3 Analogous Fields

Usually the analysis of analogous fields is used as a part of the early development planning procedure for newly discovered reservoirs. Nevertheless, this method can also be applied as part of a re-development project at a later stage in the field life. This can be especially valuable in case of mature or even depleted production units that act as a kind of reference (e.g. in terms of URF or depletion strategies) for newly discovered or less mature reservoirs in the same horizon.

The method of analogous field investigation is based on the idea that a reservoir can be characterized by a nearly unique set of properties. Looking for already known reservoirs that exhibit very similar or nearly identical characteristics can help to evaluate various cases and select the most promising strategy (Rodríguez et al., 2014).

Another important application of analogies is to estimate resources and reserves of petroleum accumulations. In the past, the OGRC (part of the SPE) established a standard technical document containing guidelines and rules for these evaluations. In 2007, the Petroleum

Resource Management System (PRMS), a joint effort of several professional societies, provided a first comprehensive summary on best practices, state of the art methods and rules for resource and reserve assessment (Etheringtonne, 2009).

According to the most recent publication of the Petroleum Resources Management System (2018) at least six major categories of properties have to be considered for the identification of analogies between different reservoirs. These categories include:

➤ Geological conditions

This part covers all aspects related to the actual deposition of the minerals, the structural changes or deformations (including the presence of natural fractures) and the effects of diagenesis on the mineral composition and lithology of the system.

➤ Petrophysical conditions

In order to consider reservoirs as analogous ones they should exhibit a high degree of similarity of parameters like porosity and permeability. Additionally, the gross thickness of the geological body, the fluid fill and corresponding saturations are compared as well. Based on that, the net pay zone and net to gross ratios can be evaluated.

➤ Reservoir Conditions

This category covers the very basic description of the reservoir including the initial pressures and temperatures as well as the depth of the accumulation and the possible presence of an aquifer. Fluid volumes initially in place (oil, gas and water) or the gross bulk volume can be used to describe the size of the reservoir.

➤ Fluid Types

Comparing two reservoirs is not limited to rock properties and fluid volumes, but also includes a comprehensive comparison of the present fluid types. Heavy oils, light oils, condensates and wet-/dry-gases exhibit entirely different production behaviour and cannot be compared to each other. Only reservoirs containing similar fluid types in terms of composition, density, viscosity, etc. can be used for analogous studies.

➤ Reservoir Driving Mechanism

Natural driving mechanisms (water drive, gas cap drive, solution gas drive, etc.) have a significant influence on the primary recovery factor of a reservoir. In order to make proper estimations of recoverable resources, the present driving mechanism has to be identified and its strength has to be quantified.

➤ Development strategies

The basic idea is that analogous reservoirs can be exploited by analogous strategies as well. Effective drainage and economic production from a new unit can be optimized by applying the knowledge gathered from analogous field investigations. This expertise includes parameters like well spacing, well and completion design, applied artificial lift methods, required surface facilities and processing plants.

2.3.1 Analogous Horizons in the Matzen Field

Reservoirs located in the 9th Tortonian horizon can theoretically be considered as analogous reservoirs. In order to have a larger pool than that during subsequent investigations, other horizons that can be considered as analogous ones to the 9th Tortonian horizon, have to be identified as well.

From a geological point of view the 8th Tortonian horizon can, according to the literature, be considered to be analogous to the 9th Tortonian. Deposition of the 8th Tortonian also took place in a fluvial and shelf dominated environment. In contrast to the 9th Tortonian, the 8th is only split up into four sublayers. The lowest of these layers, which is immediately adjacent to the 9th Tortonian, is interpreted as an extension to this layer. It clearly exhibits similar channel mouth bar, splay and bay fill sediments (Fuchs et al., 2006).

Kuffner carried out a detailed investigation of the facies and sequence stratigraphy as well as a reservoir characterization of the 9th Tortonian (Kuffner et al., 2010). As part of the results they highlighted the strong similarity between the observed lithology, sedimentary structures and the facies of both horizons.

A more detailed investigation of the analogies between individual production units located in these horizons is shown in chapter 3.2.

Chapter 3

Methodology

3.1 Analytic Description of 209-33

The focus of this study is the sandstone reservoir A015-209-33, which is located in the heavily faulted north-western part of the 9th TH in the Matzen field (Figure 8). The structure of interest represents a three-way dip closure against a major southeast dipping fault, with a thickness (distance between the OWC and the top of the structure) of around 55 m, a sand layer thickness of around 9 m, an average porosity of 26 % and the following initial conditions:

- Initial reservoir pressure 139.70 barg
- Initial avg. water saturation 21.00 %
- OIIP (low estimate) 450,000 t

The reservoir exhibits both a small gas cap drive as well as a very strong water drive. Primary production from this unit started with one well, called Raggendorf 016, in October 1963. It is important to mention that production started with an eruptive phase and the first pressure measurement was conducted in August 1966 – only three years after the start of production. Within the last 56 years, five production wells have been drilled, but only three of them are still active. The detailed well history is shown in Table 1.

Table 1: Well history of 209-33

Well	Start	End	Cumulative Oil Production
	[Date]	[Date]	[tonnes]
RAGG 16	October 1963	May 2004	116,342
RAGG 10	March 1970	May 1973	2,153
MA 476	March 1972	-	118,738
MA 229	November 1996	-	17,818
MA 145	September 2016	-	8,623

Figure 10 shows that peak production was reached in 1975, twelve years after the first oil. Within the first six years of production the water cut rose quickly to about 80 %. The temporary decline in WC to about 60 % and the gradual increase in oil production up to the peak level is related to the completion of Matzen 476 in this layer.

Throughout the last 30 years a nearly constant WC of around 95 % (indicated by the red dotted line) has been maintained. The only exception is the period from July 2003 to January 2006, during which the WC dropped to about 80 %. This reduction can be attributed to the plugging and the abandonment of Raggendorf 16, which experienced an average WC of about 99 % during the last 5 years of production. This event is also clearly visible in the significant reduction of the gross production from the reservoir.

As mentioned, the well Matzen 145 was completed in the 9th Tortonian horizon in September 2016, since then a constant rate of about 10 tonnes of oil per day at a WC of 13 % has been maintained. This can clearly be seen in Figure 10. The field WC cut was reduced by 5 % (from 95 % to 90 %) and the oil production rate was doubled instantaneously. An interesting aspect is that the start of Matzen 145 cannot be seen in the gross production rate history. However, the combined influence of a decreasing pump efficiency in Matzen 229 and Matzen 476 and the comparably low gross production of Matzen 145 kept the overall rate nearly constant. Having such a good performing producer in a mature reservoir with a currently estimated RF of around 60 % (for the low case of OIIP) already gives the first indication that undrained oil zones are left.

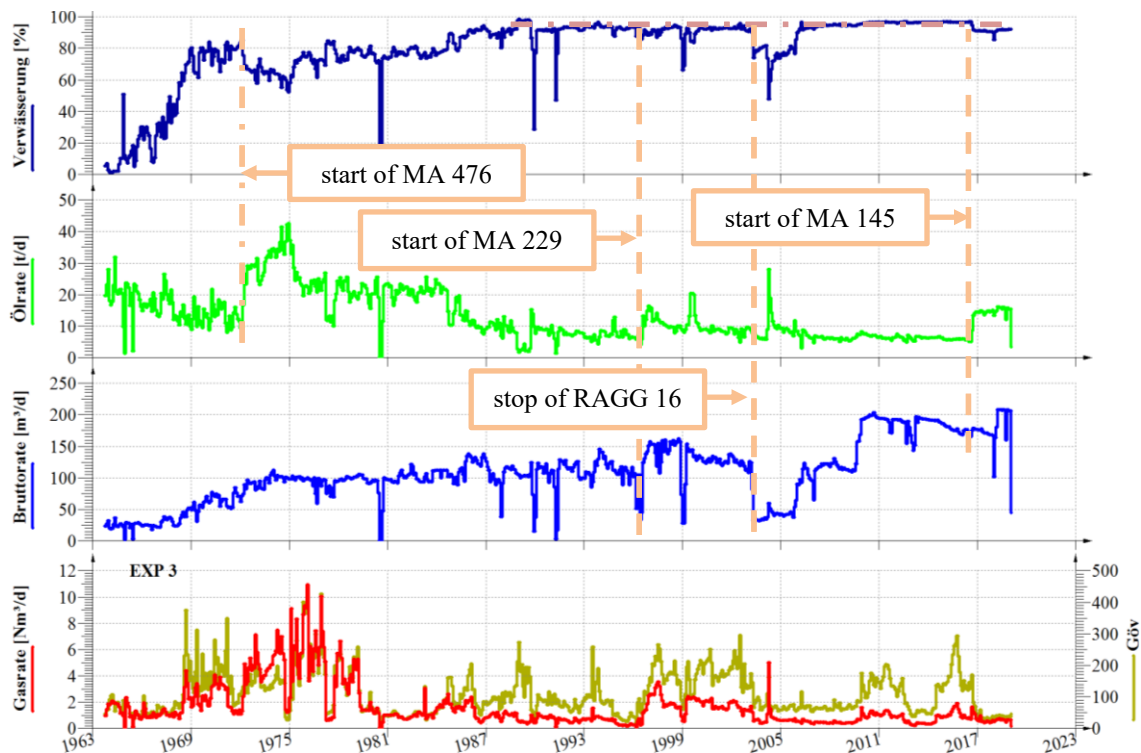


Figure 10: Production history of 209-33

Throughout its history the production unit 209-33 has undergone several revisions with respect to the estimated OIIP (shown in Figure 11). Nevertheless, there is still the unsolved issue that the currently used estimate of the OIIP is significantly too low to support the cumulative oil production of the reservoir.

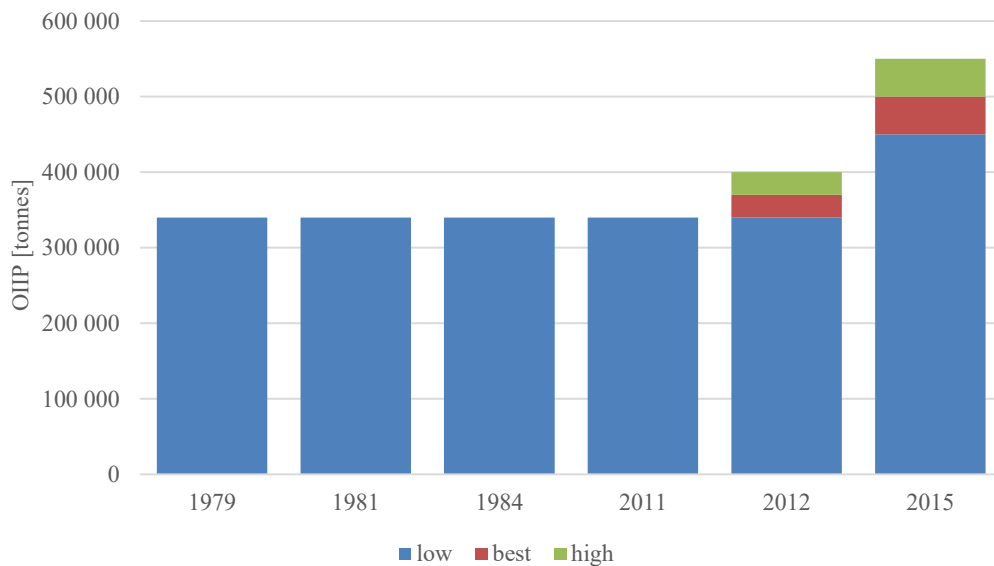


Figure 11: Revisions of the OIIP

The latest conducted volume calculations:

- based on a deterministic method resulted in an OIIP of 500,000 tonnes.
- based on a probabilistic method in GeoX resulted in a volume of 380,000 tonnes.

This probabilistic result leads to an even more unrealistic high primary recovery factor of 69 % and is also below the deterministic calculations conducted in 2012. A new evaluation of the OIIP based on the latest dynamic data is shown in chapter 3.3.

From Table 1 it can be seen that the vast majority of cumulative oil production is generated from Raggendorf 016 and Matzen 476. Both of them recovered approximately 24 % of the estimated OIIP. Looking at the spatial distribution of previous and current producers (shown in Figure 12) several interesting observations can be made. The main production is still coming from the north-eastern and central parts of 209-33. Matzen 229 is located between the top producers and its perforations are located structurally higher than in the other wells. Nevertheless, neither cumulative production nor the initial production rate reached the level of its neighbors. Most certainly, Matzen 476, which had been in production for more than 24 years when Matzen 229 was completed in 1996, already extracted the oil in this area very effectively. Having a new well in the near vicinity of a strong producer (the well-to-well distance is only about 70 m) is a consistent explanation for the comparably low performance. The reason for

this short well-to-well distance is that MA 229 first produced from deeper horizons in the Matzen field and that the 9th Tortonian horizon was only a secondary target. Raggendorf 10 was located in a central position as well (similar to Matzen 476 and Matzen 229), but its perforations were structurally deeper and close to the OWC. Consequently, a very high water cut was observed nearly instantaneously and necessitated the plugging of the well after only three years. Matzen 145 is the only well located in the south-western part of the production unit. Starting production from an area which had been undrained up until this point, is a possible explanation for the excellent performance of this well. A detailed representation of the perforated intervals, their position in the 9th Tortonian horizon and the respective deep resistivity and SP logs is given at the end of this chapter (Figure 15).

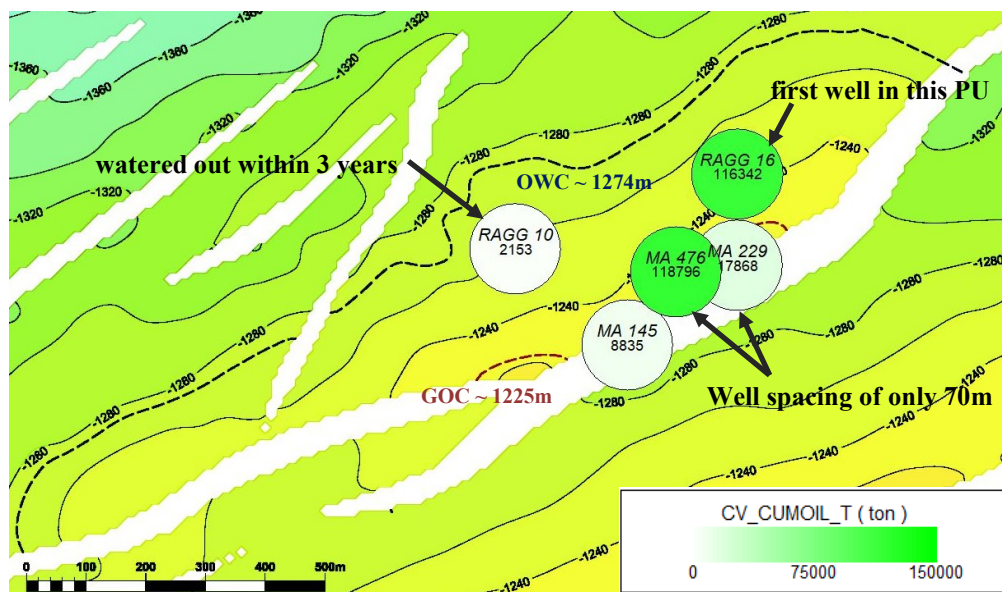


Figure 12: Bubble map of cumulative oil production in tonnes (new map)

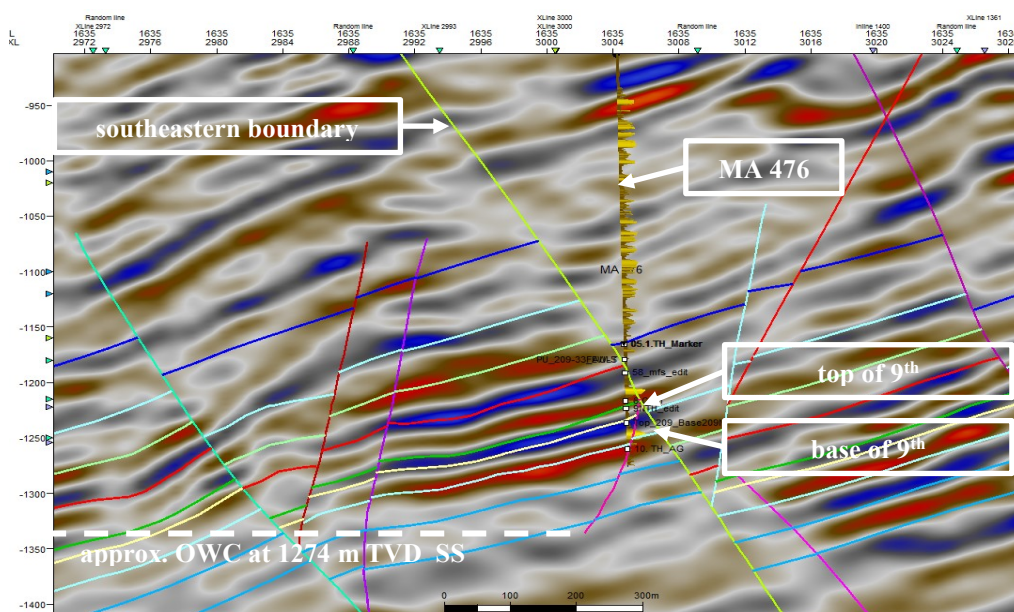


Figure 13: Seismic NW-SE inline intersecting MA 476

Another aspect is that a recently conducted seismic reprocessing (one inline is shown in Figure 13) has led to a new interpretation of the structural setting. As can be seen in the seismic chart, there is one major northeast – southwest oriented fault that represents the south-eastern boundary of the reservoir and there are also several minor faults that potentially affect the fluid flow directions inside the reservoir. So far no indications for an influence of these minor faults have been observed in the production data. Reservoir simulation based on different geological interpretations is intended to help to understand the nature and impact of these faults.

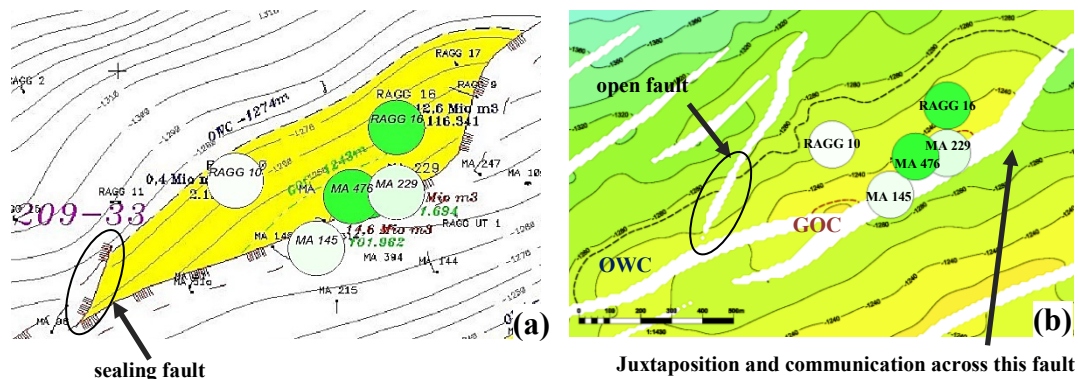


Figure 14: Comparison of the current (a) and new (b) interpretation of 209-33

Figure 14 shows a direct comparison of the current and the updated interpretation. The blue dotted line represents the OWC. Up to now it is assumed that the major northeast-southwest oriented fault is sealing, but depending on the vertical offset, a juxtaposition of 209-33 with the overlying sandstone layers (mainly from the 8th Tortonian horizon) on the opposite side of the fault is possible.

In contrast to the current model the new interpretation also suggests that the fault at the south-western end of 209-33 is not sealing. This causes an extension of the production unit in the south-western direction, along the major fault. In this case the location of Matzen 145 shifts to a more central position in the reservoir. Consequently, the undrained area to the west of Matzen 145 would increase and the respective recovery potential has to be evaluated again.

Although there is uncertainty related to the new seismic interpretation, both interpretations show that the reservoir extends either further to the west or the south-east. Therefore, both scenarios support the initial conclusion that the currently used OIIP is too low. If a juxtaposition of the 9th Tortonian horizon with the adjacent rock strata took place without having an impermeable barrier in between them or if only the areal extent of the production unit is bigger than expected, will be investigated in the reservoir simulation study.

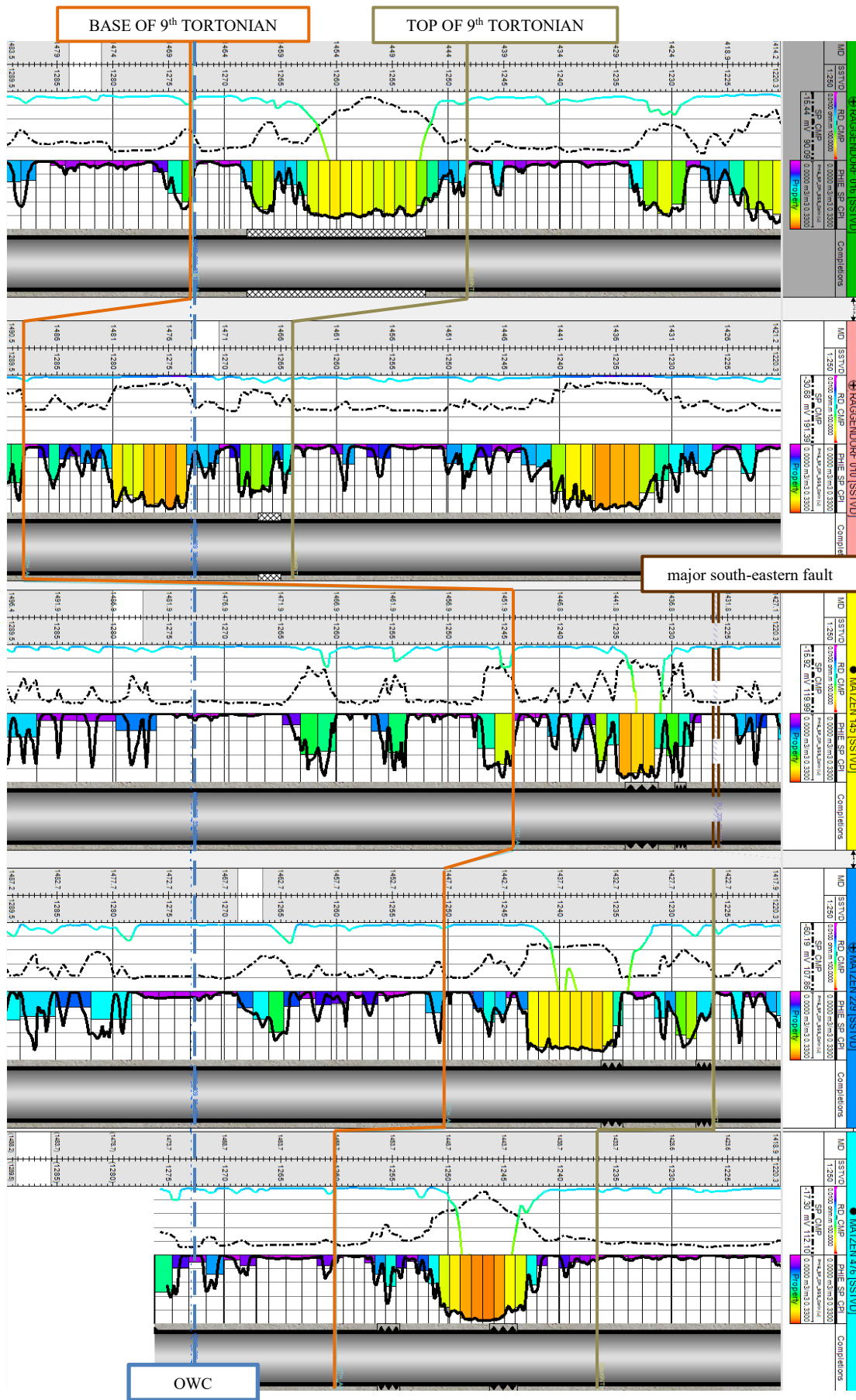


Figure 15: Completion intervals and respective log data

3.2 Analogous Investigation

In order to get a first idea of the size of the reservoir in terms of hydrocarbon volumes, an investigation of analogous fields has been conducted. As mentioned previously, the 9th Tortonian horizon is made up of one main part and nine fault blocks. These blocks are located north of the main block and are isolated (there is no hydraulic communication) from each other.

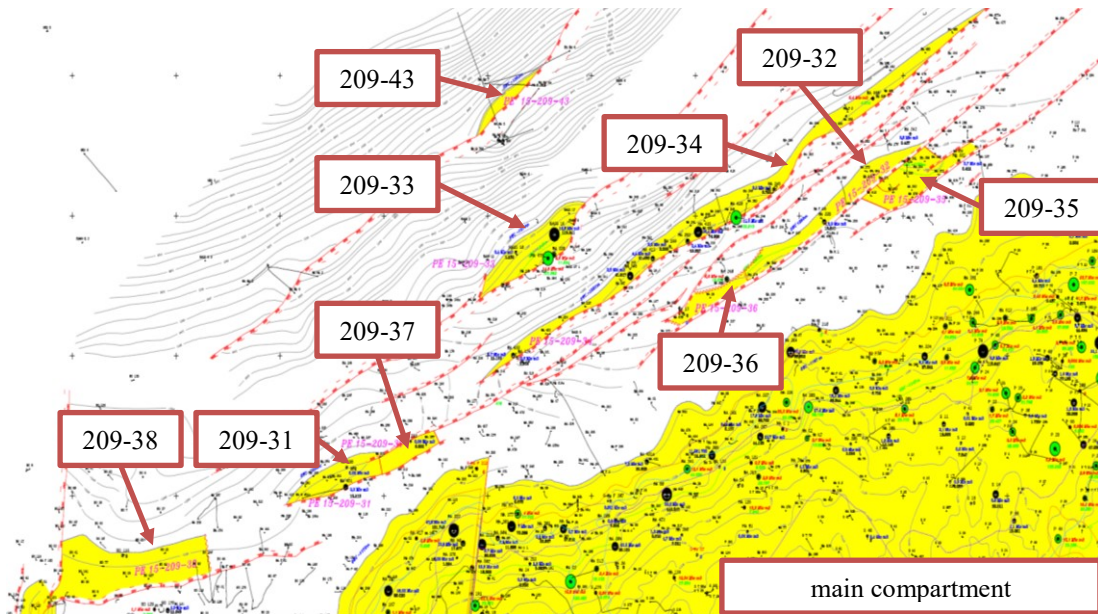


Figure 16: Current map of the northern fault blocks of the 9th TH

A first pre-screening step was carried out to identify a small set of production units that is best suited for detailed analogous investigations. Due to the fact that all the fault blocks are members of the same geological horizon, the first six categories suggested by PRMS identify each fault block as suitable analogous to 209-33. For that reason, only the production history can be taken as a proper distinguishing feature. Based on that, only production units that are already depleted or units with a sufficiently long history (close to the end of the production cycle and well characterized in terms of OIIP and remaining reserves) were taken into account for further investigations. Fault blocks that have not been exploited yet and fault blocks with a rather short history (higher uncertainty for both OIIP and reserves) are not considered as representative analogies with respect to the possible ultimate recovery factor. After this selection only three production units were left.

As seen before the 8th Tortonian horizon is the overlying layer of the 9th Tortonian horizon and it can be considered as analogous to the 9th TH as well. In Figure 17 it is seen that the general structure is similar to that of the 9th Tortonian. Again one main compartment and nine fault blocks are located in the north-west of this main part. Applying the same pre-screening procedure as to the 9th Tortonian horizon resulted in one additional analogous reservoir.

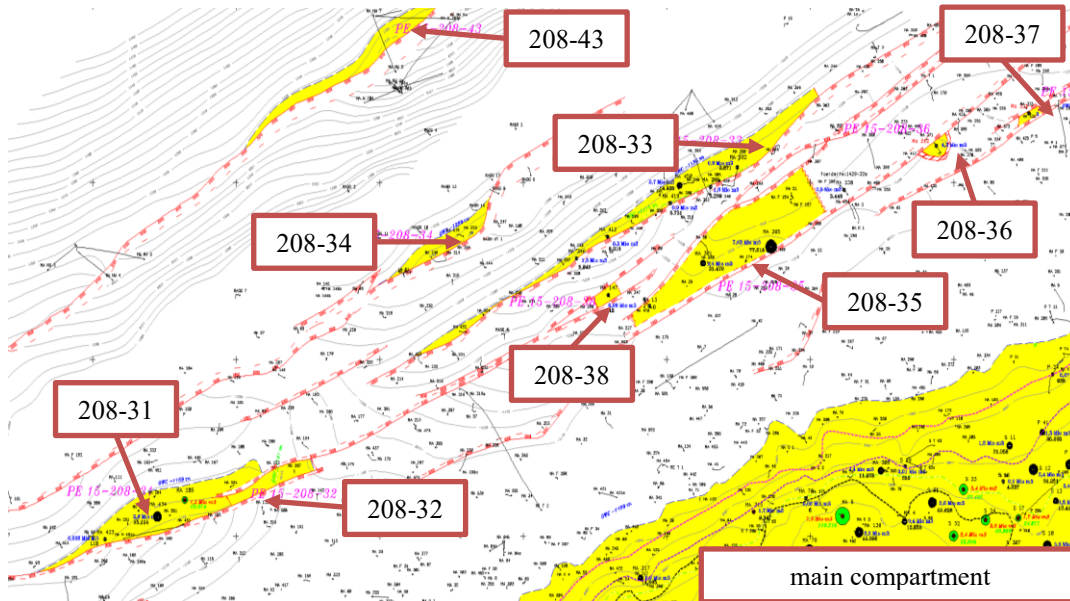


Figure 17: Current map of the north-western fault blocks of the 8th TH

Table 3 shows the parameters that have been used for comparing the selected production units with 209-33. The color-code used in the first column (the legend is given in Table 2) indicates to which group of the PRMS-classification the respective property belongs.

As mentioned before, all of the production units either have a sufficiently long production history or are already depleted. So far, no improved recovery methods have been implemented in any of these compartments. All of them exhibit a water cut of more than 95 % and a pressure decline of less than 23 % (without any artificial pressure support) during production. This is assumed to be a distinct indication for the presence of a strong aquifer drive. Dividing the size of the individual accumulations by the respective number of wells shows that the area per well is in the same order of magnitude for all the units. The main problem with this parameter is related to the actual well-to-well spacing and the shape of the units. For example, the production units 209-32 and 209-34 are very elongated and narrow fault blocks with a rather high inter-well-spacing and a comparably short distance to the reservoir boundary. In such a case, the interaction between two neighbouring wells is rather unlikely, but boundary effects possibly influence the production performance. An additional issue with 209-34 is that this unit is developed from one location at the southern end, one location in the middle and one location at the northern end. The well-to-well distance calculated for 209-34 refers to these three locations and the distance between the individual spots is not taken into account. For 209-33 it is already known that the majority of the production comes from only two of the five wells. Additionally, Matzen 229, which is located in the vicinity of the top producers Matzen 476 and Raggendorf 16, shows a rather poor performance as well. As seen in Table 3, the petrophysical properties as well as the fluid properties are very similar in all of the selected production units. Moreover, most of the properties which are related to reservoir conditions (e.g. pressure and temperature)

Table 2: Legend for the comparison of analogous fields







	Geological Conditions		Fluid Types
	Petrophysical Conditions		Driving Mechanism
	Reservoir Conditions		Development Strategies

Table 3: Comparison of selected analogous PUs to 209-33

	Unit	Case	PU 209-32	PU 209-34	PU 209-37	PU 208-33	PU 209-33
start	date	-	18.12.1984	29.05.1967	27.03.1995	04.05.1972	09.10.1963
end	date	-	-	-	23.07.1999	10.11.2014	-
prod. strategy	-	-	prim. rec.	prim. rec.	prim. rec.	prim. rec.	prim. rec.
avg. production WC	%	-	>95	>95	>95	>95%	>90
pressure change	%	-	14%	23%	N/A	17%	21%
aquifer	-	-	strong	strong	strong	strong	strong
Number of wells	-	-	4	12	1	6	5
area per well	m ²	-	52,500	42,833	73,000	56,667	53,600
avg. well spacing	m ²	-	693	223	-	250	165
OIIP	tonnes	low	107,340	400,000	2,000	100,000	450,000
	tonnes	best	140,000	425,000	3,000	125,000	500,000
	tonnes	high	160,000	453,600	32,000	158,400	550,000
cum. prod.	tonnes	-	44,663	173,215	803	36,555	263,674
	tonnes	low	47,599	174,645	803	36,555	281,951
	tonnes	best	48,696	176,298	803	36,555	285,501
Total Reserves	tonnes	high	54,099	176,898	803	36,555	290,500
	fraction	low	0.44	0.44	0.40	0.37	0.63
	fraction	best	0.35	0.41	0.27	0.29	0.57
URF	fraction	high	0.34	0.39	0.03	0.23	0.53
	fraction	high	0.34	0.39	0.03	0.23	0.53
P_{init}	barg	-	140.5	136.7	133.4	132.4	139.7
P_{actual}	barg	-	121	105	N/A	110	110
T_{res}	°C	-	55	53.8	53	53	54.7
OWC_{SSinit}	m	-	1260	1231	1189	1185	1274
Φ	fraction	-	0.25	0.25	0.25	0.25	0.26
S_{wi}	fraction	-	0.334	0.334	0.334	0.33	0.21
B_o	m ³ /m ³ (V _n)	-	1.100	1.101	1.163	1.097	1.098
B_g	m ³ /m ³ (V _n)	-	0.0076	-	-	0.008	0.007
R_s	m ³ (V _n)/m ³ (V _n)	-	35	37	36.2	35.2	35
ρ_o @ 20°C	kg/m ³	-	905	919	905	924	927

do not exhibit significant variations. Only the size of the individual accumulations varies tremendously.

As shown in Table 3, the low estimates for reserves and OIIP exhibit the highest respective ultimate recovery factors. Therefore these scenarios are used to calculate the minimum amount of OIIP required to support the currently expected reserves of 209-33. In Figure 18 it can clearly be seen that the average achievable URF in these fault blocks is approximately 41 % and independent of the size of the reservoir. The current RF of about 60 % and an expected URF of 63 % in 209-33 are a good indication that the current estimates for the OIIP do not represent the true extent of the accumulation. A different representation that emphasizes this observation is shown in chapter A.2.

The minimum amount of OIIP that is expected in 209-33 is:

$$OIIP_{min} = \frac{Reserves_{low}}{URF_{avg}} = \frac{281,951}{0.41} = 687,685 \text{ tonnes}$$

Having an RF close to the URF suggests that the PU is already close to the end of its lifetime. On the other hand, Matzen 145 has been producing 10 tonnes of oil per day at a water cut of only 13 % for more than 2 years up to now. As mentioned before, this is an unusually good performance in a reservoir with a current field water cut of 90 %. This actually emphasizes that 209-33 is still not close to the end of its lifetime and that the above calculated OIIP only acts as a lower limit for further calculations.

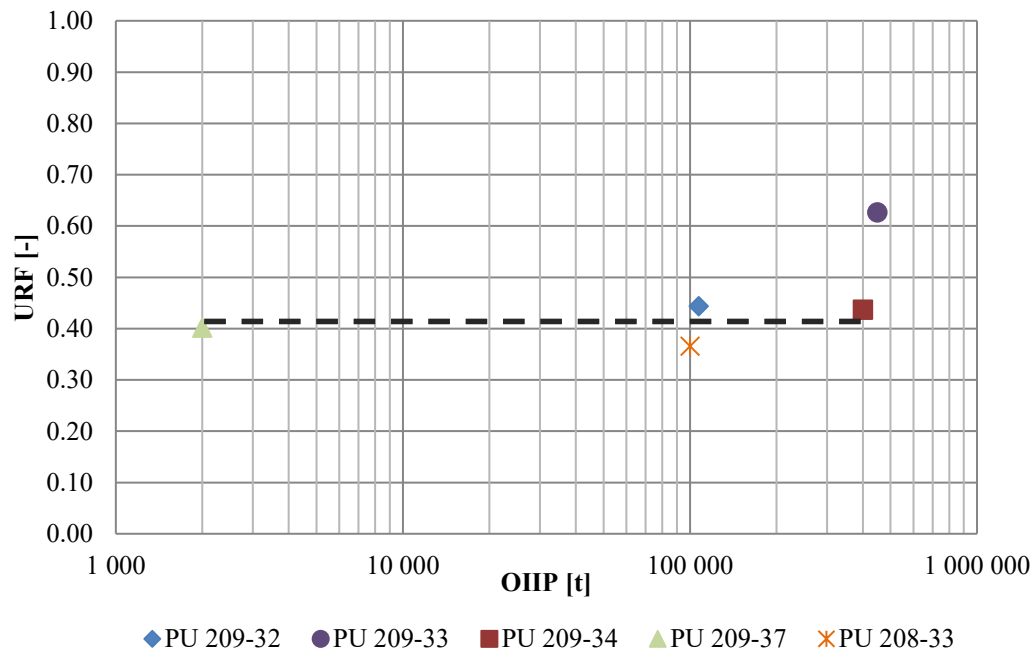


Figure 18: URF vs. OIIP

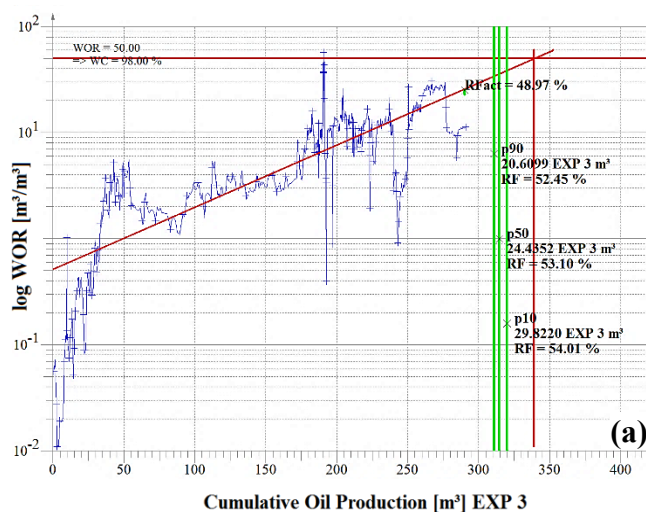
3.3 Resource & Reserve Estimation

In the course of this thesis, the estimation of resources and reserves was carried out based on three different approaches:

- an analytic approach using decline curve analysis and water oil ratio plots
- an analytic material balance approach using Petex MBAL
- a volumetric approach using Petrel (shown in chapter 3.4).

3.3.1 Analytic Approach

Two different analytic methods were used to evaluate the expected reserves or rather the expected ultimate recovery. The first one utilized a semi-logarithmic cross plot of the water oil ratio versus the cumulative oil production. An exponential trend line (the underlying equation is shown in Figure 19), portrayed as a straight line in the semi-log scaling, was used to extrapolate the historical behaviour to a pre-specified shut-in water cut. The cumulative production at this water cut was equal to the expected ultimate recovery and the remaining reserves were calculated as the difference between the expected ultimate recovery and current cumulative production. The main challenge for a proper application of this method was that a time-span that was believed to be representative for the future behaviour of the production unit had to be defined. The impact of the selected period can be seen in Figure 19. The green lines indicate the currently expected UR (P10, P50 and P90 scenarios) and a water cut of 98 % was used as the endpoint for the extrapolation. In the upper graph the entire history of the production unit 209-33 is taken into account. This resulted in expected total reserves of 314,680 tonnes (339,460 sm³) of oil. The other extreme, where only the most recent performance (since MA 145 was perforated) is included, is shown in Figure 19 (b). It is obvious that the reduction in WOR postpones the abandonment of the production unit and simultaneously leads to an increased reserve estimate of 372,530 tonnes (401,866 sm³). The corresponding difference in EUR is more than 57,000 tonnes (62,000 sm³) of oil.



General Trend Line Equation

$$WOR = a * e^{b * N_p}$$

N_p ... cum. Oil production

a, b ... fitting parameters

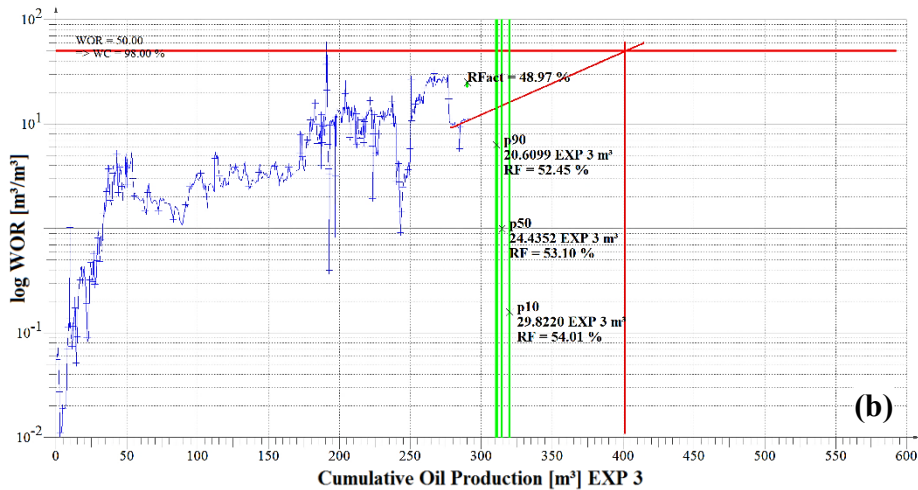
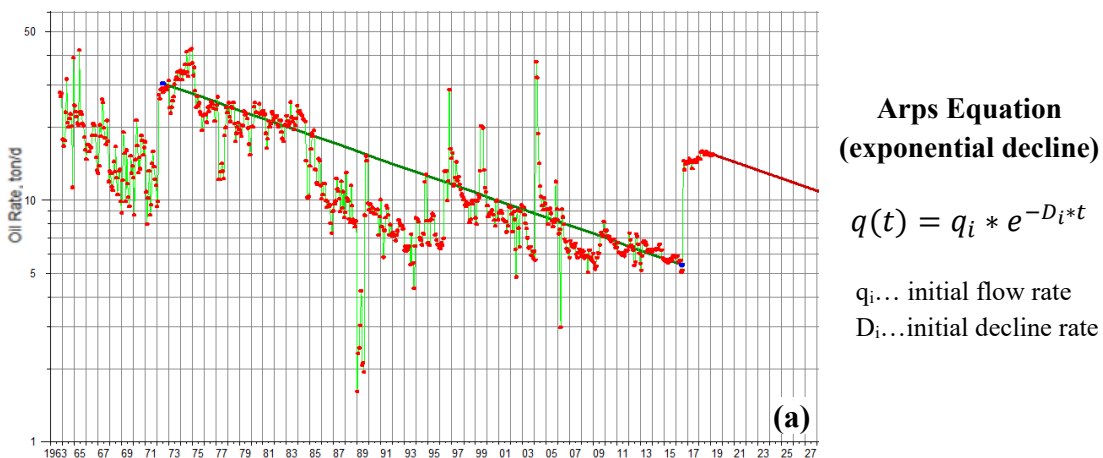


Figure 19: Reserve prediction for entire field life (a) and since Matzen 145 (b)

The second analytic method that was used is a decline curve analysis based on Arps exponential decline model. In order to make the results comparable with the ones derived from the WOR versus cumulative oil production plot, again a WC of 98 % was used as the abandonment limit. At the current gross production rate of 200 m³ per day, this is equivalent to a final oil rate of approximately 3.6 tonnes per day. Again, the main issue was the selection of a representative period that can be used to extrapolate the oil production decline. As seen in Figure 20, there is no decline observed since Matzen 145 was perforated. Consequently, this period cannot be taken into account for the DCA. Two scenarios were selected, one representing the long-term mean decline since 1973 and the second representing a more recent short-term decline. Based on the long-term trend, additional reserves of 116,500 tonnes and a respective EUR of 380,186 tonnes (410,125 sm³) were predicted. The short-term decline was investigated starting from the end of 2009, when gross production was raised to the current level, and ending when Matzen 145 was put into production. In this case remaining reserves of 67,651 tonnes and an EUR of 331,337 tonnes (357,429 sm³) of oil were estimated.



**Arps Equation
(exponential decline)**

$$q(t) = q_i * e^{-D_i*t}$$

q_i... initial flow rate

D_i...initial decline rate

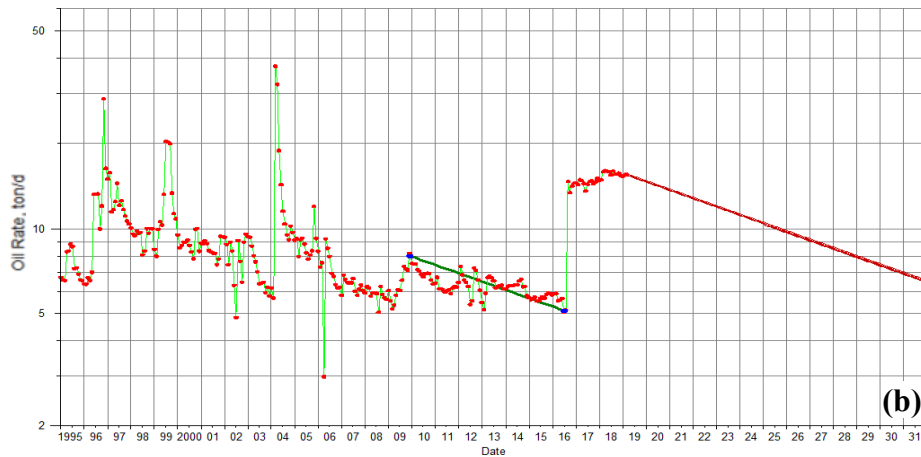


Figure 20: Reserve prediction - long term trend (a) and before Matzen 145 (b)

Using this method, the calculated difference in EUR was more than 48,000 tonnes (51,000 sm³). Comparing the results of these two approaches it can be seen that they yielded similar results.

An interesting aspect was that all of the selected scenarios resulted in remaining reserves that exceeded the current estimates. Each individual case predicted an EUR of more than 310,000 tonnes of oil, no matter if the entire field life or only the more recent history was taken into account. Comparing this value with the currently used estimates for OIIP, this leads to a:

- URF > 69 % for the low estimate (OIIP = 450,000 tonnes).
- URF > 62 % for the best estimate (OIIP = 500,000 tonnes).
- URF > 56 % for the high estimate (OIIP = 550,000 tonnes).

To sum it up, it can clearly be seen that the analysis of the dynamic data leads to high remaining reserves and consequently supports the assumption that the currently used OIIP is too low. Based on the URF determined from analogous field investigation the OIIP should be even higher than the previously estimated value of 687,000 tonnes. Due to the sensitivity of these methods with respect to the selected representative period, the minimum oil in place was kept at 687,000 tonnes for further calculations.

3.3.2 Material Balance Approach

In order to verify the order of magnitude of the results achieved from analytic investigations a simple material balance simulation for 209-33 was conducted. The main goal was to identify a range for the OIIP that is in agreement with the previously expected reserves. The individual wellbore production histories, including produced fluid volumes and static pressure measurements were used as a starting point for the simulation. A major issue related to this material balance simulation was that it could hardly distinguish between the effect of a high OIIP and a strong aquifer. This means that a wide range of OIIP scenarios can be matched by matching the aquifer size and its connectivity to the reservoir.

To simulate this reservoir a multi-tank model was built. One tank represented the actual hydrocarbon reservoir and the second was used as an aquifer (similar to the numerical aquifer used in other simulations). Generally, Petex MBAL provides the possibility to use analytical aquifers like the Carter-Tracy or Hurst-van-Everdingen Modified model for simulation. Nevertheless, an initially conducted sensitivity study showed that the modelled pressure response using the numerical aquifer lead to the most reasonable representation of the observed data. Another advantage was that the number of matching parameters was reduced to only two, namely the size of the aquifer (water in place) and its connection to the reservoir (transmissibility).

Due to the fact that only five wells are located in this unit, a well-by-well production allocation strategy was selected. This means that the production history (produced volumes of oil, gas and water) of each well was imported and subsequently allocated to the corresponding reservoir.

In reality, the aquifer is at least partially located in the same geological horizon as the oil and gas reservoir. In order to reproduce this setting the same average values for temperature, pressure and porosity were assigned to both of the tanks.

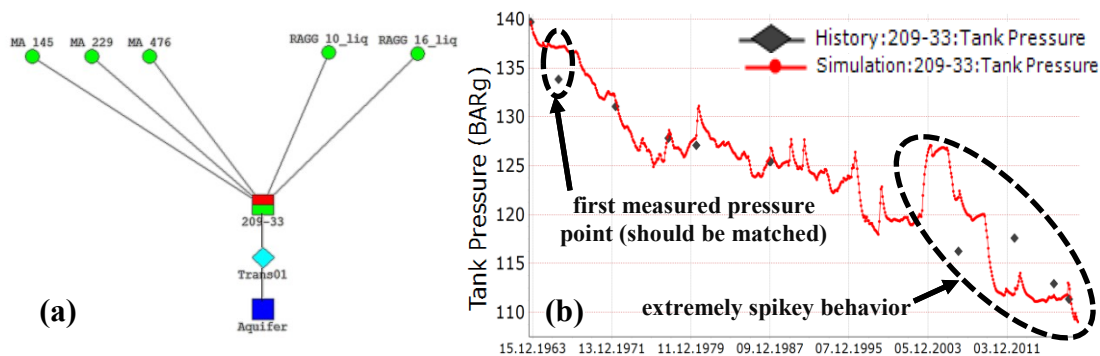


Figure 21: Model setup (a) and initial pressure history match (b)

During the initial sensitivity study mainly two different scenarios were observed for the calculated pressure response. Either, only the first data point and none of the following ones was matched or the second trend could be captured better, but the first data point was far off. The second scenario is shown in Figure 21. As can be seen, the late trend exhibits an extremely spikey behaviour which is interpreted as a numerical artefact rather than a realistic representation of the reservoir pressure. This spikey behaviour as well as the two d scenarios were observed independently of the tested aquifer model. Due to the fact that the first reliable pressure measurement (which should be matched) is exactly this first point it was concluded that the reported initial pressure might not be correct. As mentioned, production from the well Raggendorf 16 started with an eruptive flowing phase. The perforated interval is located in a TVD of 1454 m (in the middle of the perforations). Assuming that if the tubing is filled with oil, the corresponding hydrostatic pressure is about 132.4 barg. To allow for natural flow, the

actual reservoir pressure must be higher than the hydrostatic one. The best fit, capturing the full trend and exhibiting fewer spikes, (shown in Figure 22) is achieved with a p_{init} of 135 barg.

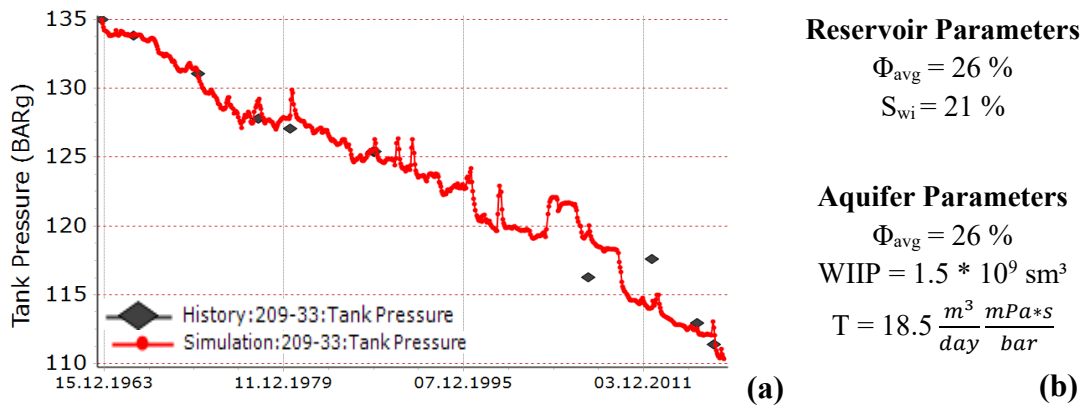


Figure 22: Pressure match with corrected p_{init} (a) and important parameters (b)

After selecting the aquifer model and correcting the initial pressure, several history matching runs were conducted to limit the possible range for the OIIP. First the lower limit of the OIIP was evaluated. Running the simulation with an OIIP of 450,000 tonnes (which represents the current low estimate) did not result in a proper match. The main problem was that the associated and free gas could not support the current cumulative gas production. For the best (500,000 tonnes OIIP) as well as for the highest estimate (550,000 tonnes OIIP), a history match could be achieved. Next, the minimum OIIP derived from analogous field investigation as well as the two extreme scenarios from analytic reserve estimation were simulated. (**Note:** To convert reserves to OIIP, the average URF calculated in chapter 3.2 was used.) Due to the strong aquifer support - according to the simulation more than 95 % of the total driving energy comes from the aquifer - an upper limit could not be identified by material balance. Even with an OIIP three times higher than the current high case and a smaller aquifer, a match was achieved. The simulation was stopped at that point because of a lack of geological plausibility. The corresponding aquifer sizes for the different scenarios varied between $1.453 * 10^9 \text{ sm}^3$ for the lowest and $1.377 * 10^9 \text{ sm}^3$ for the highest OIIP case.

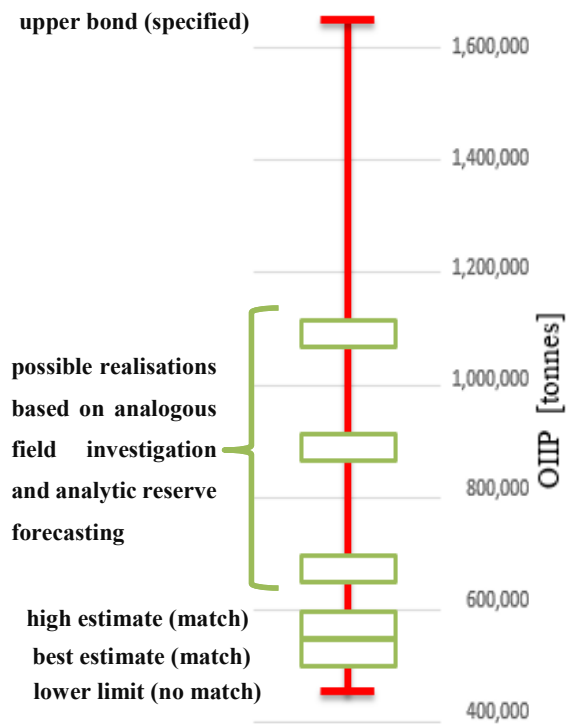


Figure 23: OIIP scenarios

3.4 Model Setup and Initialization

Due to the fact, that the major south-eastern fault exhibits a significant offset, subjacent and adjacent layers that possibly overlap with the 9th TH were part of the starting model as well. These neighbouring layers include the 10th TH below and the 7th and 8th TH on top of the main target. In order to minimize the simulation run-time, only the currently interpreted extent of the structure was used for the initialization as well as for the start of the history matching process. This means that all the cells - the used grid block size was 15*15*1 meters - south of the major fault, all neighbouring horizons and parts of the fully water saturated cells (clearly below OWC) were not considered in the simulation. So the number of active cells could be reduced from $1.12 \cdot 10^6$ to only 70,000. Any areal extension or overlap with other horizons was included later on when the history matching clearly indicated the need for that.

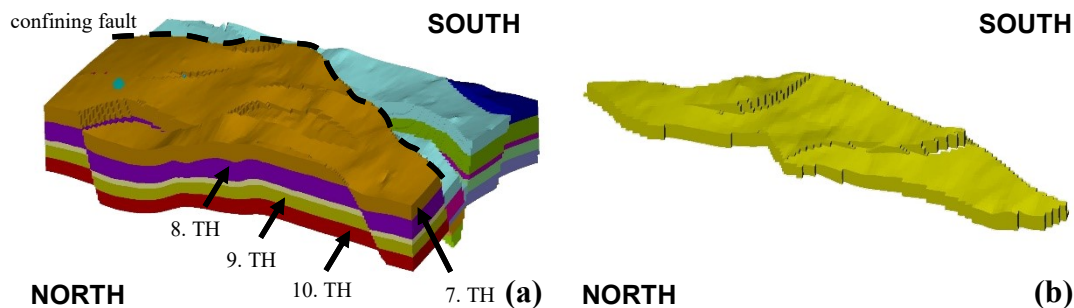


Figure 24: Entire model (a) and initial simulation domain (b)

3.4.1 Fluid Model

The main issue during the fluid modelling was that no detailed PVT- measurements were conducted for this production unit. As shown in chapter 3.2, fluid fill in 209-33 can be considered analogous to other production units in the same horizon. Therefore, the fluid model built for a comprehensive reservoir simulation study of the 9th TH (conducted in 2017) was used for this study as well. The implemented PVT functions are shown in chapter A.3.

3.4.2 Rock Physics

The measured rock data is limited to an average porosity of 26 % and an average permeability of 800 mD. No relative permeability and capillary pressure curves for the production unit were available at the start of the simulation. As described in chapter 2.2.2, the 9th TH consists of several sublayers. The rock physics functions for five layers were modelled in the previously mentioned study and were used for this simulation as well (see chapter A.4). As the presence and orientation of the individual layers cannot easily be identified, no rock-typing is included in the model. Consequently, the allocation of the capillary pressure curves and the corresponding relative permeability functions were carried out based on the absolute porosity model. A quality check of the allocation was done using the interpretation of the historical log data from the individual wells, but the allocation's inherent uncertainty should be kept in mind.

3.4.3 Initialization

The main goal of the initialization process was to select the proper rock physics functions so that the initial fluid saturations could be reproduced as closely as possible and to ensure that the reservoir is in equilibrium (quality check is shown in chapter A.5) before production starts. The investigated scenarios are described as follows:

- **Scenario (1):** The unit was assumed to be a homogenous and continuous sand layer that can be described by one single set of rock physics functions.
- **Scenario (2):** The unit was separated into two subunits. One was assumed to be the main oil bearing sand layer with low initial water saturation and the other one was a layer with a low porosity, low permeability and a varying clay content. Based on the log data, a porosity of 12 % was selected as a proper threshold.
- **Scenario (3):** The unit was separated into three sublayers. One represented the main oil bearing sand layer, the second one was also a sand layer with lower porosity and higher initial water saturation, and the third once again a clay rich rock. The chosen porosity thresholds were 8 % and 23 %.

Figure 25 shows the final results of the different initialization scenarios for the two most important producers. (**Note:** These results already use only those three rock physics functions which give the closest match to the observed data. The used set of functions for each of these scenarios is shown in chapter A.4) Comparing the simulated initial fluid distribution with the original log interpretation (indicated by the red dotted lines), it can be seen that the assumption of a continuous sand body results in a too high initial water saturation. The second scenario already lead to a better match, but still there were zones where the calculated water saturation was more than twice as high as the measured one (indicated in Figure 25). In order to reduce these extreme mismatches, a distinction between intermediate to low porosity sand and clay rich, low porosity sand was introduced. Results from the other wellbores supported the decision

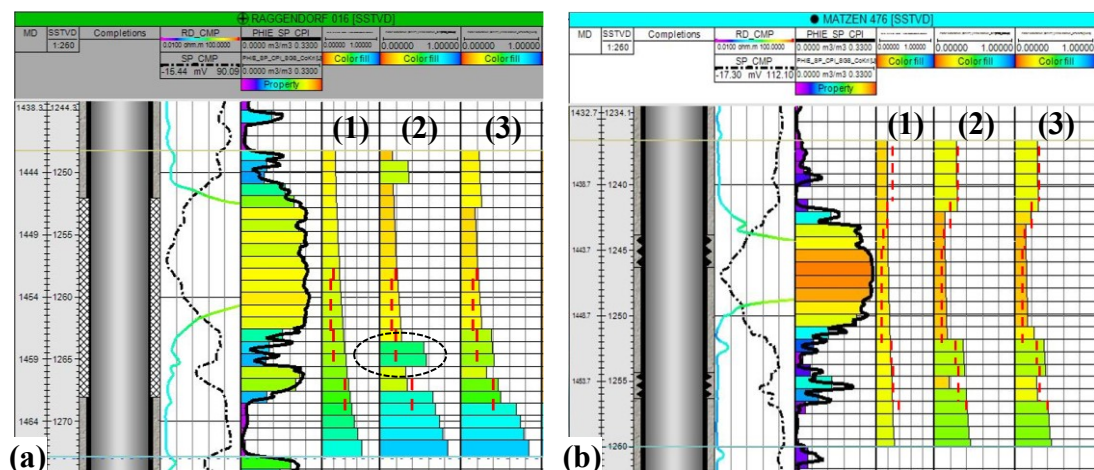


Figure 25: S_w for different initialization scenarios along RAGG 16 (a) & MA 476 (b)

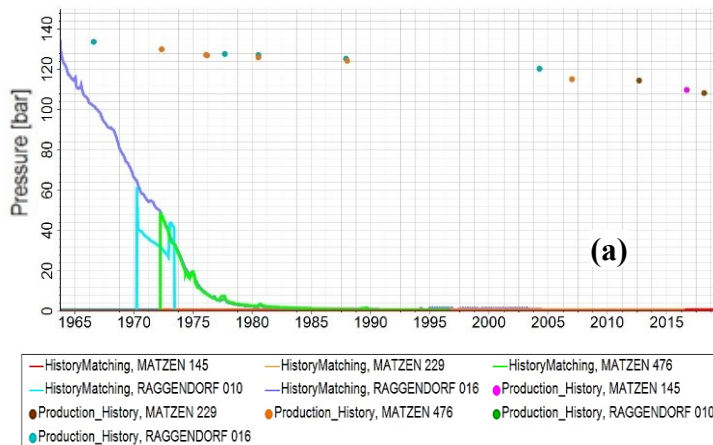
to use three sets of rock physics functions for the subsequent simulation. The calculated HC volumes for the different initialization strategies are shown in Table 4. It shows that using a volumetric approach leads to oil volumes in the range of the current low and best estimate. This can be taken as an additional validation for proper initialization, because the model (using the current interpretation) actually contains the respective estimated oil volumes. Thus, saturations not only fit on a wellbore scale, but also properly represent the fluid distribution on a field scale.

Table 4: Hydrocarbon volumes for different initialization scenarios

Name	OIP [t]	Free GIIP [sm ³]	Dissolved GIIP [sm ³]
Scenario 1	449,738	184,024	18,274,880
Scenario 2	493,395	183,304	20,048,864
Scenario 3	482,649	181,801	19,612,187

3.5 History Matching

The first step of the history matching procedure was to match the static reservoir pressure recordings. Analogous field investigation as well as the material balance simulation indicated the need and the presence of a strong aquifer drive. This observation was once more validated when the initial, reduced Petrel model was simulated without an aquifer. As seen in Figure 26, pressure declined very fast and approached zero in 1985. In order to maintain the pressure at the observed level, a numerical edge water drive was implemented (using the Eclipse keywords



AQUNUM, AQUCON and AQU DIMS). This method offers good control and a clear understanding of the reservoir rock properties (permeability and porosity), the volume of the aquifer and its connection (area and water flowing direction) to the reservoir.

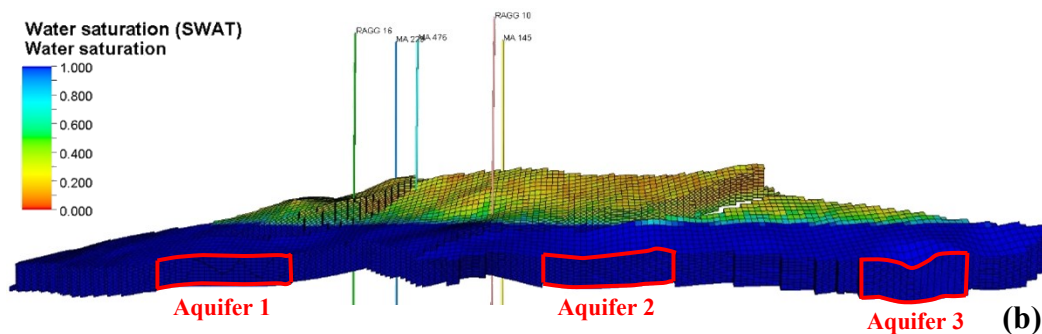


Figure 26: Pressure decline without aquifer (a) & aquifer locations (b)

The red squares in Figure 26 represent the areas of contact between the aquifer and the reservoir. In order to have a homogenous pressure distribution in the reservoir three approximately equally sized aquifers were placed along the north-western boundary of the simulation area. A pressure decline of only 20 % over more than 50 years requires strong natural water influx. To ensure that, aquifer porosity was defined corresponding to the high values observed in the main oil bearing sand layer. Furthermore, a sensitivity study (k varying from 500 mD to 2000 mD) showed that the quality of the history match was independent of the aquifer permeability. Therefore, the average production unit permeability was assigned to the aquifer as well. The exact specifications are shown in Table 5.

Table 5: Aquifer specifications

Name	Volume [sm ³]	Porosity [-]	Permeability [mD]
Aquifer 1	3*10 ⁹	0.33	800
Aquifer 2	3*10 ⁹	0.33	800
Aquifer 3	2*10 ⁹	0.33	800

Figure 27 shows the static reservoir pressure match with aquifer support. RAGG 16 as well as MA 229 exhibit very high accordance between the observed and simulated data. RAGG 10 could not be assessed, as no pressure measurements were available. Simulation results for MA 476 slightly overestimated the measured reservoir pressure and an increasing trend for this gap can be observed. As this mismatch is less than 5 %, it can still be considered as a good match.

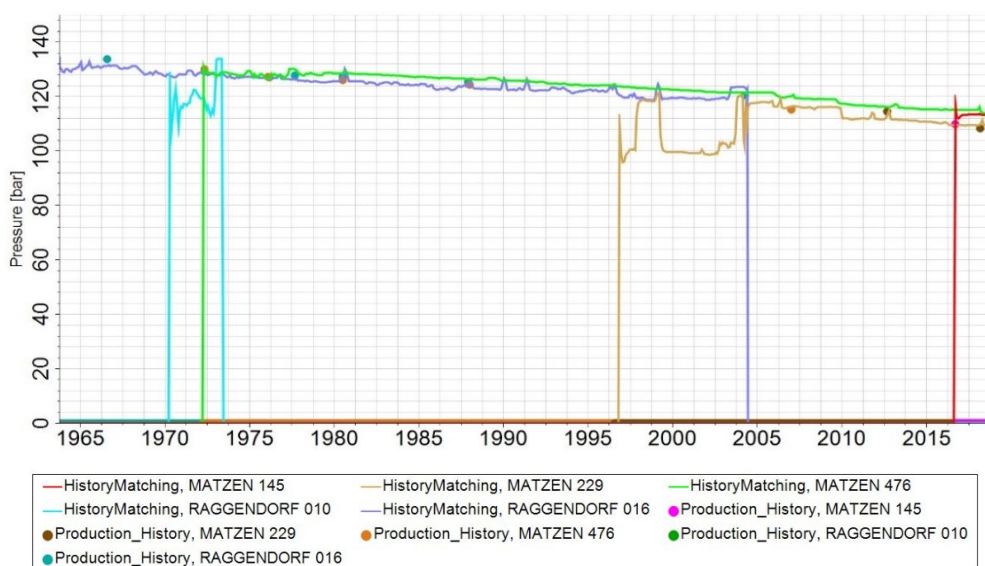


Figure 27: Static pressure history match

The next step was to check if the model could deliver the historically produced liquid volumes. For this step, water, oil and gas were not considered separately, but the corresponding reservoir volume of these fluids was matched. This was done to verify the permeability model. Both porosity and permeability distributions were modelled using a collocated Kriging approach. As can be seen in Figure 28, monthly liquid production rates for the producers are matched very

well. Only a few outliers (indicated in red) are not reproduced. After matching pressure and liquid volumes it can be assumed that the absolute permeability model is a good representation of the real reservoir.

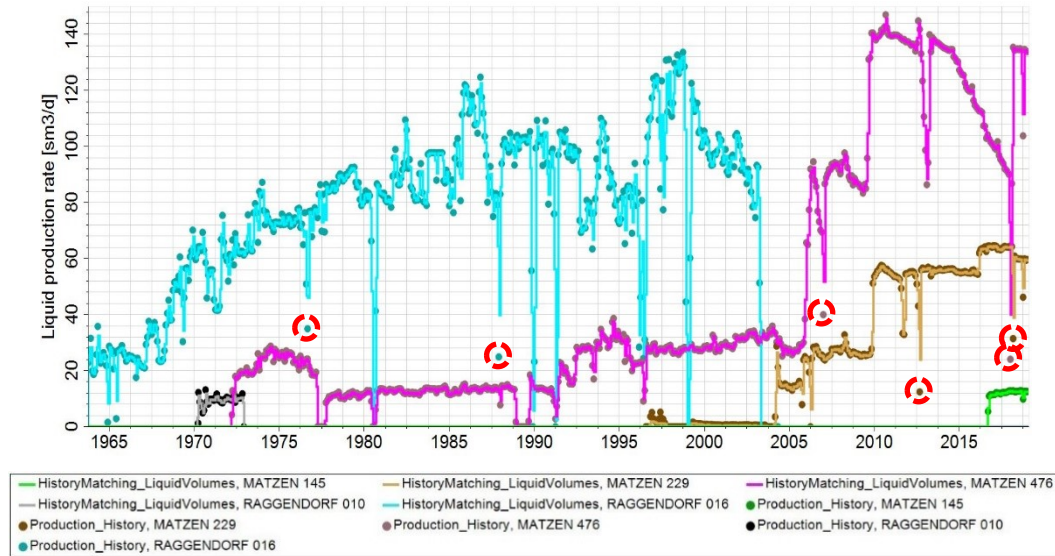


Figure 28: Liquid production rate history match

Next, the individual fluid volumes had to be matched. As the production unit 209-33 is an oil reservoir, cumulative oil production and water cut were used primarily to match the individual fluid volumes. The results are shown in Figure 29. The only well that came close to its actual production was Matzen 229. All the other wells did not reach cumulative oil production. The main issues were the huge discrepancies (in terms of absolute numbers) of Raggendorf 16 and Matzen 476. The first one reached a simulated cumulative production of 59,000 tonnes, which was about 49 % less than the true production. Having a calculated production of only 12,000

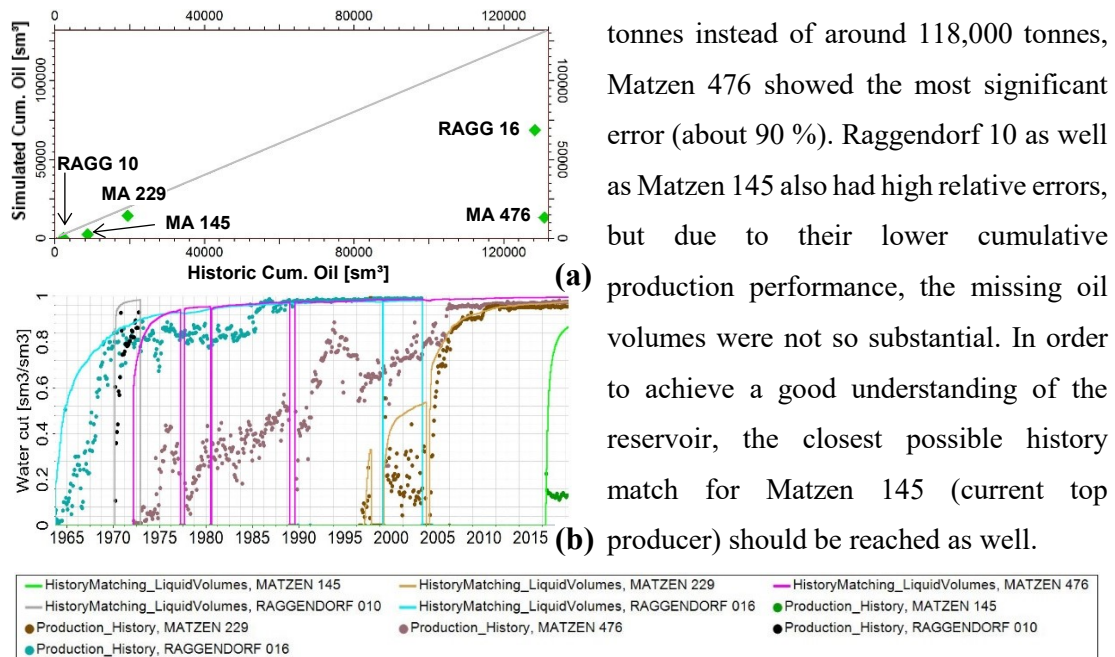


Figure 29: Historical vs. simulated cum. oil (a) and water cut (b)

tonnes instead of around 118,000 tonnes, Matzen 476 showed the most significant error (about 90 %). Raggendorf 10 as well as Matzen 145 also had high relative errors, but due to their lower cumulative production performance, the missing oil volumes were not so substantial. In order to achieve a good understanding of the reservoir, the closest possible history match for Matzen 145 (current top producer) should be reached as well.

Furthermore, it can clearly be seen that all the wells watered out considerably faster than in reality. This could be caused by the shape of the relative permeability curves (water started flowing very early) or by a too low OIIP. As RAGG 10 was drilled through the OWC and the change in pore fluid is clearly seen on the log-data (resistivity log), this depth is well known and not a matching parameter. Thus, lowering the OWC to increase the OIIP was not an option during history matching. In order to check if the bulk volume of the interpreted structure was even able to support the produced volumes two changes were made:

- Strongly water-wet conditions were established in the intermediate and high porosity sands to delay the water breakthrough and consequently keep the oil mobile for a longer period of time. (Curves are shown in chapter A.4)
- To increase the HC volumes, capillary pressure was set to zero and consequently the transition zone thickness was zero, too. Under these conditions, the OIIP changed to 601,363 tonnes. This was already higher than the current high estimate, but still lower than the minimum OIIP calculated from the analogous field investigation.

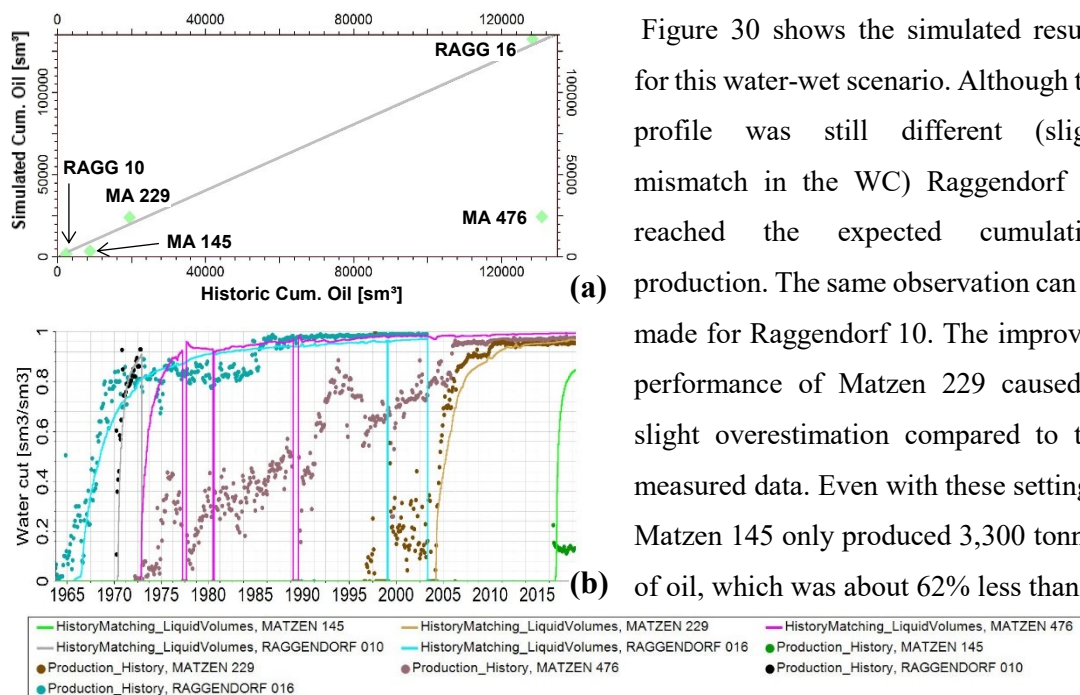


Figure 30 shows the simulated results for this water-wet scenario. Although the profile was still different (slight mismatch in the WC) Raggendorf 16 reached the expected cumulative production. The same observation can be made for Raggendorf 10. The improved performance of Matzen 229 caused a slight overestimation compared to the measured data. Even with these settings, Matzen 145 only produced 3,300 tonnes of oil, which was about 62% less than

Figure 30: Historical vs. simulated cum. oil (a) and water cut (b) with WW conditions

actually expected and the WC was also more than six times higher as it should have been. The main issue was still related to MA 476. Even though water breakthrough could be delayed and production rose to 22,000 tonnes it showed a shortfall of around 96,000 tonnes of oil.

As seen in Figure 31, the sand layer was interpreted to be discontinuous along this north-south trending internal fault (indicated by the red dotted line). RAGG 16 and MA 229 are both located east of this fault and produce from the small compartment there. In the final state it is clearly visible that RAGG 16 (already watered out) is located in an area with a water saturation of

approximately 80 %. The water saturation in the vicinity of the structurally higher lying MA 229, was around 70 % and in accordance with the expected high WC of 95 %. Additionally, a preferential or accelerated movement of water along this discontinuity (indicated by the red arrow) was observed in the western part, where MA 476 is located. This movement is a possible explanation for the very early water breakthrough in MA 476 and afterwards in MA 145.

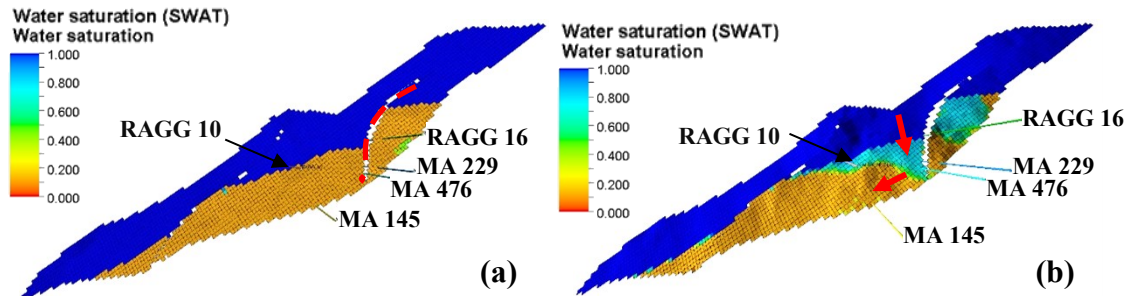


Figure 31: Water distribution initial state (a) and after 15 years (b)

To solve the previously described issues the structural interpretation was updated. First, the following changes were made:

- The continuity of the sand layer across this internal fault to reduce or even prevent the accelerated movement of water towards MA 476 was ensured.
- The compartment of the 8th Tortonian horizon, which is located south of the major confining fault and possibly in communication with 209-33, was included. The main purpose was to check if this could help to reach cumulative production in RAGG 16, MA 229 and MA 476 without using the artificial set of rock physics functions.

The main goal of this update was to implement the above-mentioned changes without changing the overall structural configuration of the first model significantly. The updated structural setting is shown below. Looking at the model it can be seen that the fault was replaced by a steeply dipping flank and the structural depression west of the previous fault was still retained. By doing that, the size of the reservoir only increased slightly compared to the first model. This allowed assessing the effect of having a continuous geological body - instead of a very low permeable fault - on the directional flow behaviour. The main volumetric change is related to the possible overlap with the 8th Tortonian horizon.

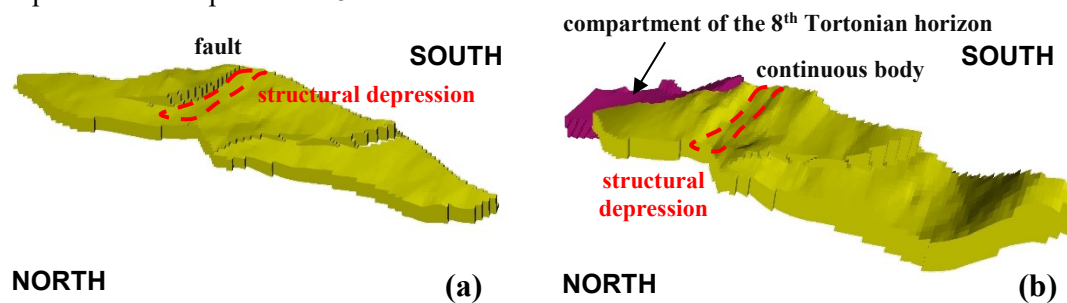


Figure 32: Initial (a) and updated (b) structural model

As a first step, only the 9th Tortonian horizon was simulated using the artificial water-wet relative permeability functions. A comparison of the historical and simulated cumulative oil production is shown in Figure 33 (a). The main improvements are:

- This new model for Matzen 476 and Raggendorf 16 reproduced the overall observed production behaviour. Previously, Raggendorf 16 matched the oil production very closely, but the error for Matzen 476 was more than 80 %. Although this model still exhibits a significant mismatch (Matzen 476 still shows a shortfall of 26,000 tonnes and Raggendorf 16 of around 15,000 tonnes) between the simulated and historical cumulative production, the deviation of the two top producers is within a similar range now.
- The shape of the water front (shown in Figure 33 (b)) is more uniform compared to the previous model (shown in Figure 31). This steep dipping flank still leads to a preferential flow of water along the flank's strike direction and consequently causes an early breakthrough in Matzen 476. Even under these conditions, the historical behaviour of the production unit is reflected more closely.

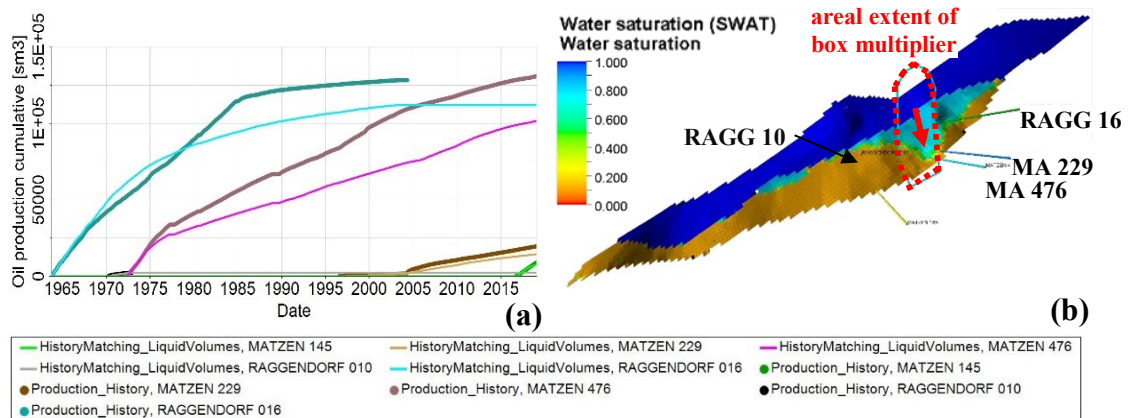


Figure 33: Cum. oil production profiles (a) and water distribution after 15 years (b)

Next, the compartment of the 8th Tortonian horizon was included into the simulation model. Using a fault transmissibility multiplier of one, unrestricted communication (as if there was no

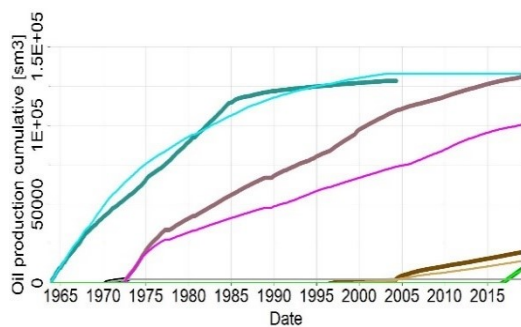


Figure 34: Cum. oil production profiles including the compartment of the 8th TH

fault) between these two compartments was established. The main goal was to check if the missing oil volumes could be delivered via this flow path. As seen in Figure 34 (**Note:** The legend shown in Figure 33 is also valid for Figure 34), the 8th Tortonian horizon solely contributes to the production of Raggendorf 16 and no influence on the nearby wells Matzen 229 and Matzen 476 is discernible. As

a result, the respective relative error related to Matzen 476 is again considerably higher than the one in Raggendorf 16. As the sand layer is rather homogenous, it can be assumed that the error of the wellbores should be within a similar range and therefore these results might be interpreted as a first indication that the major confining fault is a seal. Nevertheless, a valid judgement is only possible based on a final structural model of the 9th Tortonian horizon.

Next, so-called box multipliers were used to check if permeability and porosity alterations could help to reach the required production volumes. Box multipliers distort the initial property distribution derived from static geological modelling. In order to keep this distortion to a minimum, the area of influence was chosen to be as small as possible. For this simulation study the area of influence was defined corresponding to the highly permeable, preferred fluid flow path along the steeply dipping flank (shown in Figure 33 (b)). The aim was to ensure that the influence was focused on Matzen 476 and that the other wells remained unchanged. The two investigated scenarios were:

- a reduction of the absolute permeability to stabilize the inflowing waterfront, to delay the water production in Matzen 476 and, consequently, to increase the oil recovery from the previously bypassed zones
- a rise in effective porosity to increase the OIIP in this area. Using the same withdrawal rates, higher recoverable oil volumes also delayed the breakthrough and allow for higher cumulative production from this wellbore.

The results for both scenarios are shown in Figure 35. The red circles refer to the scenario with an altered permeability model and the blue diamonds to the case of increased porosity. As can be seen, the simulation and the historic data for Matzen 145, Matzen 229 and Raggendorf 10 yielded almost the same results. As expected, the permeability reduction (a multiplier of 0.35 was used) delayed the water production in Matzen 476, but the incremental recovery was still

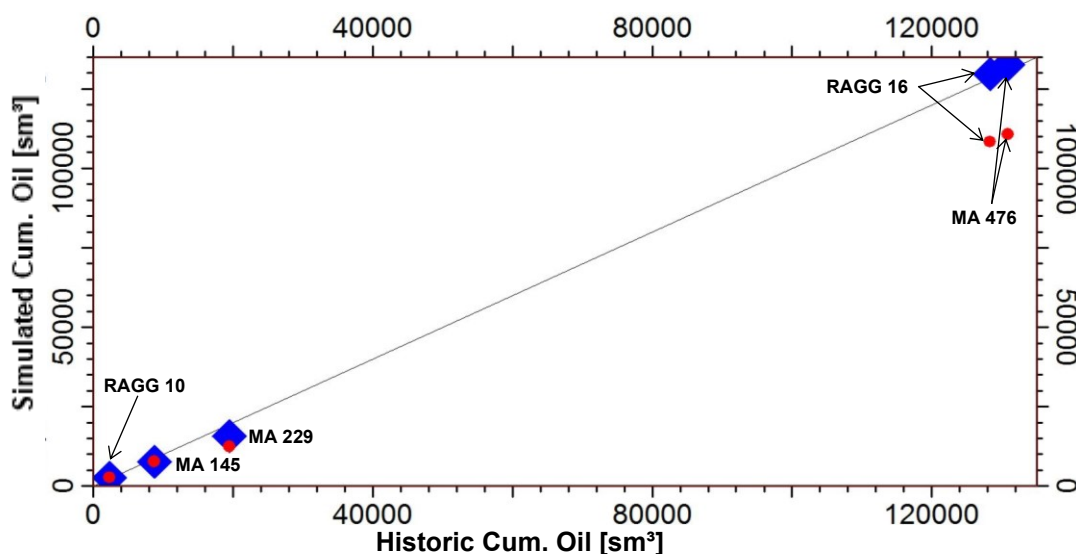


Figure 35: Error plot for permeability (red) and porosity (blue) box multiplier scenarios

not sufficient to support the historical volumes. For the second scenario, a porosity multiplier of 2.2 was used in the model. As Figure 35 shows, this increased the production of the two top producers to the historical levels. The detailed cumulative oil production profiles are shown in chapter A.6. Simulation results using the updated structural interpretation lead to the following conclusions:

- Removing the internal fault reproduced the desired overall trend in cumulative oil production. Based on that, it was assumed that no permeability barrier is present in this area and the reservoir can be modelled as a continuous body.
- Early breakthrough of water coming from Matzen 476 caused the water cut in Matzen 145 to rise very quickly. As this cannot be observed in the measured data, the presence of a flow restriction between these two wells was concluded.
- Including the compartment of the 8th Tortonian horizon only affected Raggendorf 16. As the structural model of the 9th Tortonian horizon still required modifications, no valid judgement regarding possible juxtaposition and crossflow between these layers could be made.
- Using a box multiplier to reduce permeability to only 35 % of the initial model lead to a good match during the early production phase, but it also clearly indicated the need for additional OIIP on a long-term basis. The second box multiplier scenario in which only the porosity was changed (no permeability alteration) emphasized this as well.

The two major aspects that suggested another update of the structural model were: First of all, a porosity multiplier of 2.2 would lead to a very high peak effective porosity value of close to 70 %. This is not in accordance with the characterization of the reservoir rock and physically not plausible either. Second, there is a certain amount of inherent uncertainty related to the seismic interpretation (presence and connectivity of faults, shape of rock layers, etc.), which is transmitted to the structural model as well. In order to achieve a satisfactory history match without the necessity for a porosity multiplier of 2.2, a second re-interpretation regarding the structural setting of the reservoir was carried out. The most important aspect was to check if the structural depression could be replaced by a smooth transition zone and if a permeability barrier between MA 145 and MA 476 could be implemented, in a way that both features were still in accordance with the seismic data.

Additional test scenarios at the end of this process loop showed that the effect of using the water-wet relative permeability setup for the low porosity sand did not lead to a considerable increase in oil production. On the other hand, using the observed data set instead (saturation function 4) nearly matched the water cut behaviour of the individual wells. Therefore, the new model considered extremely water-wet conditions only for the main oil bearing sand layer.

The updated structure that incorporates previously mentioned changes and satisfies seismic measurements is shown in Figure 36. In addition, a possible flow barrier between MA 229 and MA 476 was identified. As this feature is hardly visible on the seismic cross-section and the vertical offset is minor, it was only implemented as a simulation fault instead of explicitly modelling it as a part of the structural framework. This made a quick adaption of the transmissibility possible. Taking the geology of the PU into account, a permeability reduction of one order of magnitude was implemented in the near vicinity of the present faults as well.

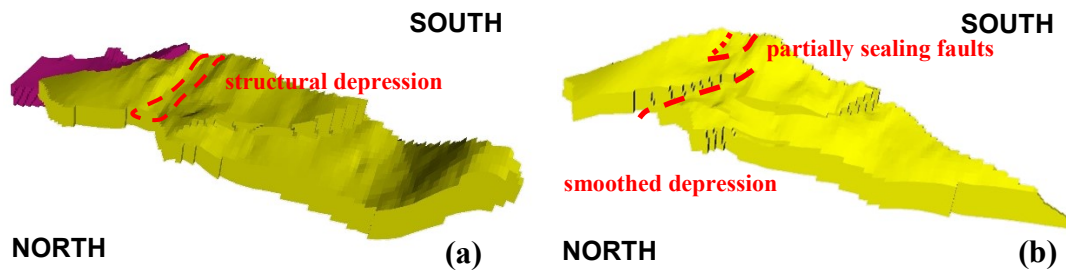


Figure 36: First (a) and final (b) update of the structural model

Running the history matching case under these conditions resulted in no water production from MA 145. Having pure oil production for almost three years is rather atypical for the Matzen field in general. Nevertheless, the constant observable low water production does not fit the historical water cut behaviour (constantly increasing trends) of all the other wells in the production unit either. Assuming that the observed data does not reflect the actual behaviour of the reservoir, a technical cause for the water production was hypothesized. In order to identify possible water sources, a water control diagnostic plot according to (Chan, 1995) was developed for MA 145. This method utilizes a log-log plot of the WOR and the time derivative of the WOR against time to differentiate between various causes for water production. The same analyses were carried out for MA 476 and RAGG 16 and were used as a reference for MA 145. The results and the corresponding diagnostic plots are shown in chapter A.7 of the appendix.

According to (Chan, 1995), the two top producers both exhibit a behaviour that can be classified as multi-layer channelling. In reality, the 9th Tortonian horizon consists of several sublayers. Therefore, these results are in accordance with the geological and stratigraphic knowledge of the horizon. In contrast to that, the result for MA 145 looks entirely different. The diagnostic plot representing stable coning best describes the overall behaviour there. Water cones usually develop over time when water gradually approaches the wellbore. Due to the fact that MA 145 is perforated well above the OWC, a low gross production rate of around 13 sm³/day was used, and water production started right from the beginning. Therefore, coning cannot be the root cause of the water production. The only possible explanation left is related to the history of MA 145 in the 10th Tortonian horizon. Before starting production from the unit 209-33, MA 145

produced from a subjacent fault block located in the 10th Tortonian horizon. Due to the low oil production rate of approximately 0.6 tonnes per day and a corresponding high water cut (~98 %), this perforation interval has been conserved (only plugged but not cemented), and production from the 9th Tortonian horizon started in 2016. The production interval in the 9th TH is only one meter above the bridge plug, therefore forces and deformation related to the perforation job can endanger its sealing capability. Another aspect is that the tubing conveyed perforation (TCP) gun could not be recovered and remained on top of the plug. Any subsequent fishing operations could also create leakage paths, which could allow fluid flow from the 10th TH to the productive part of the wellbore. Thus, it is assumed that the water produced in MA 145 is coming from the subjacent layer and not from the current production unit.

In order to check this concept, one part of the 10th Tortonian horizon was included in the simulation model (south view seen in Figure 37). The open perforation intervals (green discs) and the approximate location of the bridge plug (red square) are indicated in the figure as well.

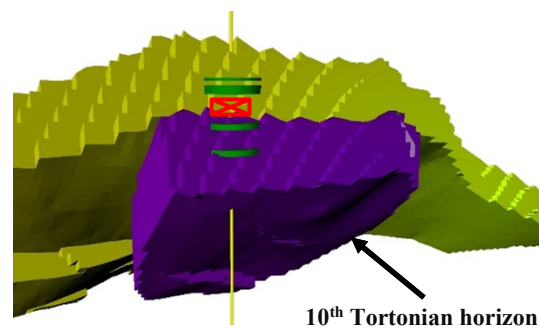


Figure 37: Subsection of 10th TH

For simplification (and to prevent the need for creating a second history match) the minor amounts of oil left in the lower reservoir were neglected and water was considered to be the only mobile phase there. The results for this simulation scenario are shown in Figure 38. Although there is a mismatch (in terms of absolute values) in the water cut of MA 145, this is the first time that the overall production behaviour (oil and water) of all the wells was reproduced by the simulation. Additionally, the error in cumulative oil production of MA 476 was less than 10 %. Only RAGG 16 still showed a comparatively big error of approximately 23 %.

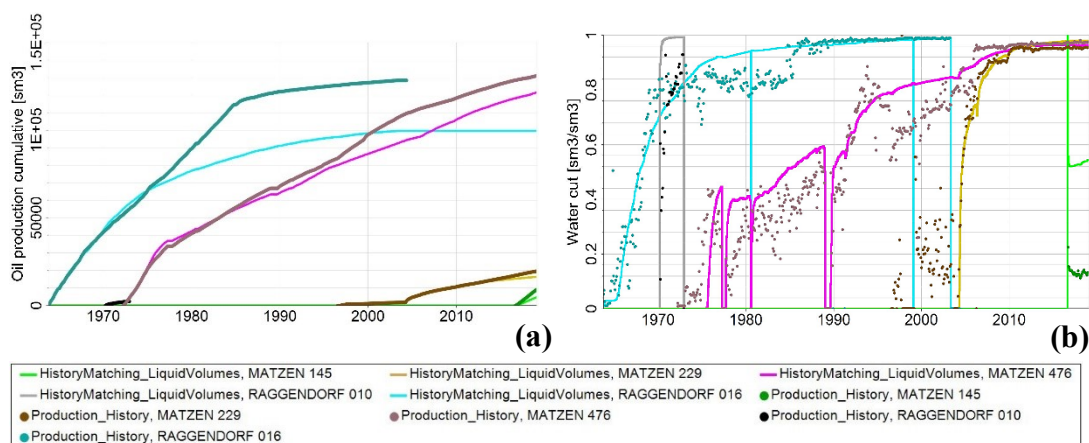


Figure 38: Production behaviour including the perforations in the 10th TH

To verify the assumption concerning the source of water once more, a detailed analysis of the water produced in MA 145 was conducted in the OMV laboratories. The results are shown below.

Table 6: Water analysis

		sample	comparative data	
		Matzen 145	Matzen 476	Matzen 394
sample collection		29.04.2019	06.05.2019	01.04.1970
horizon		209-33 or 210-32	209-33	210-32
alkalinity_{pH4.3} (m-Wert)	[mmol/l]	24.2	24.1	24.65
alkalinity_{pH3.5} (m-Wert)	[mmol/l]	25.2	24.9	25.45
total hardness	[°dH]	33.4	35.7	26
chloride	[mg/l]	14884	14279	14270
bromide	[mg/l]	73.3	62.7	78
iodide	[mg/l]	23.4	48.9	41
sulphate	[mg/l]	1.2	0.7	7
lithium	[mg/l]	1.24	1.38	- *
sodium	[mg/l]	9408	9298	9507
ammonium	[mg/l]	72.7	71.2	70
potassium	[mg/l]	108	79.7	107
magnesium	[mg/l]	75.2	61.9	57
calcium	[mg/l]	106	142	92
strontium	[mg/l]	17.5	23.3	- *
barium	[mg/l]	1.5	2.9	- *
boron	[mg/l]	33.7	31.4	29
silicon	[mg/l]	13.1	11.4	10.3
iron	[mg/l]	<0.1	<0.1	<0.1

There are two main issues related to this water analysis. First of all, there is a lack of comparative sample data and therefore no representative mean values and ranges for the individual concentrations could be specified. Second, the formation waters for both production units exhibit very similar compositions (seen in Table 6). Based on that, an exact determination of the water source was not possible.

In summary, it was not possible to identify the source of water by diagnostic plots or water analyses reliably. MA 145 is the current top producer and the amount of associated water is minor, therefore no further immediate actions have been taken, but the need for an integrity test of the plug has been included in the next actual regular workover program. These possible leakages are the current best estimate and the only way to reproduce the behaviour of MA 145, therefore this assumption was used for all further simulations.

*) data not measured

Detailed investigation of the previous simulation results exhibit both good displacement and sweep efficiency in the north-eastern part of the reservoir. Thus, the underperformance of RAGG 16 could not be explained by modelling artefacts or undrained reservoir zones. The only possible explanation left is that there is a crossflow between the compartment of the 8th Tortonian horizon and the PU 209-33. As a result, this compartment was once again included in the simulation model.

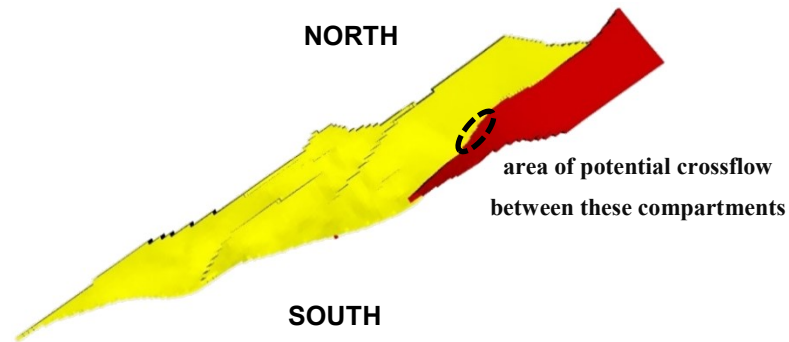


Figure 39: Simulation model including the compartment of the 8th TH (red)

The effect of this assumed crossflow was the same as described in the second history matching loop. In the simulation oil production from RAGG 16 significantly increased ($\sim 10,000 \text{ sm}^3$) whereas the production of the other wellbores remained nearly unchanged. Results for this simulation run are shown in Figure 40. Although the water cut history was reproduced very closely, the model still underestimated the historically produced oil volumes.

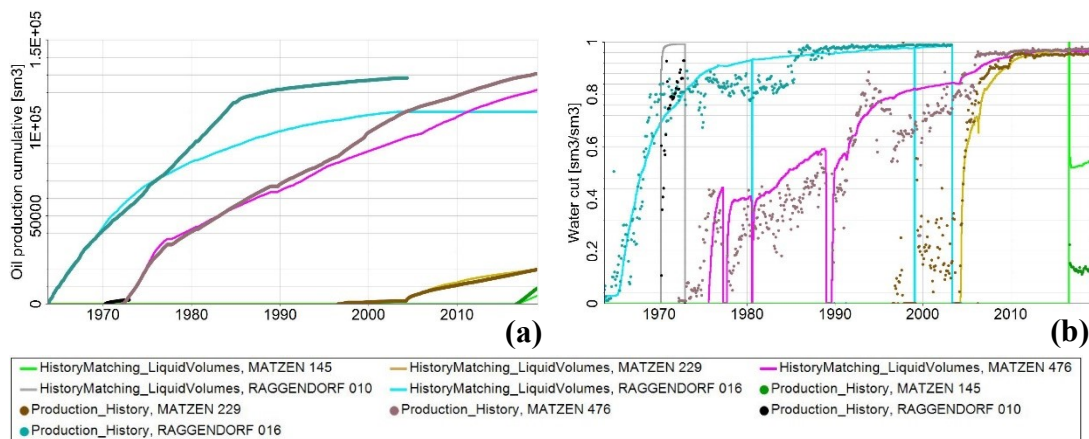


Figure 40: Production behaviour of the final simulation model

Now all structural interpretation options were exhausted and porosity was the only parameter left that could be used to reach the final history match. Beside the previously mentioned box multiplier used to reduce permeability in the near vicinity of the faults, box multipliers to increase porosity and therefore the recoverable oil had to be implemented. As these box multipliers should not influence the evaluation of the future development strategy, their areal extent (shown in chapter A.8) was limited to the approximate drainage area of MA 476 and RAGG 16. A porosity multiplier of 1.2 was required to match the historical oil production

volumes on a well scale and on a reservoir scale. This was a big improvement compared to the previously used multiplication factor of 2.2. Nevertheless, the most important achievement was that the resulting peak porosity values were kept below 40 %. Therefore, physical plausibility is given and the porosity model is in line with the rock characterization.

As seen in Figure 41, the production behaviour of MA 145 was not affected by including the 8th Tortonian horizon or the porosity modification and consequently there was still an overestimation of the water production. The reason was that the perforations located in the 10th Tortonian horizon were fully connected to the wellbore. The main reason is that the assumed restriction created by the leaking plug cannot be modelled using Eclipse. Due to the fact that the full-field oil production match was excellent and the rate behaviour of MA 145 was reproduced as well, it was decided that no rock property modification (permeability reduction in the 10th TH) should be implemented to mimic this restriction.

The final results of the history matching process are shown below.

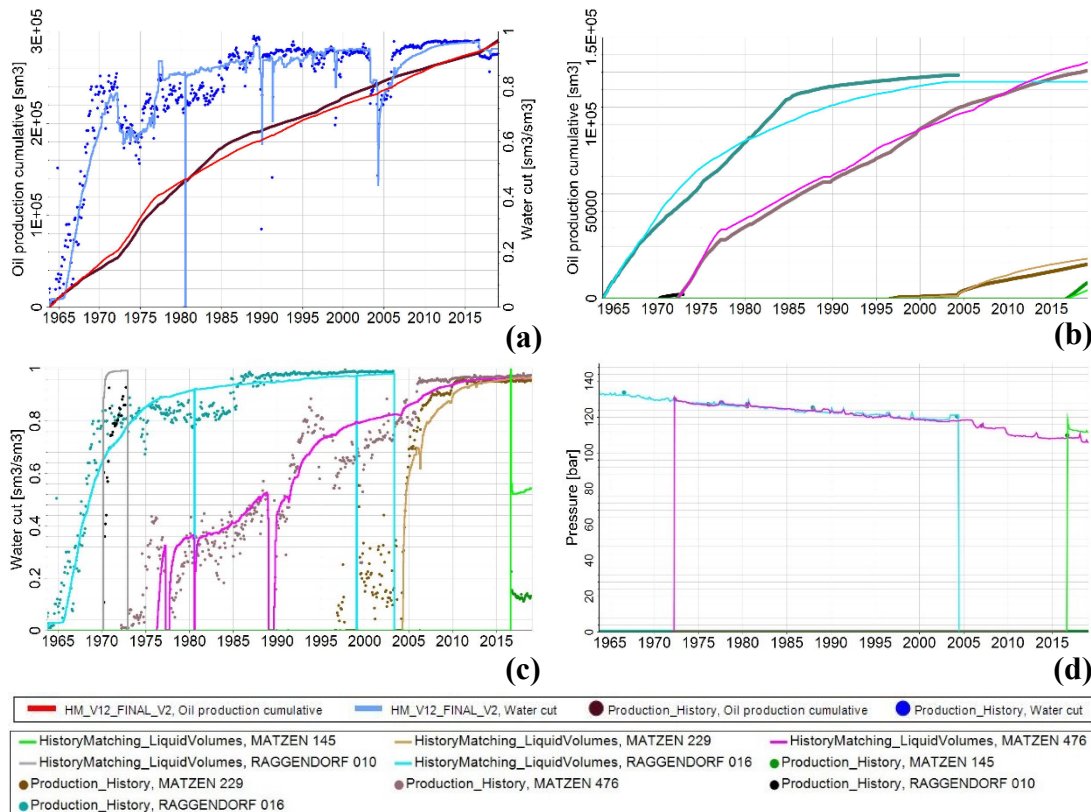


Figure 41: Final history matching results

One final aspect that has to be mentioned is that MA 145 and several other offset wells used to calculate the porosity model are located close to the major sealing fault. As this fault has a significant offset, the presence of several minor (sub-seismic) faults in the near vicinity of the main fault is very likely. This can lead to the fact that some of these wells - like MA 145 - do not penetrate the entire sand layer and the thickness observed on the log-data does not represent the true net thickness. Figure 15 (shown in chapter 3.1) clearly shows this distinct decrease in

sand thickness from more than 8 m in the eastern area around RAGG 16 to only 3 m in the central part and western part around MA 145. This consequently biases the porosity model towards a thinner sand layer. So assuming that the true layer thickness is similar to the one observed in the eastern area, the required porosity multiplier would be even lower in parts of the reservoir model.

To sum it up, the final model

- reproduces the historical field production volumes with an error of less than 1.0 %
- reproduces the overall production trends (oil production and water cut development) of the individual wellbores
- reproduces the historically observed pressure measurements
- only requires minor modifications regarding its petrophysical properties and all these changes are still in accordance with all geological and petrophysical interpretations.

Therefore, the model is considered to be a satisfactory representation of the true reservoir that can be used for further forecasting and predictive tasks.

3.6 Development Scenarios & Production Forecasting

In order to identify the optimum future development strategy, different scenarios were analysed. As a first step, the focus was put on rather cheap and easily implementable measures related to already existing wells. Details regarding these workover potentials are given in chapter 3.6.1. Next, the infill drilling potential for the production unit 209-33 was evaluated. The reservoir target zones were defined using a screening and selection process based on the k^*h product (product of absolute formation permeability and formation thickness) and the simulated current oil saturation. The parameters used to further optimize the target location are

- the distance to the neighbouring wells
- the distance to the oil water contact
- the distance to the faults.

The suggested wellbore locations and completion intervals for different infill well scenarios are given in the chapters 3.6.2 and 3.6.3.

Forecasting should be as realistic as possible, therefore it was assumed that production from a possible infill well could start in 2021 at the earliest and the prediction and assessment period was limited to ten years. Wellbore shut-in criteria used for all different scenarios were

- a minimum oil production rate of 0.5 tonnes per day
- and a maximum water cut of 99.3 %.

3.6.1 Workover Potential

The primary drilling campaign in this area took place between 1949 and 1955. Based on that, there is a theoretical number of five wells that could be considered as workover candidates. Nowadays only three of these wells are still active in other production units.

- RAGG 9 is located east of RAGG 16 in the already watered out zone. Therefore, it is not considered for workover operations.
- MA 314 is located between the active wells MA 145 and MA 476. The short well-to-well distance of around 120 m and its good oil production rate of around 2 tonnes per day (from the 8th Tortonian horizon) eliminate the well as a potential workover candidate.
- MA 394 is also located between the active wells MA 145 and MA 476. The distance to MA 476 is even less than 60 m. Its relative position to MA 476 is similar to the one of MA 229, but it is located in the western part of the reservoir. MA 229 was perforated in 1996 and it did not reach the expected rates, therefore MA 394 is also not considered to be a good candidate.

3.6.2 Vertical Infill Drilling

For placing the infill well, spatial as well as petrophysical limitations were specified. A minimum distance of 15 m to the faults and to the current oil-water contact were to be fulfilled. Additionally, the minimum inter-well spacing should not be less than 200 m – this is an experience value used for infill drilling and re-completion work in the Matzen area.

As mentioned above, the $k \cdot h$ product and the current oil saturation state were used as petrophysical selection criteria. The product of these two parameters was normalized by its maximum so that the final decision parameter is a dimensionless value between 0 and 1. To ensure good inflow from the reservoir only the upper quartile (normalized $k \cdot h \cdot S_{oil} > 0.75$) was considered as a potential drilling target. As the reservoir still stretches around 800 m to the west (measured from MA 145), two infill wells are theoretically possible in the production unit. Figure 42 shows the potential infill well locations for a single-well and a two-well scenario.

The planned well-to-well distances are:

- ~ 400 m from MA 145 to the single infill well
- ~ 300 m from MA 145 to Well 1
- ~ 200 m from Well 1 – Well 2.

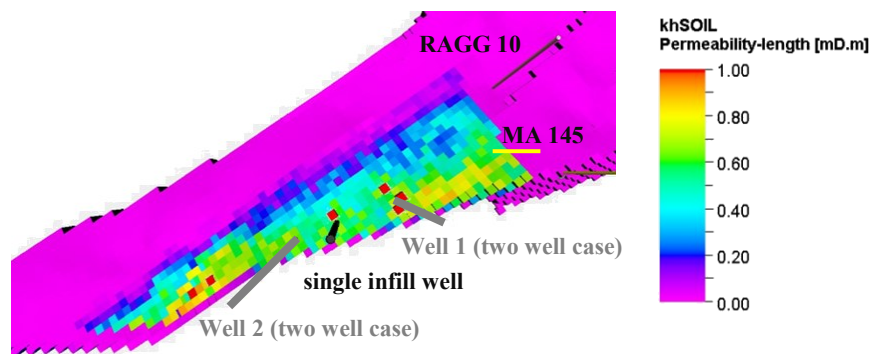


Figure 42: Reservoir target locations

The highlighted red squares represent the calculated reservoir target locations. As can be seen, only well 2 of the two-well scenario cannot be placed accordingly because the well-to-well distance would be less than the previously defined 200 m.

The corresponding expected production profiles (oil rate and cumulative oil) for a single infill well (black curve) and for two infill wells (grey curves) are shown in Figure 43. As this is a mature reservoir, it was decided to use a production strategy similar to the one in the successful well MA 145. In the simulation production started with a moderate gross rate of 20 sm^3/day . The main goal was to have a stable displacement front, to prevent water coning and therefore to delay water production from the infill wells. Due to the fact that gross rate increases did not bring about the desired net oil increase in the past, the production rate for the new well was assumed to be constant throughout the entire prediction period. Based on that, the single-well

scenario lead to the highest predicted production per wellbore, but the two-well scenario lead to a higher total recovery. A detailed evaluation of the expected project net present value (NPV) is conducted in chapter 3.7.

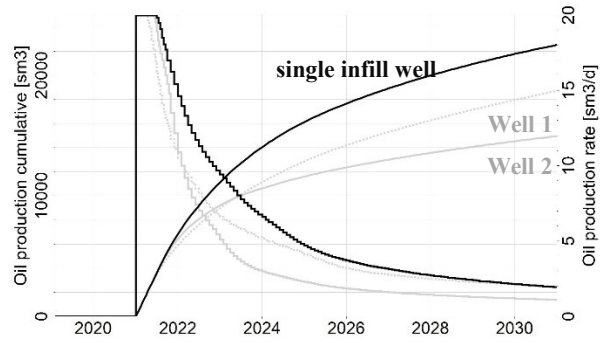


Figure 43: Oil production prediction

3.6.3 Horizontal Infill Drilling

This option utilized the same spatial decision criteria as vertical infill drilling before. The main goal for this scenario was to maximize the contact area between wellbore and reservoir. Therefore, the azimuth of the well was directed in the south-western direction (parallel to the confining fault) and the horizontal section was located in the main oil bearing sand layer. This specific well placement eliminated the need for calculating the petrophysical selection criterion mentioned in chapter 3.6.2. Nevertheless, it can also be clearly seen that the horizontal section of this well penetrates the calculated reservoir targets (indicated in red). The planned trajectory and completion interval is shown in Figure 44 (a). As one can see, an openhole completion was assumed for the horizontal section.

Production forecasting results are displayed below. For the horizontal infill well it was specified that the initial net production rate should be approximately twice as high (~ 40 m³/day) as the one of a vertical well. The previously mentioned shut-in conditions were also applicable for this scenario.

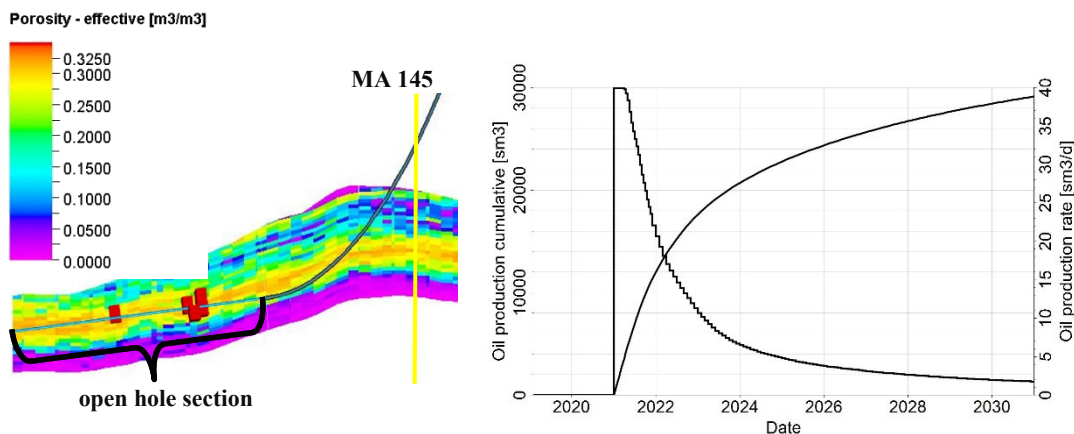


Figure 44: Wellbore trajectory (a) and cumulative oil production (b)

3.7 Economic Assessment

For the final selection of the optimum development strategy an economic assessment was carried out as well. Development scenarios were ranked based on their expected net present value (NPV) and the calculation was done according to the following equation:

$$NPV = \sum_{t=0}^N \frac{(revenue - expenses)}{(1 + i)^t}$$

t specific point in time

i interest/discounting rate

As mentioned previously, the assessment period for the economic feasibility is ten years. Both the gas price as well as the operating expenses were assumed to be constant. Oil price variations were implemented according the currently used mid-term planning scenario. Its exact development is included in the corresponding graphs. The NPV was calculated annually on a year-end basis and the used economic boundary conditions are summarized in Table 7.

Table 7: Economic framework

Parameter	Unit	Value
Oil price (average)	€/tonne	448
Gas price (average)	€/m ³ (Vn)	0.23
OPEX	€/boe	11.5
Royalties gas	%	19
Royalties oil	%	15
Corporate Income Tax	%	25
Inflation	%	2

At this early planning stage, the project costs were estimated based on average costs known from the most recent drilling activities in the Matzen field. The term drilling costs not only refers to the actual drilling, but it also includes casings and cementing activities. On the other hand, tie-in costs cover all expenditures (for pipelines, well site, completion activities, pump jack, etc.) which are necessary to integrate the well into the existing transport system.

Table 8: Project cost estimation

Parameter	Unit	Vertical wellbore	Horizontal wellbore
Drilling costs	€/m	1,200	1,700
Measured depth	m	1,550	2,150
Drilling costs	€	1,860,000	3,655,000
Tie-in costs	€	1,000,000	1,000,000
Total costs	€	2,860,000	4,655,000

In order to create a proper decision basis, not only absolute key performance indicators like the cash flow profiles but also relative ones like the discounted profitability index were calculated for the different infill well opportunities.

Although the total oil recovery is highest in the case of two infill wells, this option leads to the lowest economic benefit. Well 2 does not even reach a positive NPV within the first ten years of production. The high initial investment costs delay breakeven and reduce the predicted NPV for the horizontal infill well to about € 620,000. Breakeven for the single infill well will be reached in 2023 (more than one year earlier than in any other scenario) and with an estimated NPV of more than € 1,000,000 it is nearly 70 % more economic than the horizontal well.

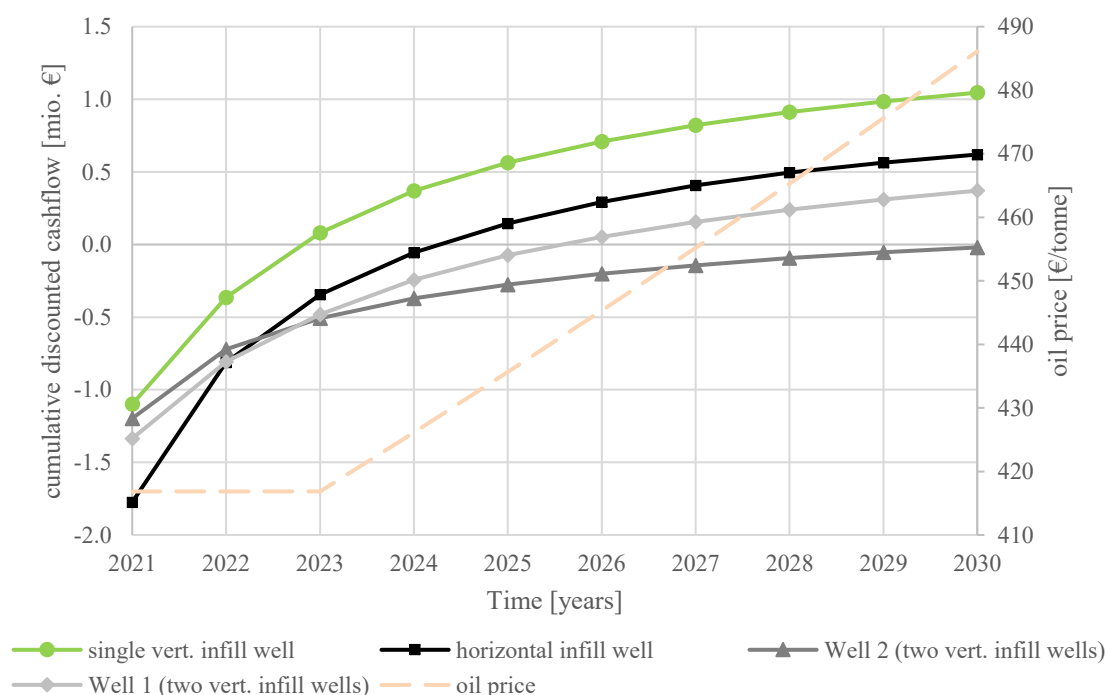


Figure 45: Cash flow profiles

The discounted profitability index (DPI) is calculated as the ratio between the net present value and the discounted CAPEX. It can be seen that well 1 is as profitable as the horizontal one and the single well option is more than twice as profitable as these two options. Thus, these best case (P50) evaluations, clearly indicate that a single vertical infill well outperforms the other options on an economic basis and consequently represents the development strategy of choice.

Table 9: DPI for P50 scenarios

Case	Unit	DPI
Single vertical infill well	-	0.37
Well 1 (Two vertical infill wells)	-	0.13
Well 2 (Two vertical infill wells)	-	-0.01
Horizontal infill well	-	0.13

Based on the previous selection, two alternatives covering a low (P90) as well as a high (P10) estimate condition were calculated. For the low case a slightly modified set of absolute permeabilities was used in the simulation. This already caused an early water breakthrough in MA 145, which has not been observed in reality. Having an advanced water front compared to the best estimate also causes early water breakthrough in the infill well and consequently reduces oil production rates and expected recovery. In the high case scenario it was assumed that the property modifier that was required during history matching was not limited to the eastern and central parts, but also extended to the western part of the reservoir. Again, the same economic and technical boundary conditions were used. The range of cumulative oil production ranges from about 17,800 tonnes in the low case scenario to nearly 26,500 tonnes in the high case. This means that even the P90 case, with a calculated NPV of € 350,000 suggests that the single infill well is economically viable.

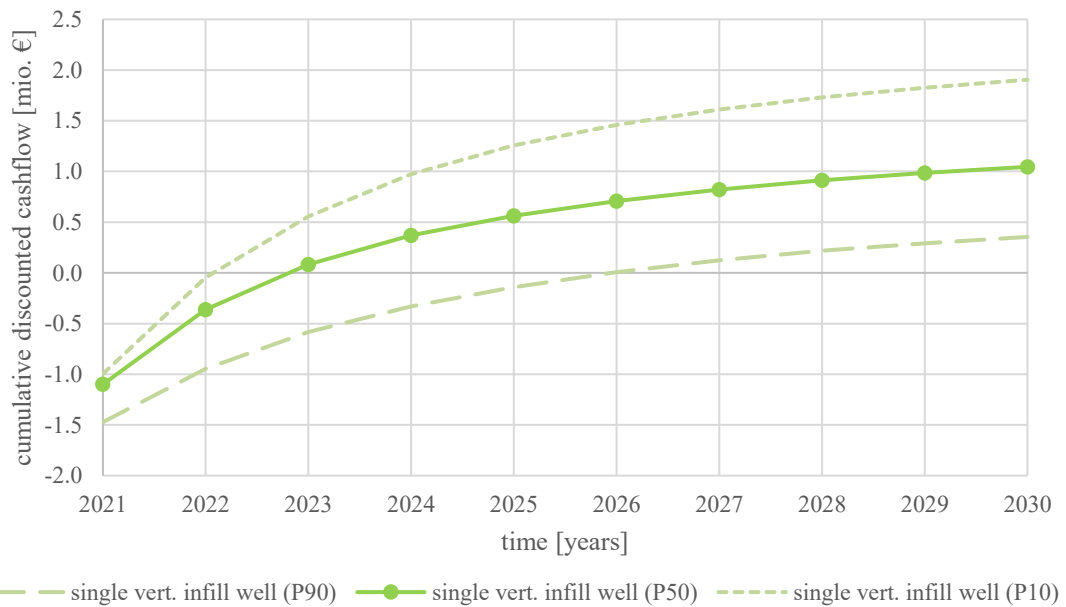


Figure 46: P10, P50 and P90 scenarios for a single infill well

Chapter 4

Results & Discussion

In the course of this thesis, a reservoir model that reproduces the historical behaviour of the production unit 209-33 in the 9th Tortonian horizon of the Matzen field was developed. As the reservoir is located in the Matzen fault system the presence of sealing and non-sealing faults was expected beforehand.

In order to reduce complexity, the internal sublayer structure was modelled by using only three sets of rock physics functions. The validity of this approach was checked by comparing the modelled initial state of the reservoir with the historical log-interpretations and by comparing the simulated OIIP with the current estimates.

Nevertheless, the simulation results clearly indicated that the previous estimations of the oil in place were significantly too low to support the historical production behaviour. Even the implementation of water-wet relative permeability curves and the neglect of capillary pressure in the highly porous sand layer was not enough to match historical production data with the initial geological model.

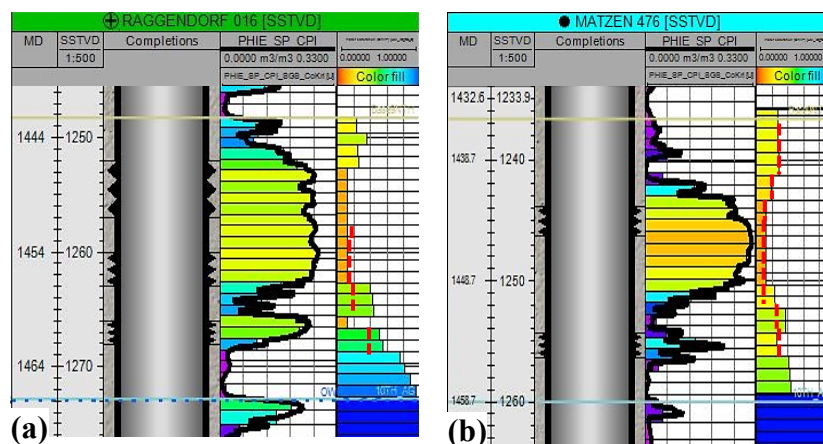


Figure 47: S_w for final initialization scenario along RAGG 16 (a) & MA 476 (b)

Additionally, the simulation also confirmed the presence of a strong natural aquifer drive. The number of unknown parameters regarding the aquifer was reduced and the pressure match improved by using a numeric aquifer realization instead of an analytic model.

Early water production (low OIIP and strong influx from the aquifer) was an issue throughout all simulation models. In order to delay the water breakthrough, the artificial set of rock physics functions was kept in the final model as well. The initial saturation state of the final model is shown in Figure 47 (red lines indicate the original log-interpretation). As the endpoint saturations (connate water saturation and residual oil saturation) were not modified, the modelled and actually measured (indicated in red) saturations were well in line.

Calculating the corresponding oil initially in place lead to around 840,000 sm³, which is equivalent to 778,680 tonnes of crude oil. Using that figure, the current recovery factor and ultimate recovery (URF derived from analogous field investigations) are given by the following expression:

$$RF = \frac{\text{Current Recovery}}{OIIP} = \frac{263,674}{778,680} = 33.8 \%$$

$$\text{Expected Ultimate Recovery} = OIIP * URF_{avg} = 778,680 * 0.41 = 319,259 \text{ tonnes}$$

A primary recovery factor of 33.8 % (in a low and best estimate) is more realistic than the previously calculated one of around 60 %. Additionally, the estimated ultimate recovery of 319,000 tonnes is perfectly within the range (314,000 – 380,000 tonnes) derived from analytic methods like the decline curve analysis and water oil ratio plots.

Through history matching the presence of faults and their effects on the fluid flow directions were shown. Several different realizations with varying faults (extension, position, offset, etc.) and possible communication paths between the 8th and 9th Tortonian horizons were evaluated. Modelling the reservoir as a continuous sand body did not reproduce the historical behaviour. Only reduced or now transmissibility across internal faults lead to the expected and observed production history. In contrast to previous reservoir models, the final one - in which all faults and their properties are defined - suggests that the assumed crossflow from the 8th into the 9th Tortonian horizon is likely. By including the compartment of the 8th TH into the model, the cumulative oil production as well as the oil and water production rates and consequently the water cut can be matched closely.

Neither the water control diagnostic plots nor a detailed water analysis could clearly identify the source of production water in MA 145. Nevertheless, the wellbore's workover history and simulation results give good indications that the 10th Tortonian horizon and not the production unit 209-33 is the actual source.

The final results of history matching still include porosity box multipliers in the eastern and central parts of the reservoir. These slight modifications are required to match cumulative recovery and do not contradict the historical rock characterization.

It can clearly be seen that MA 145 and other offset wells exhibit a significant decrease in net-pay thickness in the log-measurements. Depositional history of the reservoir does not indicate such a thinning trend. Moreover, the reservoir is located in a fault system and most of these offset wells are located in the vicinity of the major confining fault. Thus, it is more likely that these wells intersect sub-seismic faults (or a similar feature) and only partially penetrate the sand layer. This biases the porosity model to a lower net sand thickness, reduces the OIIP and therefore adversely affects the simulation. Therefore, porosity box multipliers are even more plausible.

Regarding the future development of the reservoir it has been shown that re-completion of existing wells does not create any benefits. On the other hand, infill well drilling leads to additional recovery and economic success. This additional recovery created from different infill drilling cases compared to a no further activity case is shown below.

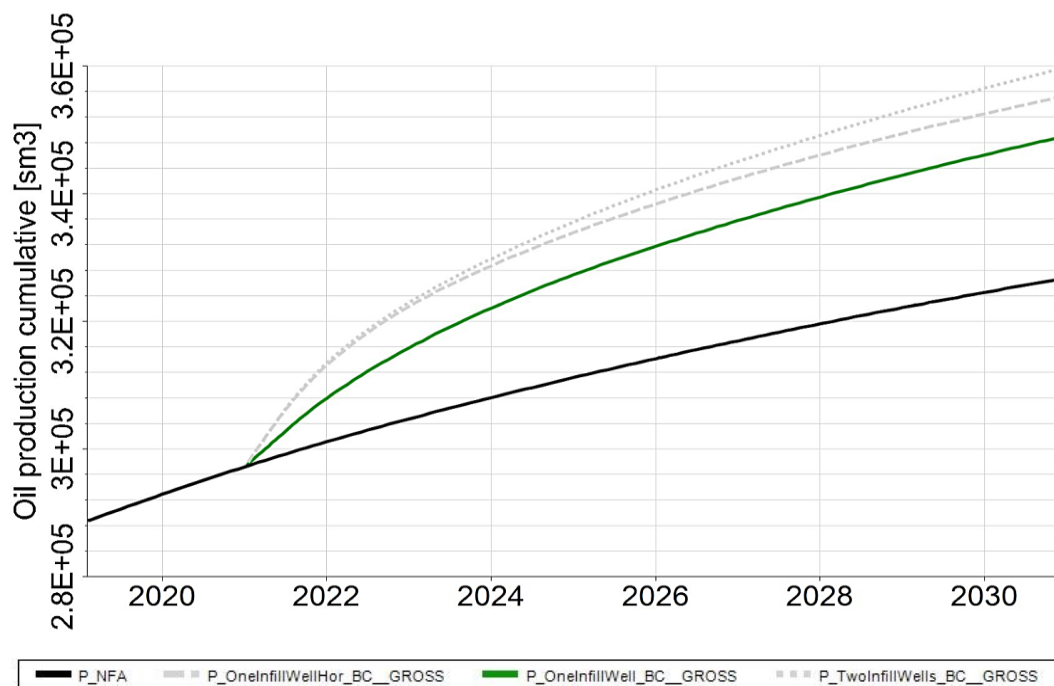


Figure 48: Cumulative oil production in a P50 scenario – all cases

The NFA scenario itself predicts a recovery of approximately 327,000 sm³, which is equivalent to around 303,000 tonnes of oil, by the end of 2030. Comparing that to the lower estimates given by the DCA analysis and WOR-plots, the respective errors are less than 10 %. The long-term WOR-plot leads to the best match with the simulated NFA scenario and the corresponding error is less than 4 %.

Table 10: Predicted future RF

Case	Incremental Recovery	RF in 2031
	[sm ³]	[%]
Single vertical infill well	~22,000	41.5
Two vertical infill wells	~34,000	42.9
Horizontal infill well	~29,000	42.3

The technically best development strategy that leads to the highest incremental oil recovery is the two vertical infill well case. Besides that, all cases reach final RFs higher than the average URF derived from analogous field investigations. Nevertheless, these expected recovery factors are still below the maximum values found during analogous field investigations. The production units 209-32 and 209-34 both exhibit a URF of 44 % and therefore all predictions are still well in line with the observed data.

This thesis also clearly shows that the highest technically recovery does not necessarily translate to the highest economic success. Based on detailed economic evaluations, using a single vertical infill well (lowest incremental oil recovery) is the most profitable development strategy.

Chapter 5

Conclusion

5.1 Summary

As a result of this thesis, a representative reservoir model that fits the static as well as the dynamic data has been developed. Moreover, it has been shown that the historical behaviour of MA 145 does not represent the actual reservoir behaviour and possible technical root causes for the water production have been suggested.

It has been shown that the ultimate recovery predicted using simple analytic tools like decline curve analysis and water oil ratio plots are well in line with the results derived from full field simulations.

Based on the derived reservoir model, different opportunities regarding the future development of the production unit 209-33 have been technically and economically assessed and the optimum strategy has been selected.

5.2 Evaluation

In order to come up with the final development strategy, several sub-goals had to be fulfilled. One essential part of this thesis was the integrated approach used in history matching. A reservoir that is located in a fault zone exhibits significant structural uncertainty, especially related to the presence and the offset (related to transmissibility) of faults. Thus, the development of a representative and realistic model requires the usage of static and dynamic data.

One shortcoming of this model is the lack of relative permeability and PVT measurements related to the investigated production unit. Several neighbouring fields located in the same geological horizon have been investigated and strong analogies for both rock and fluid characteristics have been identified between these reservoirs and 209-33. Therefore using relative permeability and PVT data from these analogous fields is not only a reasonable, but also the best possible approximation that can be carried out.

The prediction scenarios are set up in a realistic time frame so that actual execution (drilling, completion and tie-in of the infill well) is possible and production can start as planned. To prevent any bias towards improved profitability, economic boundary conditions based on OMV's mid-term planning scenario have been used.

5.3 Future Work

The evaluation and selection of the optimum future development strategy, including the definition of the reservoir target has been completed. The next steps will have to target the actual realization and execution of the project and include

- a subsurface peer review
- the planning of the wellbore (only after a successful peer review)
- the drilling and tie-in (only after a successful peer review).

Chapter 6

References

- Barron, J. (2018). *Oil company additions to proved reserves in 2017 were the highest since 2013*. [online] Eia.gov. Available at: <https://www.eia.gov/todayinenergy/detail.php?id=36532> [Accessed 11 Feb. 2019].
- Bjørndal, E., Bjørndal, M., Pardalos, P. and Rönnqvist, M. (2013). *Energy, Natural Resources and Environmental Economics*. Berlin: Springer Berlin, p.35.
- Carmalt, S. W., Moscariello, A. (2017). What is a Giant Field?. In: R. K. Merrill and C. A. Sternbach, ed., *AAPG Memoir 113: Giant fields of the decade 2000-2010*. AAPG, pp.9-14.
- Chan, K.S., (1995). *Water Control Diagnostic Plots*, Paper SPE 30775. SPE Annual Technical Conference and Exhibition, 22-25 October 1995, Dallas, U.S.A.
- Eia.gov. (2019). *Table Definitions, Sources, and Explanatory Notes*. [online] Available at: https://www.eia.gov/dnav/pet/TblDefs/pet_crd_pres_tbldef2.asp [Accessed 10 Feb. 2019].
- Etherington, J. (2009). *Managing Your Business Using Integrated PRMS and SEC Standards*, Paper SPE 124938. SPE Annual Technical Conference and Exhibition, 4-7 October 2009, New Orleans, Louisiana.
- Finsterwalder, R., Hujer, W., Kuffner, T., Mikuz, T., Perez, J., Ramberger, R., Rieser, E. (2013). *9.TH Matzen Study*. OMV internal study, Vienna, August 2013
- Fuchs, R., Hamilton, W. (2006). New Depositional Architecture for an Old Giant: The Matzen Field, Austria. In: J. Golonka and F. J. Picha, ed., *AAPG Memoir 94: The Carpathians and their foreland: Geology and hydrocarbon resources*. AAPG, pp.205-219
- Fuchs, R., Ramberger, R., Veit, Ch. (2001). *Das Matzen Projekt: Renaissance der größten Öl- und Gasfeldes in Österreich (Wiener Becken)*: Hamburg/Wien, Erdöl Erdgas Kohle, 117 Jg., Heft 11, 2001, pp. 528-540

- Fouad, K., Knox, P. R. (2001). *Neural Network Analysis of 3-D Seismic Data Delineates Slope- to Basin-Floor Fan Bodies in a High-Frequency Falling-Stage Systems Tract, Matzen Field, Austria*, Paper OTC 13160. Offshore Technology Conference, 30 April–3 May 2001, Houston, Texas.
- Gumpenberger, T., Kornberger, M., Deckers, M., Clemens, T., (2013). *POLYMER VISCOSITY IN POROUS MEDIA AND NEAR WELLBORE BEHAVIOUR OF A POLYMER PILOT IN THE MATZEN FIELD, AUSTRIA*, Paper OMC-2013-166. 11th Offshore Mediterranean Conference and Exhibition, 20 – 22 March 2013, Ravenna, Italy
- Gronister, Ch. (2004). *STREAMLINE SIMULATION FOR WATERFLOOD RESERVOIRS, Findings 9th Tortonneian Reservoir (A015-209-91)*. OMV internal study, Vienna, July 2004
- Kuffner, T., Hujer, W. (2010). *Facies, Sequence Stratigraphy and Reservoir Characterization of the 9.TH*. OMV internal (LEP) Report, Gänserndorf, October 2011.
- Knox, P. R., Fouad, Khaled, Zinke, S., Light, Malcolm, Skolnakorn, J., Shi, S., Von Lunen, E., Yeh, J. S., Finley, R. J., Barba, R. E., Jr., Holtz, M. H., Mercer, M., Handford, R., Martinez, C., Sipahioglu, O., Rassi, Claudia, Hamiltonne, D. S., Akhter, M. S., Clift, S. J., Dunlap, D. B., Mahoney, M., Treviño, R. H., Bullen, G., Chang, C. Y., Ramberger, R., Fuchs, R., Gstrein, M., Zier, N., Baltas, P., Jarnik, M., (2000). *Optimizing hydrocarbon recovery from the Matzen Field, Vienna Basin, Austria*, The University of Texas at Austin, Bureau of Economic Geology, final report prepared for OMV, under agreement no. UTA98-0377, pp.5.45-5.53
- Kröll, A. (1984). *Die Erdöl- und Erdgasregion Matzen/Schönkirchen aus geologischer Sicht*, Erdöl-Erdgas, 100 Jg., Heft 5, Mai 1984
- Martín Rodríguez, H., Escobar, E., Embid, S., Rodríguez Morillas, N., Hegazy, M. and Lake, L. (2014). New Approach to Identify Analogous Reservoirs. *SPE Economics & Management*, 6(04), pp.173-184.
- Palzor Shenga (2018). THE OIL & GAS EXPLORATION WINNERS OF 2018. [online] Available at: <https://www.rystadenergy.com/newsevents/news/press-releases/fs-2018-discoveries/> [Accessed 10 Feb. 2019].
- Petroleum resources management system. (2018). 1st ed. Society of Petroleum Engineers, pp.25-26.
- Poldlehner, A. (2009). *Optimization and Debottlenecking of the Underground Gas Storage (UGS) Schönkirchen-Reyersdorf*. University of Leoben.

List of Figures

Figure 1: Development of global conventional oil & gas discoveries	2
Figure 2: Changes in proved reserves 2016 to 2017	3
Figure 3: Location of the Matzen field	5
Figure 4: Structure of the Matzen field.....	7
Figure 5: Type log of the Matzen field	8
Figure 6: Paleographic setting of the 6 th layer (top) and 1 st layer (bottom)	10
Figure 7: Schematic layering of the 9 th TH (North-South cross section).....	12
Figure 8: Current iso-map of the 9 th TH	12
Figure 9: Oil production history and WC of the main compartment in the 9 th TH.....	13
Figure 10: Production history of 209-33.....	18
Figure 11: Revisions of the OIIP	19
Figure 12: Bubble map of cumulative oil production in tonnes (new map)	20
Figure 13: Seismic NW-SE inline intersecting MA 476.....	20
Figure 14: Comparison of the current (a) and new (b) interpretation of 209-33	21
Figure 15: Completion intervals and respective log data.....	22
Figure 16: Current map of the northern fault blocks of the 9 th TH.....	23
Figure 17: Current map of the north-western fault blocks of the 8 th TH	24
Figure 18: URF vs. OIIP.....	26
Figure 19: Reserve prediction for entire field life (a) and since Matzen 145 (b).....	28
Figure 20: Reserve prediction - long term trend (a) and before Matzen 145 (b).....	29
Figure 21: Model setup (a) and initial pressure history match (b).....	30
Figure 22: Pressure match with corrected p_{init} (a) and important parameters (b).....	31
Figure 23: OIIP scenarios	31
Figure 24: Entire model (a) and initial simulation domain (b)	32
Figure 25: S_w for different initialization scenarios along RAGG 16 (a) & MA 476 (b).....	33
Figure 26: Pressure decline without aquifer (a) & aquifer locations (b).....	34
Figure 27: Static pressure history match.....	35
Figure 28: Liquid production rate history match	36
Figure 29: Historical vs. simulated cum. oil (a) and water cut (b).....	36
Figure 30: Historical vs. simulated cum. oil (a) and water cut (b) with WW conditions	37
Figure 31: Water distribution initial state (a) and after 15 years (b).....	38
Figure 32: Initial (a) and updated (b) structural model	38
Figure 33: Cum. oil production profiles (a) and water distribution after 15 years (b).....	39
Figure 34: Cum. oil production profiles including the compartment of the 8 th TH	39
Figure 35: Error plot for permeability (red) and porosity (blue) box multiplier scenarios	40
Figure 36: First (a) and final (b) update of the structural model.....	42
Figure 37: Subsection of 10 th TH.....	43
Figure 38: Production behaviour including the perforations in the 10 th TH.....	43
Figure 39: Simulation model including the compartment of the 8 th TH (red)	45
Figure 40: Production behaviour of the final simulation model	45
Figure 41: Final history matching results	46
Figure 42: Reservoir target locations	49
Figure 43: Oil production prediction	50
Figure 44: Wellbore trajectory (a) and cumulative oil production (b).....	50
Figure 45: Cash flow profiles	52
Figure 46: P10, P50 and P90 scenarios for a single infill well	53
Figure 47: S_w for final initialization scenario along RAGG 16 (a) & MA 476 (b).....	55
Figure 48: Cumulative oil production in a P50 scenario – all cases	57

List of Tables

Table 1: Well history of 209-33.....	17
Table 2: Legend for the comparison of analogous fields.....	25
Table 3: Comparison of selected analogous PUs to 209-33	25
Table 4: Hydrocarbon volumes for different initialization scenarios	34
Table 5: Aquifer specifications	35
Table 6: Water analysis.....	44
Table 7: Economic framework.....	51
Table 8: Project cost estimation.....	51
Table 9: DPI for P50 scenarios	52
Table 10: Predicted future RF	58

Nomenclature

B_g	formation volume factor gas	$[\text{m}^3/\text{m}^3(\text{V}_n)]$
B_o	formation volume factor oil	$[\text{m}^3/\text{m}^3(\text{V}_n)]$
k	absolute permeability	$[\text{mD}]$
N_p	cumulative oil production	$[\text{sm}^3]$
p	pressure	$[\text{barg}]$
R_s	solution gas ratio	$[\text{m}^3(\text{V}_n)/\text{m}^3(\text{V}_n)]$
S_w	water saturation	$[-]$
S_{wi}	initial water saturation	$[-]$
T	temperature	$[^\circ\text{C}]$
ρ_o	oil density	$[\text{kg}/\text{m}^3]$
Φ_{avg}	average porosity	$[-]$

Abbreviations

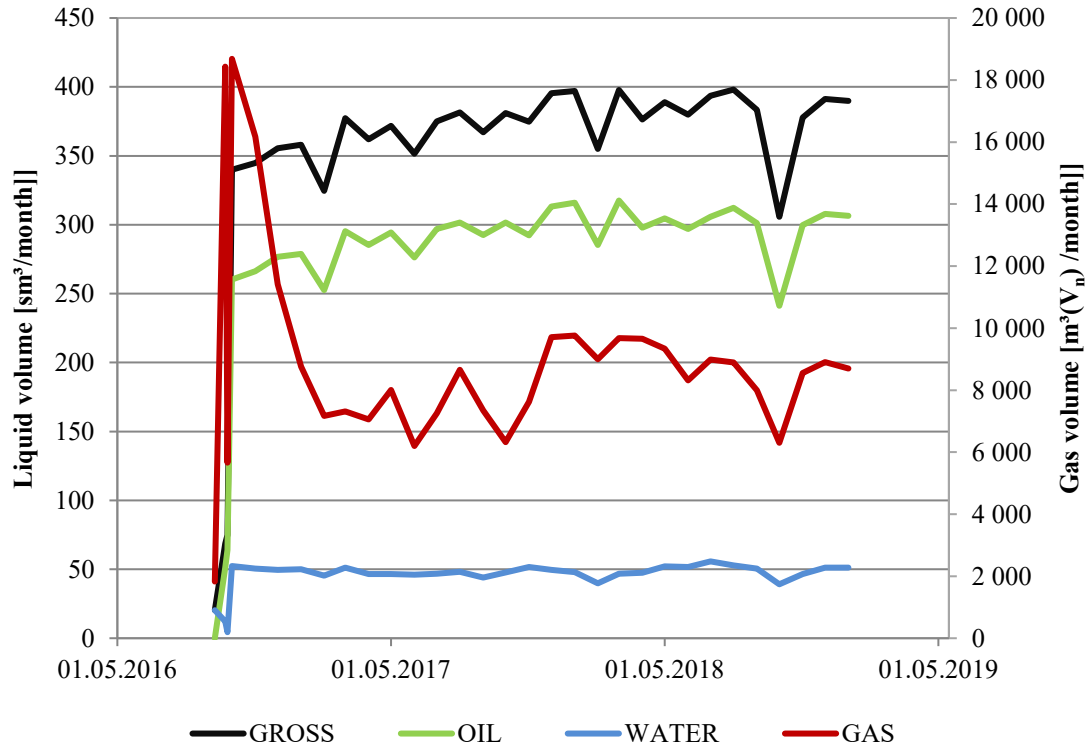
CAPEX	Capital Expenditures
DPI	Discounted Profitability Index
EOR	Enhanced Oil Recovery
EUR	Expected Ultimate Recovery
GDB	Production Data Base
GOC	Gas Oil Contact
HC	Hydrocarbon
MA	Matzen
NFA	No Further Action
NPV	Net Present Value
OIIP	Oil Initially In Place
OGRC	Oil and Gas Reserves Committee
OPEX	Operational Expenditures
OWC	Oil Water Contact
PRMS	Petroleum Resource Management System
PU	Production Unit
PVT	Pressure, Volume, Temperature
RAGG	Raggendorf
RF	Recovery Factor
SPE	Society of Petroleum Engineers
SS	Sub Sea
TH	Tortonian Horizon
TVD	Total Vertical Depth
URF	Ultimate Recovery Factor
WC	Water Cut
WIIP	Water Initially In Place

Appendix A

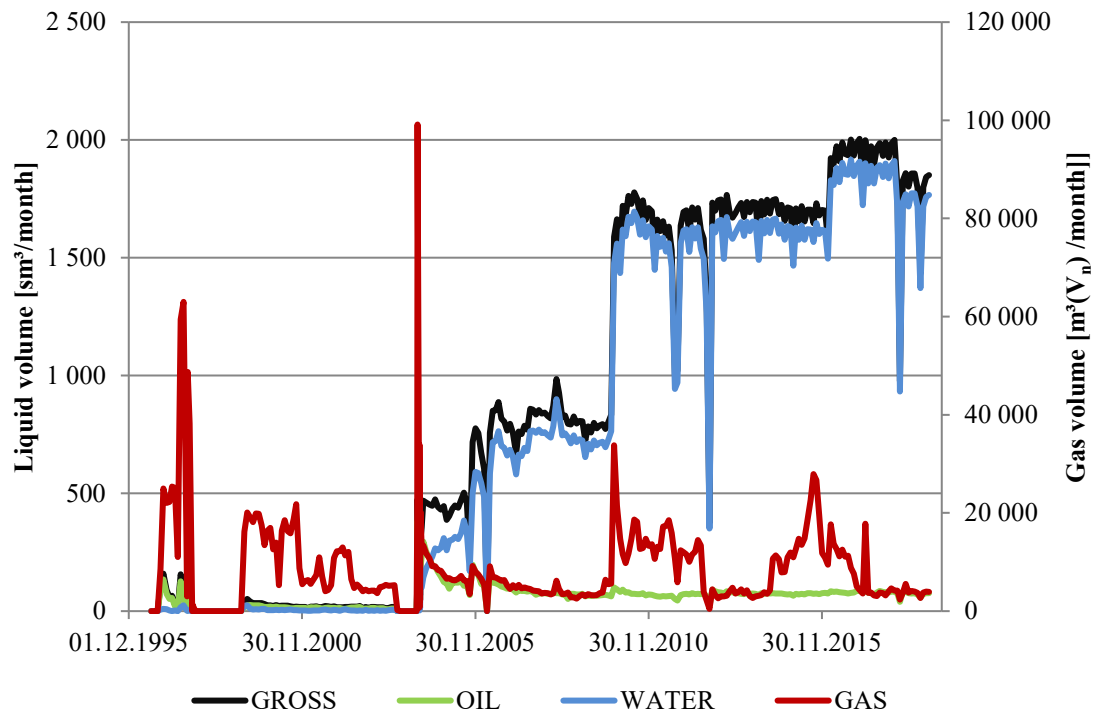
Appendix

A.1 Wellbore production history (209-33)

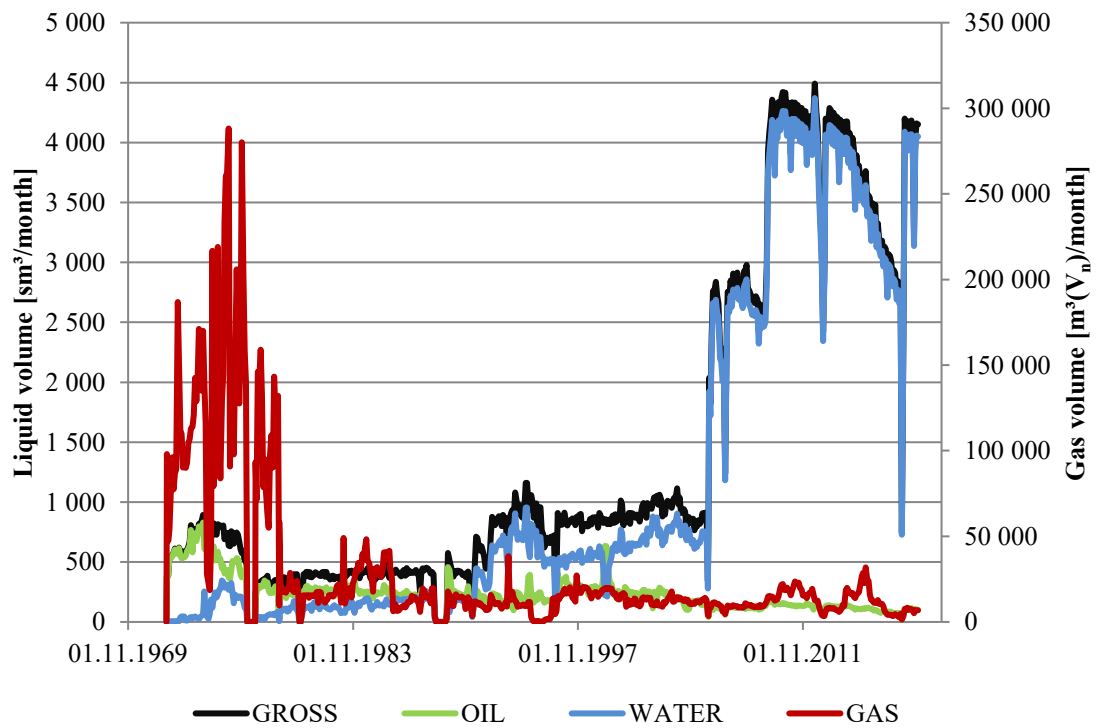
Matzen 145



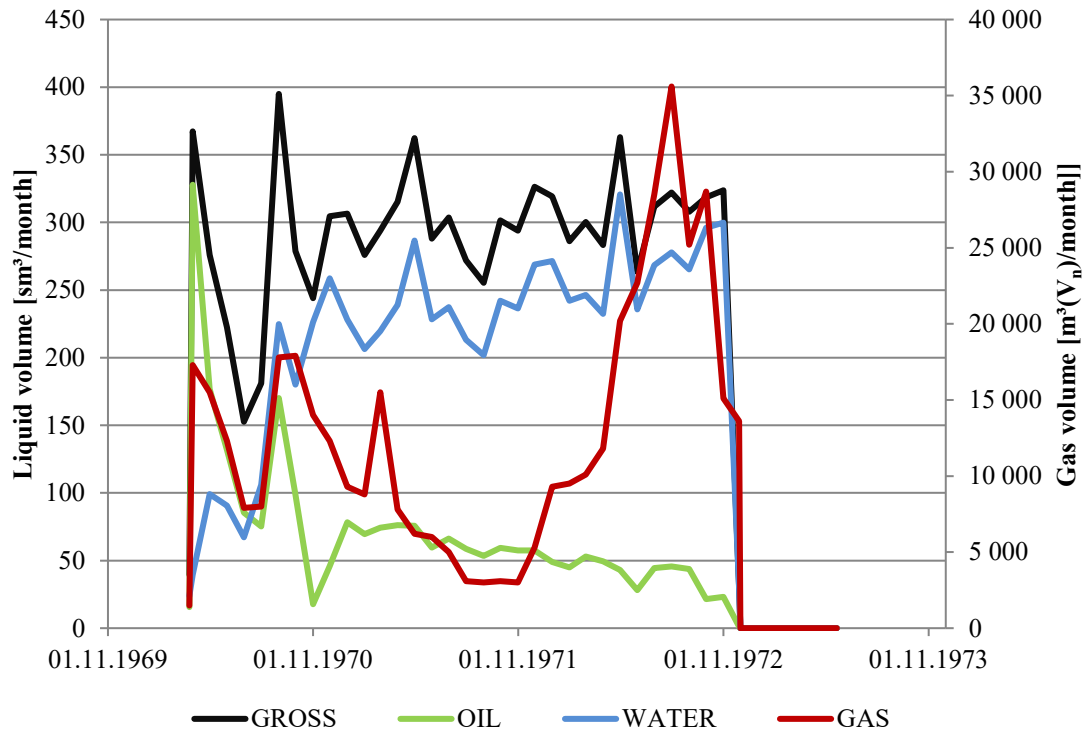
Matzen 229



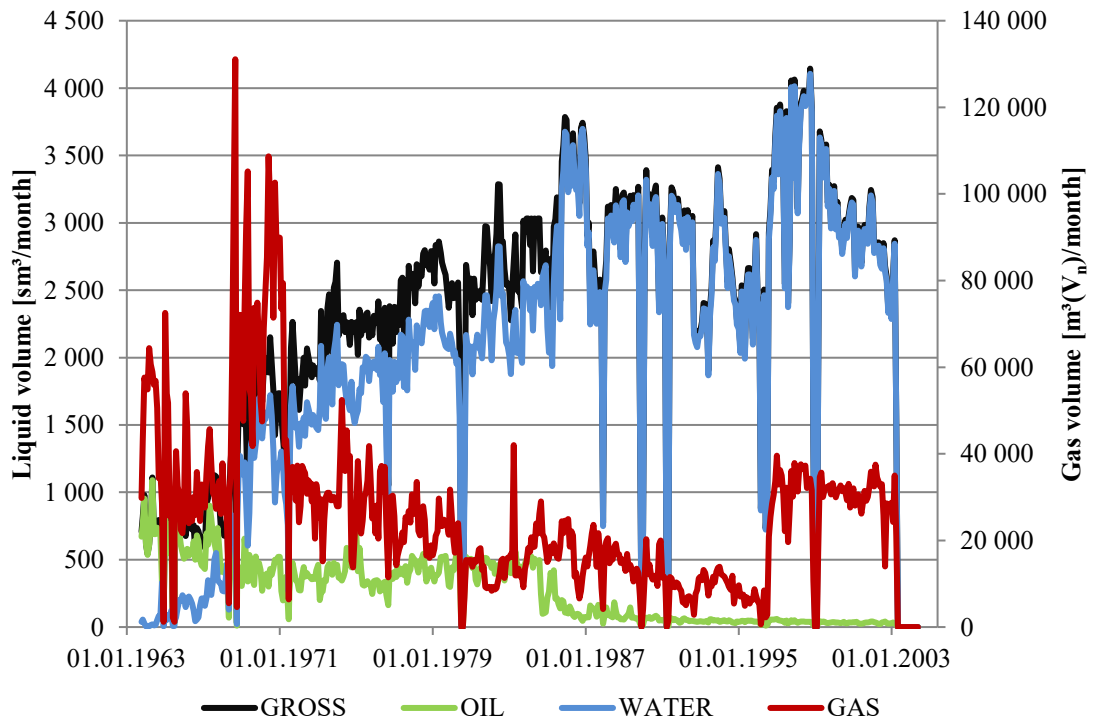
Matzen 476



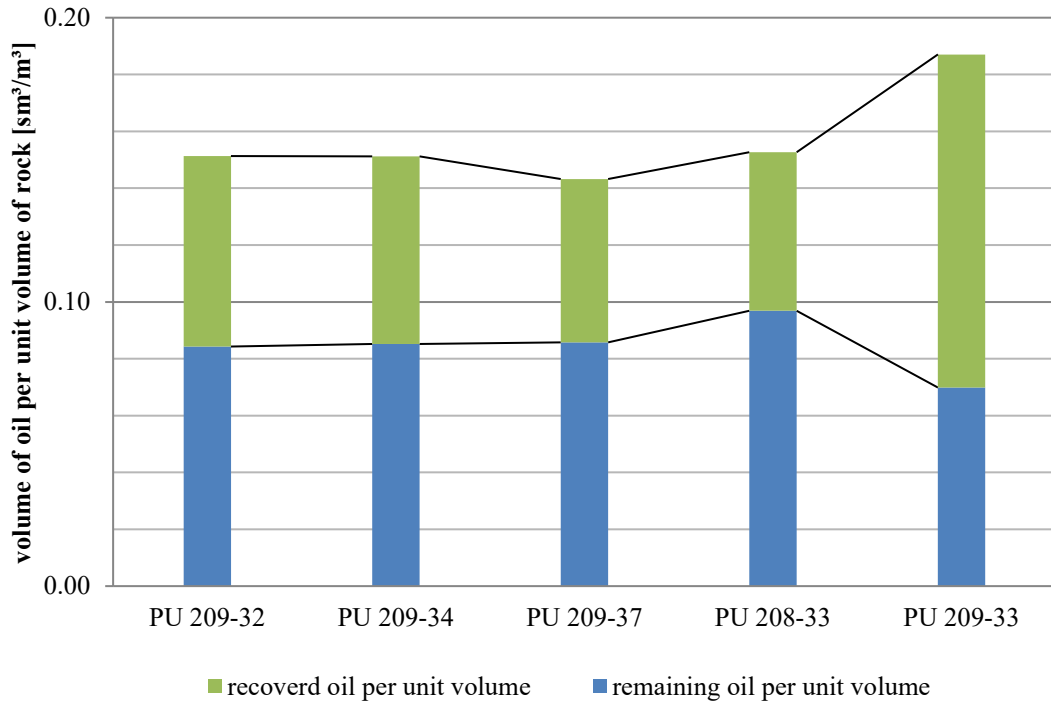
Raggendorf 010



Raggendorf 016

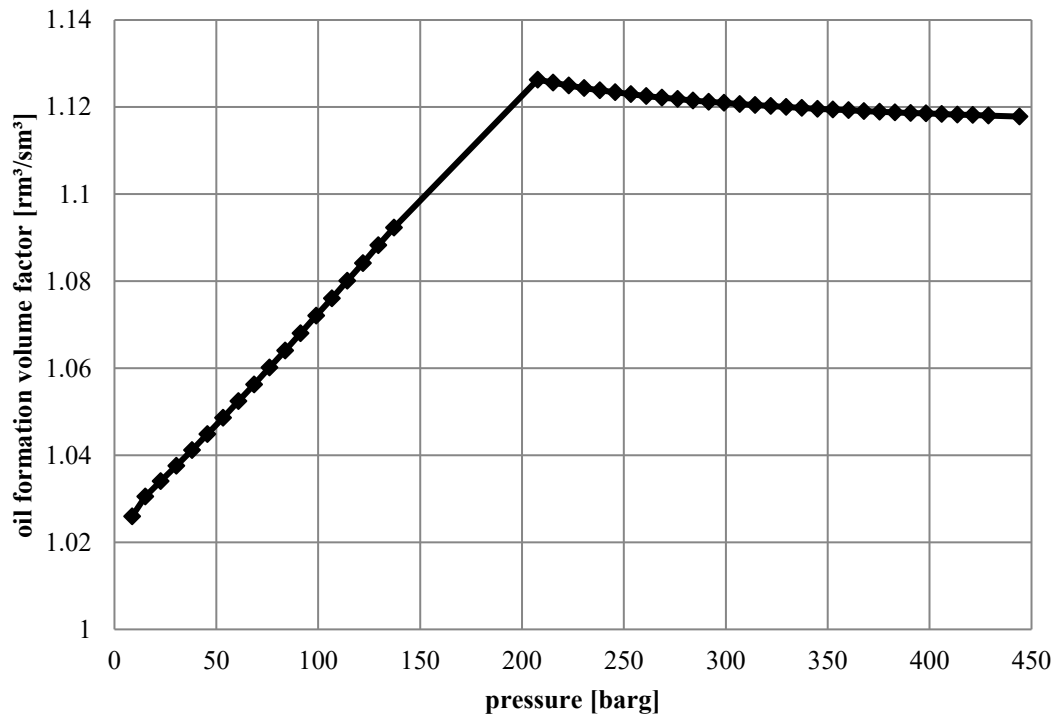


A.2 Comparison of recovered & remaining oil

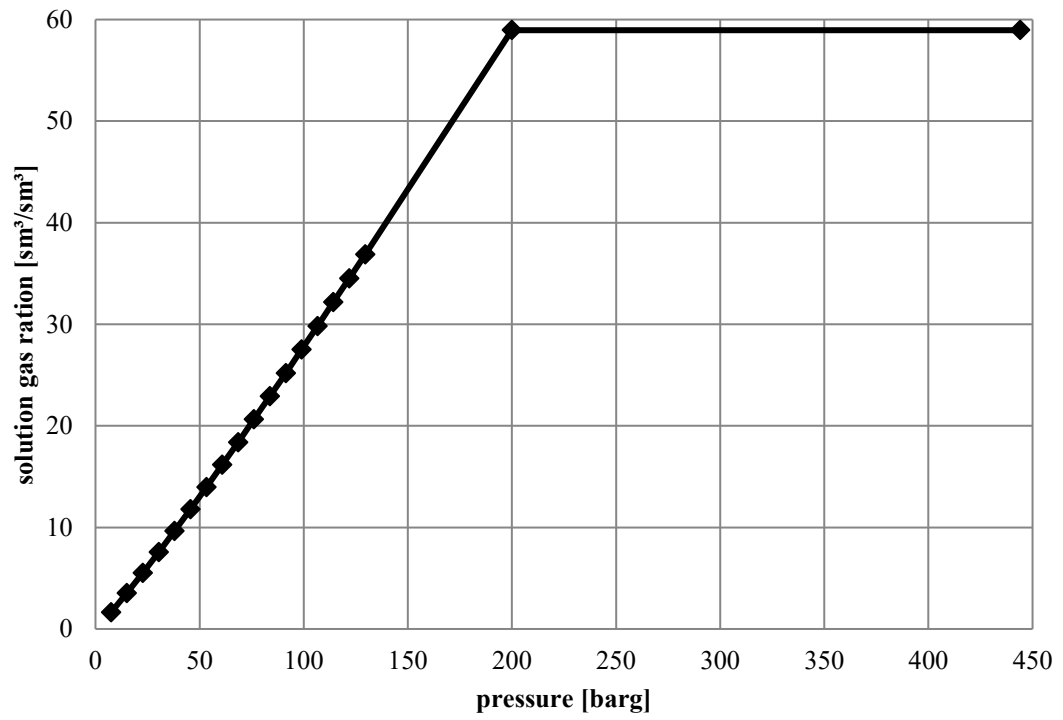


A.3 Fluid model

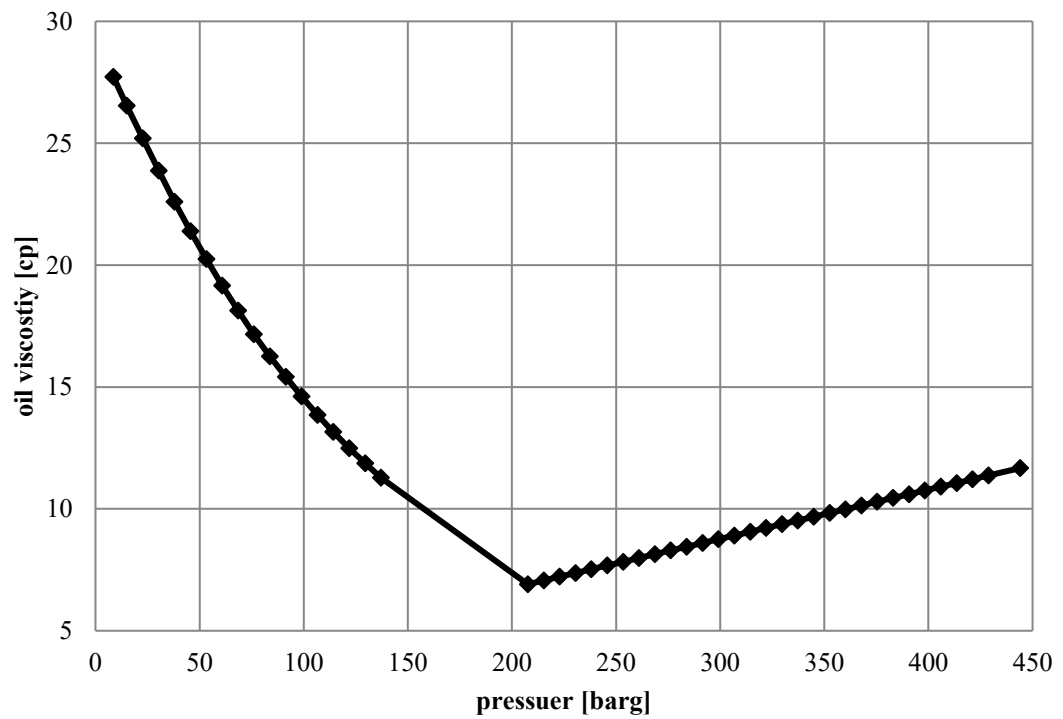
Oil Formation Volume Factor



Solution Gas Ratio

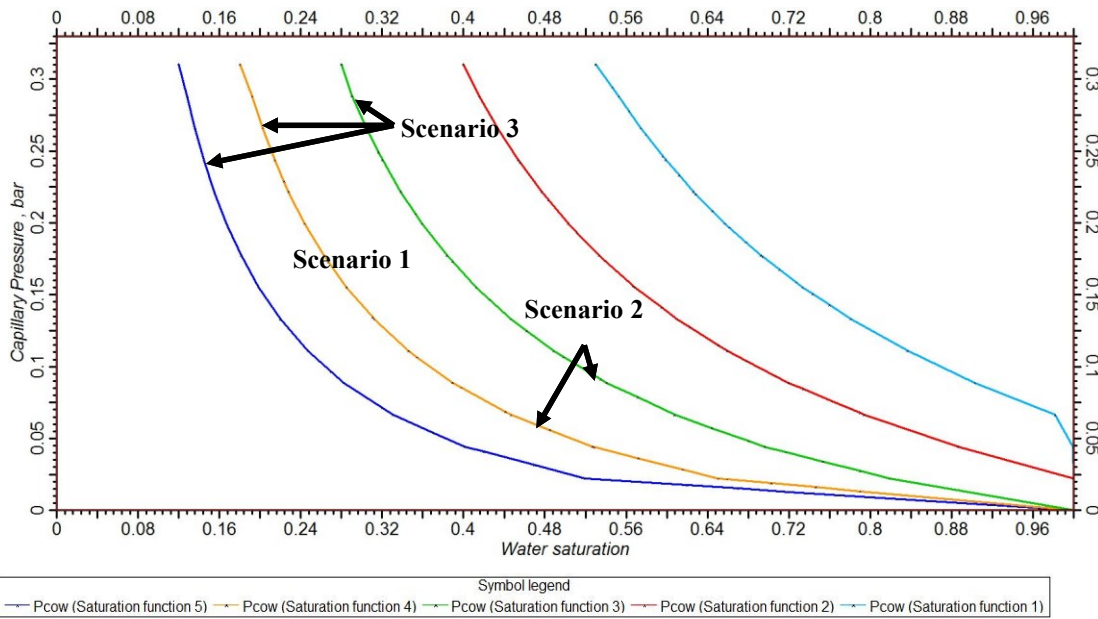
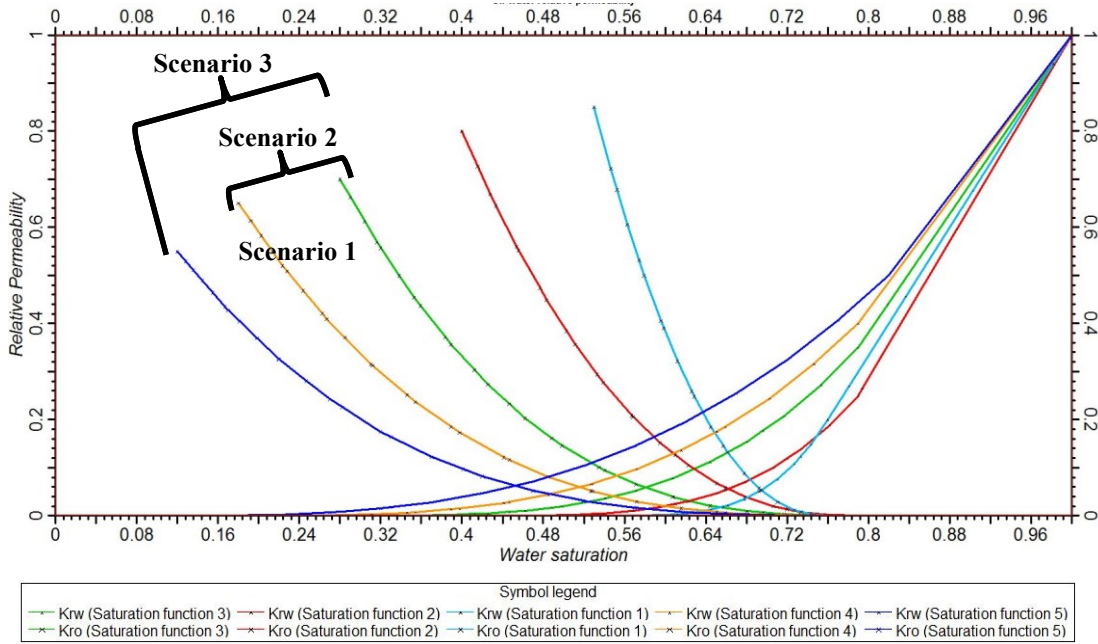


Oil Viscosity

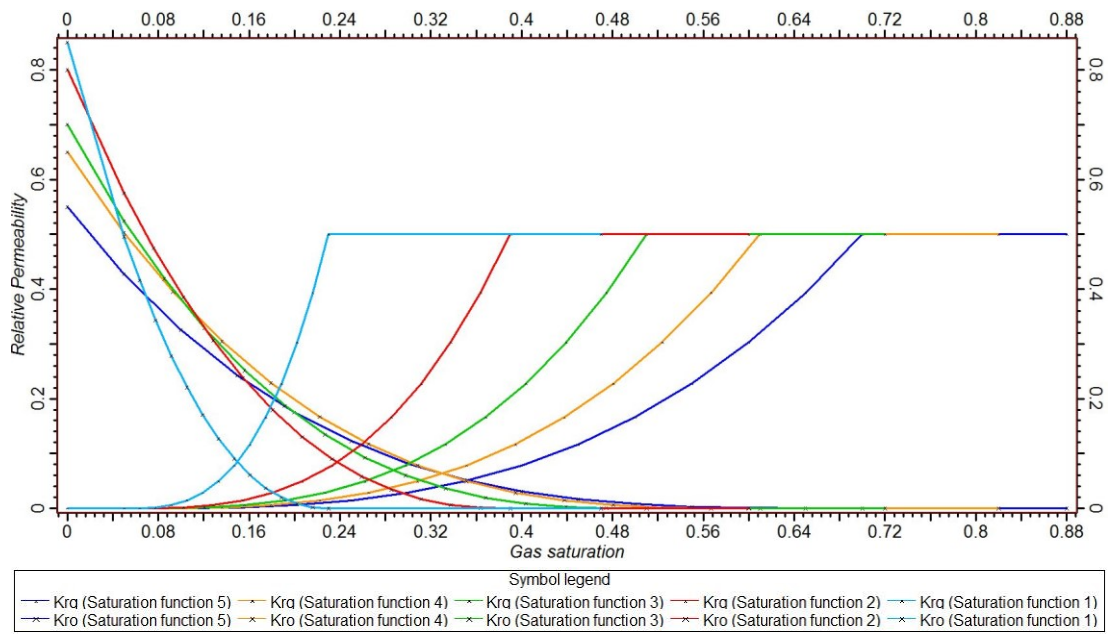


A.4 Rock physics

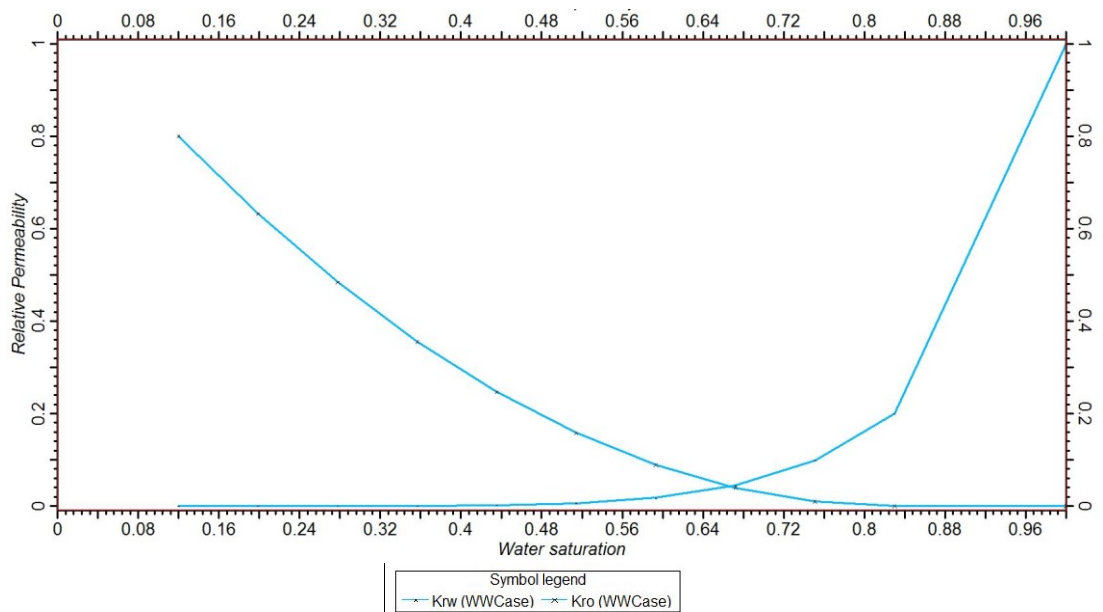
Measured functions (water – oil system)



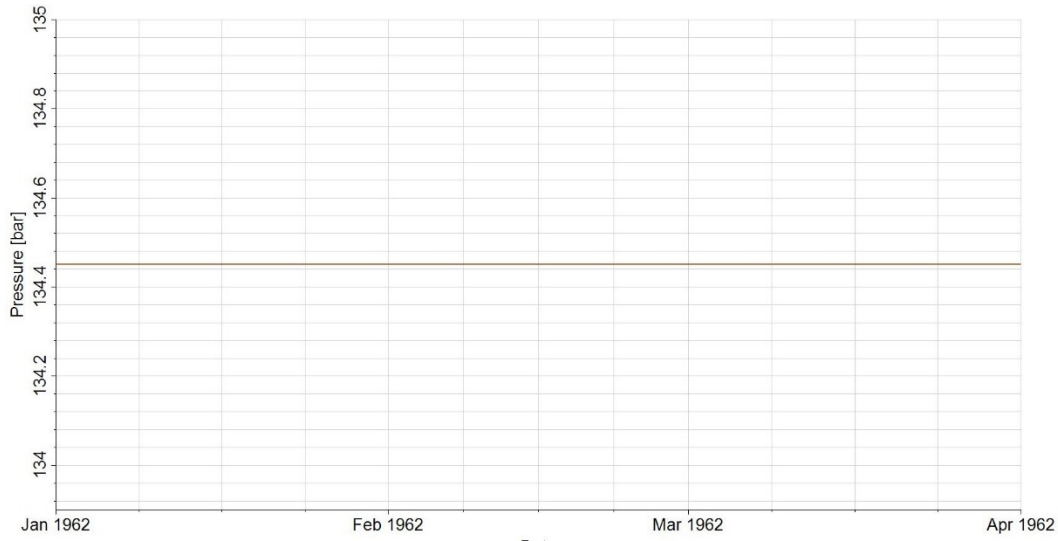
Measured functions (gas – oil system)



Artificial function (extremely water-wet conditions)

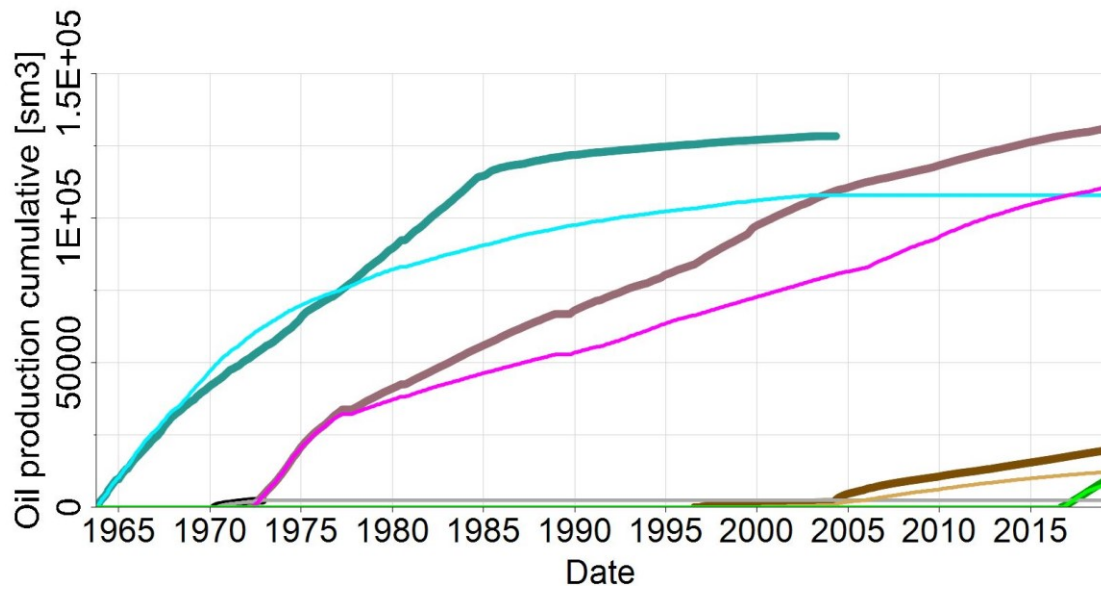


A.5 Equilibrium check for initialization

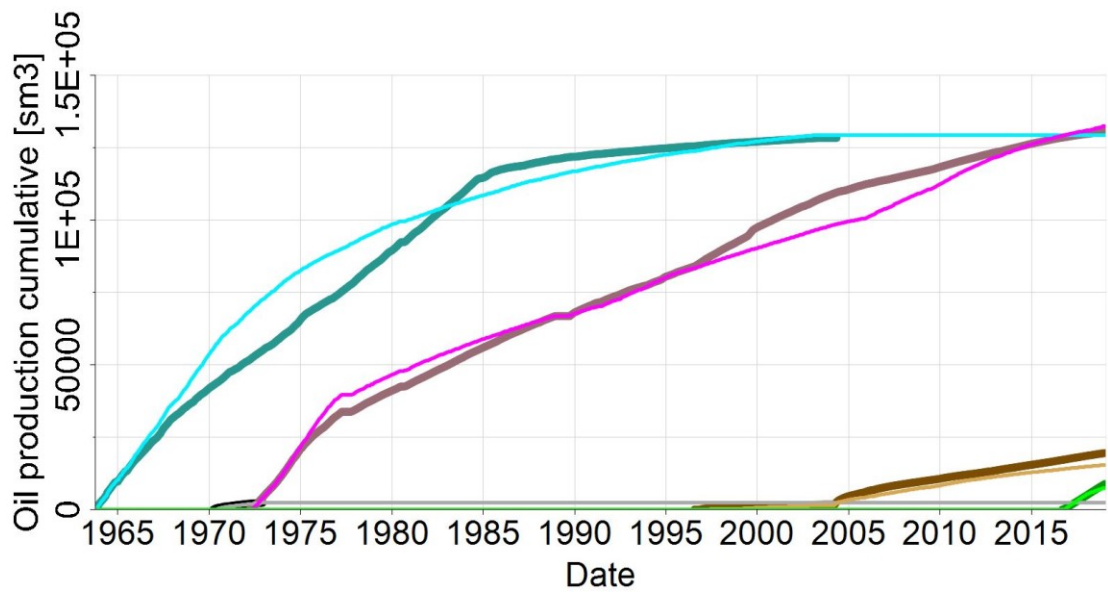


A.6 Cumulative oil production profiles

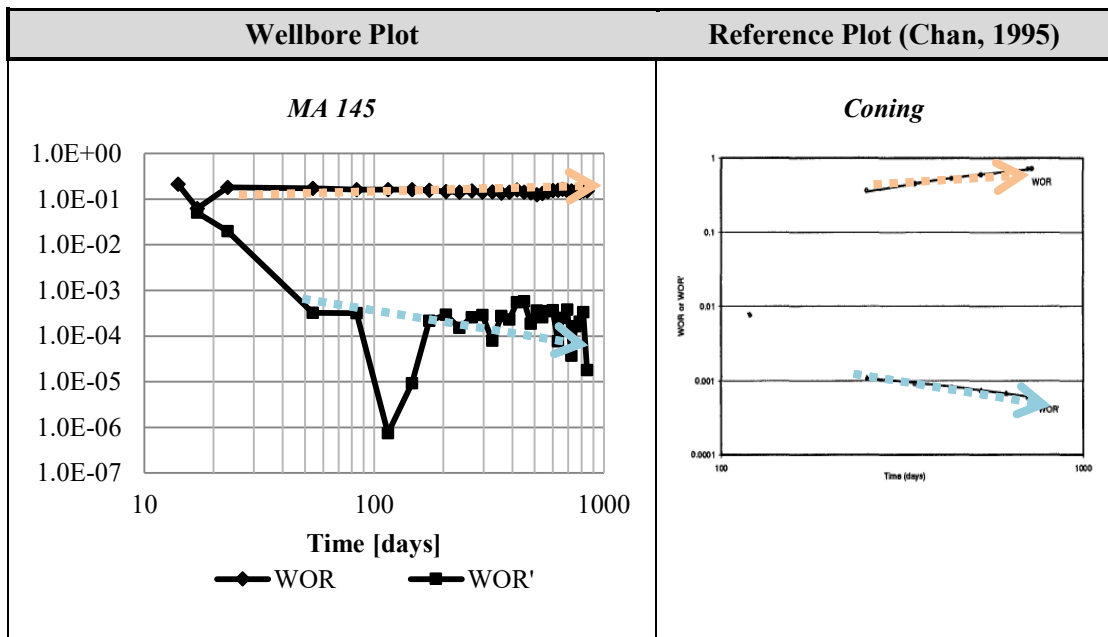
Box multiplier for permeability reduction (Factor = 0.35)

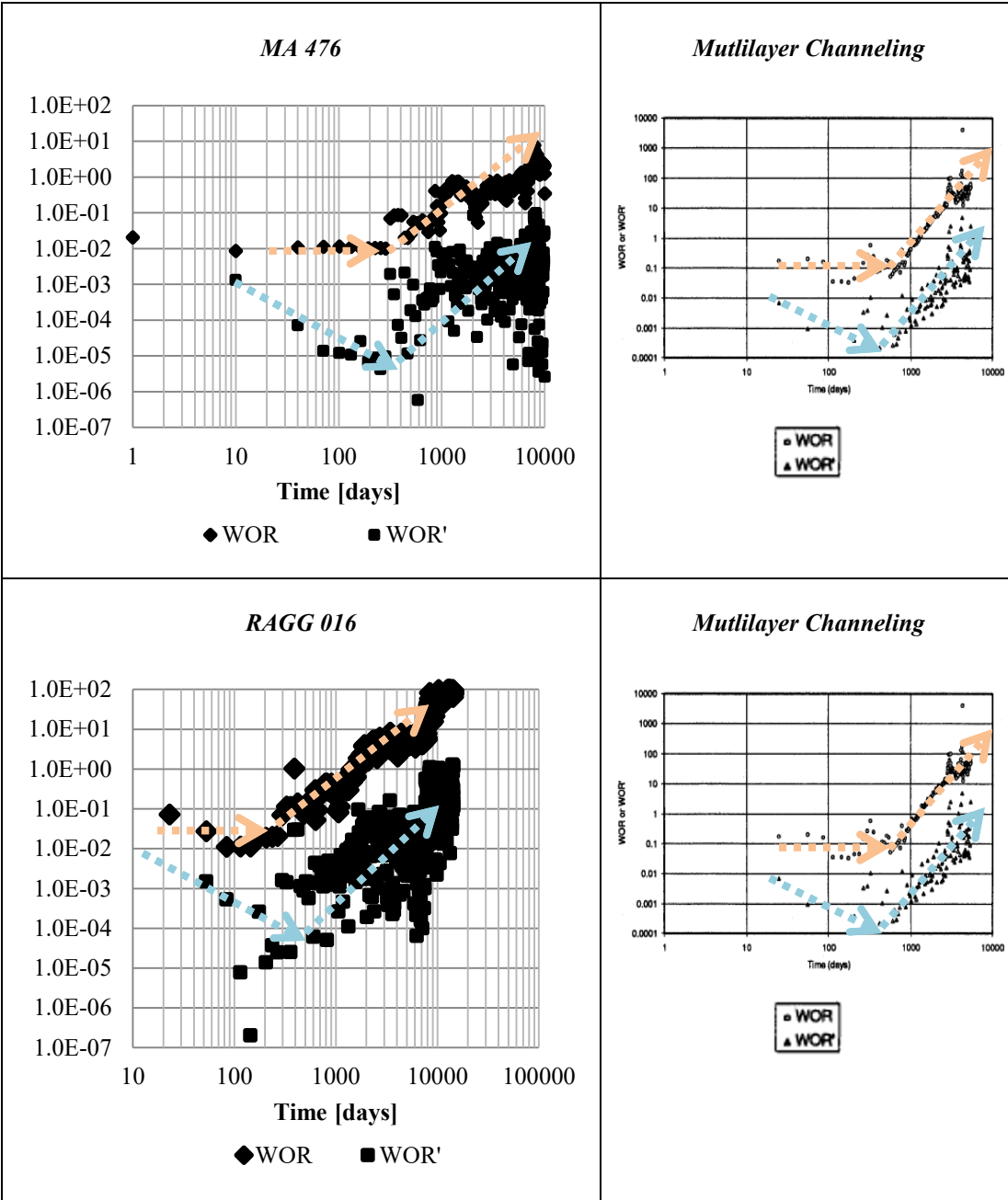


Box multiplier for porosity increase (Factor = 2.2)



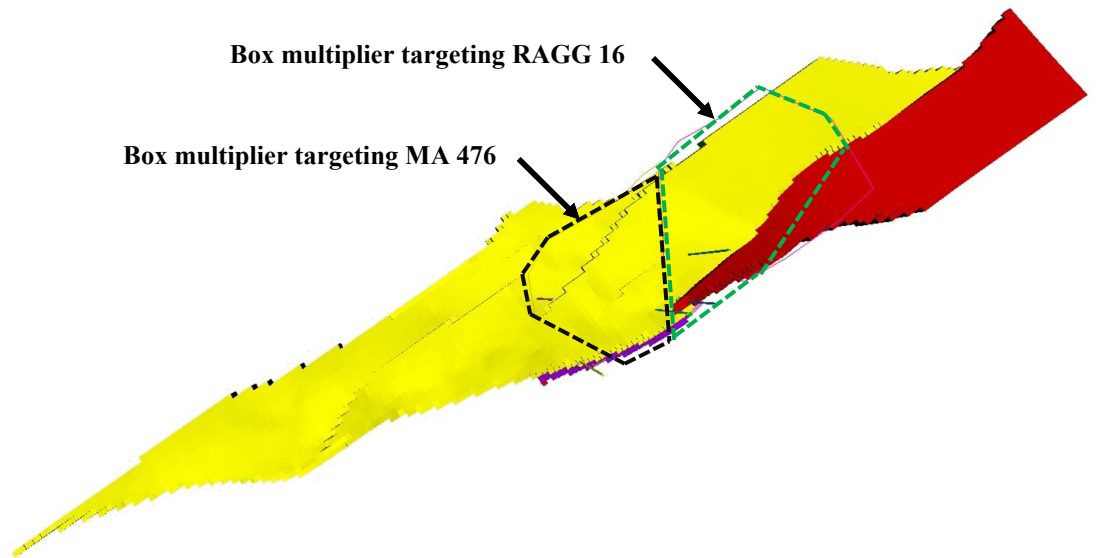
A.7 Water control diagnostic plots





A.8 Final box multipliers

Area of the final porosity box multiplier (only for the 9th Tortonian horizon)



Area of the final permeability box multiplier (near vicinity of the faults)

